Repair Methods for CFRP Aircraft Structures with Functional Inserts

Master of Science Thesis

Martino Giobbio

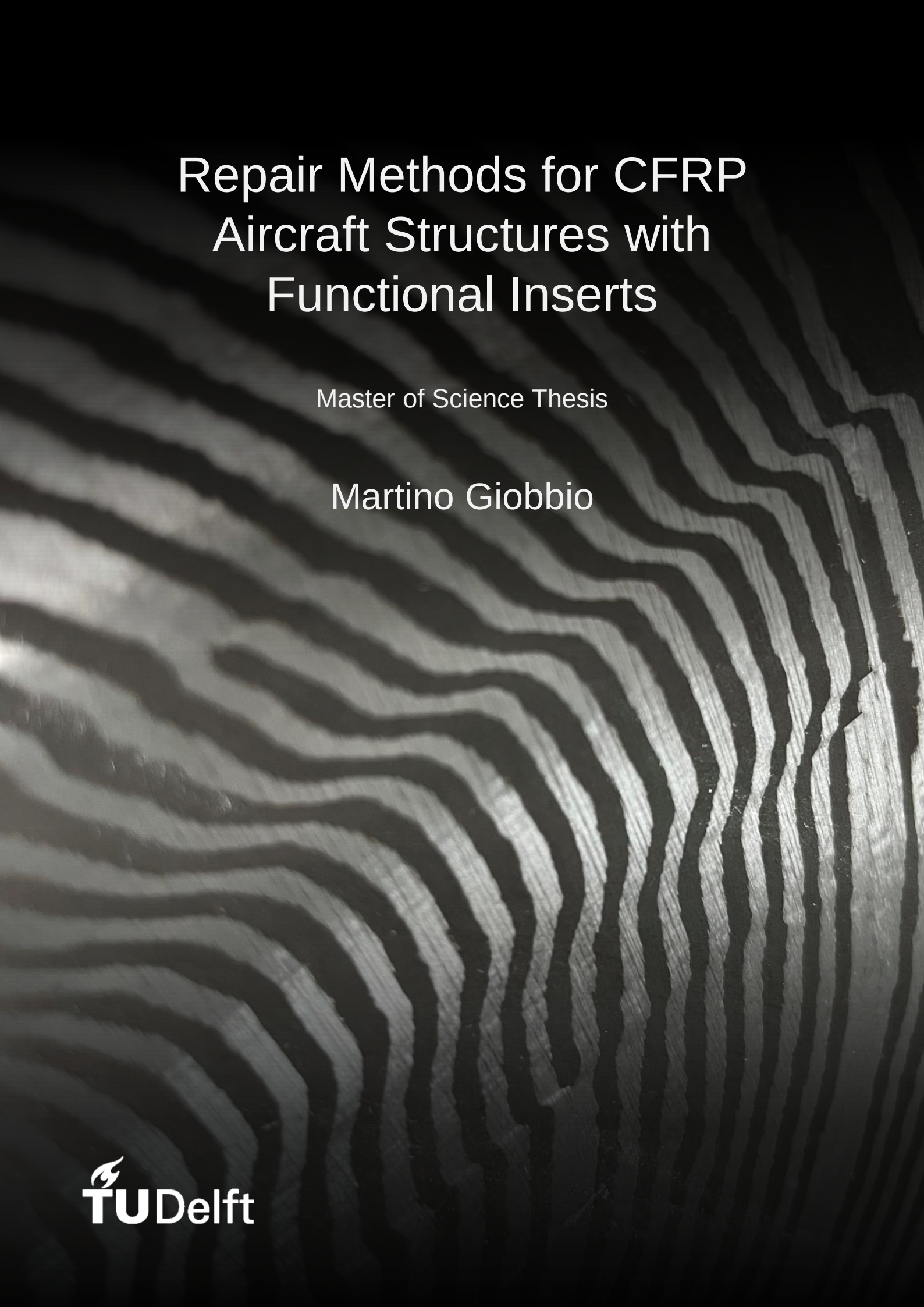

TU Delft

Repair Methods for CFRP Aircraft Structures with Functional Inserts

Master of Science Thesis

For obtaining the degree of Master of Science in Aerospace Engineering
at Delft University of Technology

Martino Giobbio

4814096

January 26th, 2024

Faculty of Aerospace Engineering · Delft University of Technology

The work in this thesis was supported by Airbus Defence and Space GmbH. Their cooperation is gratefully acknowledged.

Delft University of Technology
Faculty of Aerospace Engineering
Department of Aerospace Structures and Materials

GRADUATION COMMITTEE

Date: 26/01/2024

Chair:

Dr.ir. René Alderliesten

Committee members:

Dr.ir. John-Alan Pascoe

Dr.ir. Daniël Peeters

Dr. Sofia Teixeira de Freitas

TU Delft Delft University of Technology

Preface

This master thesis represents the culmination of my studies in aerospace engineering at TU Delft. This work aims to contribute to the development of repair procedures for composite aircraft structures. This project was fully conducted at Airbus Defence and Space GmbH, whose cooperation is gratefully acknowledged.

While writing this thesis, a general knowledge of composite materials, aerospace and structural engineering aspects was assumed. Readers interested in an overview of the topic can find this in Part I. Readers interested in the details of the work performed in this investigation can find all the information in Part II and III. Readers interested in the main outcomes of this thesis are advised to consult Part IV.

I would like to extend my gratitude to my academic supervisors, Dr.ir. John-Alan Pascoe and Dr. Sofia Teixeira de Freitas, for their availability, guidance, expertise and insightful feedback throughout this thesis. I would also like to thank my supervisor at Airbus, Stefan Seifert, for giving me the opportunity to undertake this research and the freedom to define its direction.
Additionally, I would like to express my thanks to my parents and siblings for their unwavering support, encouragement and trust throughout my entire academic journey.
At last, I would like to thank the fellow students I met during my time at university: studying and working together has definitely enriched my learning experience. A special thanks to those with whom I shared the most time, for their support and companionship.

Martino Giobbio
Ingolstadt, December 2023

Abstract

Aerospace manufacturers increasingly rely on composite materials for the most advanced aircraft, due to their superior performance and tailorability. As the adoption of such structures grows, so does the occurrence of various kind of damages throughout their service life. Therefore, there is the necessity to develop robust, reliable and repeatable procedures to fully restore the structural integrity of composite components. An additional challenge is posed by composite structures that include functional inserts: the functionality of such inserts needs to be re-instated on top of the integrity of the overall structure, while ensuring a seamless repair finish. This thesis considered two damage scenarios in a CFRP fuselage access panel whose edges are wrapped with a functional material, and defined the most suited repair procedure to tackle them.

The first scenario is represented by damages located in the CFRP structural part of the component. The scarf repair method was identified as the optimal one for this instance, research effort was therefore directed towards its improvement. Indeed, such technique does not currently allow to achieve a fully flush surface, as a mismatch between the repaired area and the undamaged one remains noticeable. Eliminating such unevenness is crucial for stealth and eventually aerodynamic reasons, and therefore needs to be investigated. Two repair configurations were implemented: the first one consists of re-milling the surface once the repair is completed, while the second one relies on a thinner repair patch that — once properly aligned — allows for a flush surface. The first option allowed for an improvement of over 80%, reducing the surface unevenness from more than 1/2 of a millimeter to less than a 1/10, while ensuring a smooth, continuous surface finish. At the same time, it proved capable of meeting all the mechanical requirements, performing closely to a reference repair configuration in several tests. On the other hand, the second option only partially improved the surface finish, but fell short of the fatigue life requirement by a large margin and also showed a significantly poorer mechanical performance compared to the reference repair and the other configuration.

The second scenario is represented by small, cosmetic damages located in the functional edge of the component. It was identified that such damages are best addressed with repair procedures based on a filler compound. Guidelines to define such repair compound were defined, although the impossibility of performing electromagnetic tests prevented from determining an optimal composition and left with a few alternatives to be further compared. Then, two repair procedures based on the use of such compounds were thought out: the first one is similar to conventional filling repair procedures, while the second one relies on a bespoke tool to inject the repair compound. The former was implemented and produced promising results: it allowed to precisely restore the original profile and achieve a seamless surface finish; however, the ability to reinstate the material's functionality could not be assessed. Damages affecting both the structural and functional parts were also briefly addressed, paving the way for future developments.

Contents

Preface iii

Abstract iv

List of Abbreviations ix

List of Symbols x

List of Figures xi

List of Tables xv

1 Introduction 1

1.1 Relevance . . . 1
1.2 Background . . . 3
1.3 Thesis structure . . . 4

I Literature Study 6

2 Damages and repairs overview 7

2.1 Damage types . . . 7
2.2 Damage sources . . . 8
2.3 Repair classification . . . 9
2.4 Repair techniques . . . 9
2.5 Adhesive bonding . . . 11
2.5.1 Adhesion mechanisms . . . 11
2.5.2 Adhesive joints failure modes . . . 12

3 Structural Material Repairs 13

3.1 Scarf joints . . . 13
3.2 General repair procedure . . . 14
3.2.1 Damage identification and assessment . . . 15
3.2.2 Material removal . . . 15
3.2.3 Surface treatment . . . 16
3.2.4 Adhesive application . . . 17
3.2.5 Repair patch application . . . 17
3.3 Repair parameters . . . 18
3.3.1 Scarf angle and geometry . . . 18
3.3.2 Adhesive thickness . . . 20
3.3.3 Laminate thickness & stacking sequence . . . 20

3.3.4 Plies mismatch . . . 20
3.3.5 Overply . . . 21
3.4 Failure modes . . . 21
3.5 Repair flushness . . . 22
3.6 Innovative configurations . . . 23
3.7 Certification . . . 25
3.8 Additional aspects . . . 26

4 Functional Material Repairs **27**
4.1 Stealth technology . . . 27
4.2 Microwave absorbing materials . . . 28
4.2.1 Absorption mechanisms . . . 28
4.2.2 Materials . . . 28
4.3 Particles dispersion in polymer composites . . . 29
4.4 Applicable repair methods . . . 29
4.4.1 Filling repairs . . . 29
4.4.2 Injection repairs . . . 30
4.4.3 Other methods . . . 30

5 Research questions **31**

II Structural Material Repairs **33**

6 Problem statement **34**
6.1 Background and approach . . . 34
6.2 Concepts definition . . . 36
6.3 Specimen and tests selection . . . 36
6.4 Workflow . . . 37

7 Adhesive selection **39**
7.1 Specimen characteristics . . . 39
7.2 Specimen production . . . 40
7.2.1 Manufacturing . . . 40
7.2.2 Quality control . . . 43
7.3 Testing . . . 44
7.3.1 Test set-up . . . 44
7.3.2 Test conditions . . . 46
7.4 Results and discussion . . . 47
7.4.1 Failure cycles . . . 47
7.4.2 Fracture surfaces . . . 47
7.4.3 Adhesive selection . . . 49

8 Specimens production and analysis **51**
8.1 Laminate production . . . 51
8.1.1 Layup . . . 51
8.1.2 Curing . . . 52
8.1.3 Scarf . . . 52
8.1.4 Surface treatment . . . 53
8.2 Repair concepts implementation . . . 55
8.2.1 Conventional patch specimens . . . 55
8.2.2 Re-milled patch specimens . . . 55
8.2.3 Re-designed patch specimens . . . 56
8.3 Surface flushness . . . 59
8.3.1 Conventional patch specimens . . . 61
8.3.2 Re-milled patch specimens . . . 63
8.3.3 Re-designed patch specimens . . . 64

9 Testing and results **66**
9.1 Quasi-static tests . . . 66
9.1.1 Results . . . 66
9.1.2 Failure mode and path . . . 70
9.2 Fatigue tests . . . 71
9.2.1 Fatigue life . . . 72
9.2.2 Failure mode and path . . . 73
9.2.3 Residual strength . . . 73

10 Discussion and conclusions **78**
10.1 Repair configuration . . . 78
10.1.1 Discussion . . . 78
10.1.2 Conclusion . . . 80
10.2 Patch type . . . 81
10.2.1 Discussion . . . 81
10.2.2 Conclusion . . . 82
10.3 Additional remark . . . 82

III Functional Material Repairs **83**

11 Problem statement **84**
11.1 Background . . . 84
11.2 Approach and limitations . . . 85
11.3 Workflow . . . 86

12 Repair compound design **88**
12.1 Repair compound definition . . . 88

12.2 Compounds comparison . . . 90
12.2.1 Comparison plate manufacturing . . . 90
12.2.2 Visual comparison . . . 90
12.3 Compounds mechanical testing . . . 93
12.3.1 Centrifugal tests . . . 93
12.3.2 Specimen & test details . . . 94
12.3.3 Results & discussion . . . 95
12.4 Selection . . . 97

13 Repair procedures **99**
13.1 Manual repair procedure . . . 99
13.2 Injection repair procedure . . . 102

14 Discussion and conclusions **104**
14.1 Repair compound . . . 104
14.2 Repair procedures . . . 104

15 Outlook **106**

IV Conclusive Remarks **109**

16 Conclusions **110**
16.1 Summary . . . 110
16.2 Answers to the research questions . . . 111

17 Recommendations **115**

References **117**

A EN6066 Static tests **125**

B EN6066 Fatigue tests **129**

C EN6066 Residual strength tests **130**

List of Abbreviations

CFRP	Carbon Fibre Reinforced Plastics
CLT	Classical Laminate Theory
DIC	Digital Image Correlation
EASA	European Union Aviation Safety Agency
EMI	Electromagnetic Interference
FAA	Federal Aviation Administration
FEM	Finite Element Method
FRP	Fibre Reinforced Plastics
GFRP	Glass Fibre Reinforced Plastics
IQR	Inter-Quartile Range
LHS	Left Hand Side
LO	Low Observable (technology)
MAM(s)	Microwave Absorbing Material(s)
MCLS	Modified Crack Lap Shear
NDI	Non-Destructive Inspection
RHS	Right Hand Side
RTM	Resin Transfer Moulding
SLS	Single Lap Shear
UD	Uni-directional
UTS	Ultimate Tensile Strength
VID	Visible Impact Damage
WIWeB	Wehrwissenschaftliches Institut für Werk- und Betriebsstoffe

List of Symbols

A	Specimen's cross-sectional area	[mm^2]
b	Specimen's width	[mm]
E	Young's modulus	[GPa]
E_x	Laminate tensile modulus	[GPa]
f	Frequency	[Hz]
F_c	Centrifugal force	[N]
F_{max}	Ultimate tensile load	[kN]
m	Mass	[g]
r	Radius	[m]
t	Specimen's thickness	[mm]
α	Scarf angle	[rad]
ε_{max}	Elongation at break	[-]
ε_u	Allowable strain	[-]
σ	Standard deviation	[-]
τ_p	Ultimate design stress	[MPa]
ω	Angular velocity	[rad/s]

List of Figures

1.1 Percentage of composites in terms of weight adopted in various military and large civil aircraft over time (edited chart from [3]) . . . 2
1.2 Nose of the Lockheed-Martin F-35A, showcasing composite panels with functional material inserts on their edges . . . 2
1.3 Graphic representation of a composite structure with functional inserts, demonstrator structure considered during this master project [4] . . . 4
1.4 Flowchart outlining the overall structure of this thesis . . . 5

2.1 Micrographic pictures of some damages in a composite material at lamina and laminate level . . . 8
2.2 Schematic representation of a scarf repair [7] . . . 10
2.3 Schematic representation of an external patch repair [7] . . . 10
2.4 Schematic representation of a resin injection repair [13] . . . 10
2.5 Schematic representation of a mechanically fastened repair [7] . . . 11
2.6 Schematic representation of a plug repair [7] . . . 11
2.7 Schematic representation of various adhesive joint failure modes [15] . . . 12

3.1 Schematic representation of a scarf joint under tensile load [18] . . . 13
3.2 Top and side views of a scarf repair under tensile load [18] . . . 14
3.3 Normalized shear and peel stress distribution along the scarf length L of a 2D scarf joint (red lines) and a 3D scarf repair (blue lines). For the latter, the stresses are plotted along three distinct loading directions φ (refer to Figure 3.2 for a graphical definition of φ) [18] . . . 14
3.4 Schematics of the necessary steps to implement a scarf repair in a composite structure [22] . . . 15
3.5 Relative bond stress (shear and peel) as function of the scarf angle (edited from [29]) . . . 19
3.6 Schematic representation of common tensile failure modes for scarf repairs [41] . . . 22
3.7 Schematic section views of possible soft-patch scarf repair configurations [48] . . . 23
3.8 Schematic representation of some innovative repair designs [41] . . . 24
3.9 Photograph and schematic representation of the stitched scarf repair concept [57] 25

6.1 Flush scarf repair geometries previously tested at Airbus (dimensions in mm) [5] . . . 35
6.2 Cross sections of the flush scarf repair concepts considered in this thesis . . . 36
6.3 EN6066 specimen geometry, side and top view (dimensions in mm) . . . 37
6.4 Flowchart depicting the steps performed to tackle the research questions related to the repairs localised in the structural part of the demonstrator structure . . . 38

7.1 Modified Crack Lap Shear (MCLS) specimen geometry, side and top view (dimensions in mm) . . . 39
7.2 Flowchart depicting the manufacturing steps of the MCLS specimens . . . 41
7.3 Manufacturing steps for the MCLS specimens with the film adhesive . . . 41
7.4 Manufacturing steps for the MCLS specimens with the paste adhesive . . . 42
7.5 Micrographs showing the bondline of the MCLS specimens . . . 43
7.6 Adhesive bondline thickness of the MCLS specimens, both with film and paste adhesive . . . 44
7.7 Locations along the bondline of the adhesive thickness measurements (dimensions in mm) . . . 44
7.8 Crack tip location in the specimen MCLS_PA_5, used to identify the critical strain level corresponding to the crack front for the paste adhesive . . . 45
7.9 Crack growth as function of the number of cycles for the MCLS specimens with the film adhesive . . . 48
7.10 Crack growth as function of the number of cycles for the MCLS specimens with the paste adhesive . . . 49
7.11 Fracture surfaces and failure modes for the MCLS specimens with film and paste adhesive . . . 50
7.12 Micrographs depicting imperfections — or the lack of — in the bondline of the MCLS specimens . . . 50

8.1 Flowchart depicting the manufacturing steps of the EN6066 specimens . . . 51
8.2 Vacuum lay-up followed for the produced laminates (thicknesses not to scale) . . . 52
8.4 Creation of the scarf surface via a CNC milling procedure . . . 53
8.3 Autoclave curing cycle for the 8552/IM7 laminates [86], [87] . . . 54
8.5 Division into strips and first sanding direction for the surface treatment (dimensions in mm) . . . 54
8.6 Manufacturing of the scarf repair with the conventional patch . . . 55
8.7 Manufacturing of the scarf repair with the re-milled patch . . . 56
8.8 Manufacturing of the scarf repair with the re-designed patch . . . 59
8.9 Location on the EN6066 plates where the thickness was measured via ultrasonic inspection (dimensions in mm) . . . 60
8.10 Sketch of the modified patch configuration, depicting the concavity at the interface between the parent laminate and the repair patch . . . 61
8.11 Surface flushness of the plate repaired with the conventional patch . . . 62
8.12 Side view and top surface analysis of a conventional patch specimen, obtained with a laser microscope . . . 62
8.13 Surface flushness of the plate repaired with the re-milled patch, before re-milling . . . 63
8.14 Surface flushness of the plate repaired with the re-milled patch, after re-milling . . . 63
8.15 Side view and top surface analysis of a re-milled patch specimen, obtained with a laser microscope . . . 64
8.16 Surface flushness of the plate repaired with the modified, thinner patch . . . 64
8.17 Side view and top surface analysis of a modified patch specimen, obtained with a laser microscope . . . 65

9.1 Ultimate tensile load reached by the different patch configurations during static testing . . . 67
9.2 Ultimate tensile strength reached by the different patch configurations during static testing . . . 67
9.3 Elongation at break reached by the different patch configurations during static testing 68
9.4 Tensile modulus of the different patch configurations, obtained from static testing data . . . 69
9.5 Fracture surfaces of the EN6066 specimens, static tests (in every picture: parent laminate on the LHS, repair patch on the RHS) . . . 70
9.6 Schematic, cross-sectional illustrations of the fracture paths of the EN6066 specimens, static tests (in all the figures: parent laminate on the LHS, repair patch on the RHS) . . . 71
9.7 Fatigue life of the different patch configurations . . . 72
9.8 Fracture surfaces of the EN6066 specimens that failed below the threshold during the dynamic tests (in both pictures: parent laminate on the LHS, repair patch on the RHS) . . . 73
9.9 Ultimate tensile load reached by the different patch configurations during the residual strength static tests . . . 74
9.10 Ultimate tensile residual strength reached by the different patch configurations during the residual strength static tests . . . 74
9.11 Elongation at break reached by the different patch configurations during the residual strength static tests . . . 75
9.12 Tensile modulus of the different patch configurations, obtained from the residual strength static testing data . . . 75
9.13 Fracture surfaces of the EN6066 specimens, static tests (in every picture: parent laminate on the LHS, repair patch on the RHS) . . . 77

11.1 Repair procedure for damages in the functional material, based on the use of hard patches [4] . . . 84
11.2 Repair procedure for damages in the functional material, based on the use of a ”sacrificial” patch [4] . . . 85
11.3 Repair procedure for damages in the functional material, based on the use of pre-preg soft patches [4] . . . 85
11.4 Flowchart depicting the steps performed to tackle the research questions related to the repairs localised in the functional part of the considered composite component 86

12.1 Range of all the possible repair compounds for the functional material . . . 89
12.2 Drawings of the comparison plate manufactured with the functional material (dimensions in mm) . . . 91
12.3 Comparison tool filled with different repair compounds . . . 91
12.4 Photomicrographs depicting the cross section of the larger hole for the different repair compounds . . . 92
12.5 Photomicrographs depicting the cross section of the smaller hole for the different repair compounds . . . 93
12.6 Test equipment used to measure the tensile strength of different repair compounds 94

12.7 Overview of the ultimate tensile strength and failure modes recorded during the centrifugal tests for all the tested compounds 96
12.8 Correlation between ultimate tensile strength and additive content, based on the median values for each tested compound 96
12.9 Fracture surfaces of some tensile centrifugal test specimens, depicting at least an example of all the encountered failure modes 97

13.1 Impact damages on the edge of the demonstrator component addressed with this repair procedure 100
13.2 Component repaired after removing the entire damaged areas via grinding 100
13.3 Positioning of the component in a jig intended to keep the repair compound in place while curing 101
13.4 Repaired component at the end of the curing cycle, prior to the final surface post-processing 101
13.5 Repaired component at the end of the procedure, after the final post-processing intended to re-fine the edge contour 101
13.6 Micrographs depicting the considered demonstrator component and some repaired areas 102
13.7 Step-by-step repair procedures to address small damages in the functional material using a paste-like repair compound 102
13.8 Injection repair procedure to address small damages on the functional edge 103
13.9 Drawings of the concept tool defined for injection repairs (dimensions in mm) . . . 103

15.1 Conceptual repair procedure to address damages impacting both the structural and the functional parts of the demonstrator component 107
15.2 Conceptual repair procedure to address damages impacting both the structural and the functional parts of the demonstrator component, damage located in the transition area between the two materials 107

A.1 Stress-strain curves for the EN6066 specimens, static tests 126
A.2 Fracture surfaces of the EN6066 specimens, static tests (in every picture: parent laminate on the LHS, repair patch on the RHS) 128

B.1 Fracture surfaces of the EN6066 specimens failed below 54000 cycles during the fatigue tests (in every picture: parent laminate on the LHS, repair patch on the RHS)129

C.1 Stress-strain curves for the EN6066 specimens, residual strength static tests . . . 131
C.2 Fracture surfaces of the EN6066 specimens, residual strength tests (in every picture: parent laminate on the LHS, repair patch on the RHS) 132

List of Tables

3.1 Overview of surface treatment techniques (edited from [20]) 17
3.2 Advantages and disadvantages of different repair patch configurations 18

4.1 Comparison of different techniques to incorporate particles in polymer composites 29

5.1 Overview of the research questions considered in this thesis 32

6.1 Parameters and characteristics of the EN6066 specimens 37
6.2 Goal and scope of the first part of the thesis, aimed at investigating structural repairs 38

7.1 Parameters and characteristics of the MCLS specimens 40
7.2 Curing conditions of the two adhesives used for the MCLS specimens 42
7.3 Parameters used for the surface treatment of the MCLS specimens and their straps 42
7.4 Measurements of the bondline thickness for the MCLS specimens 43
7.5 Fatigue testing conditions for the MCLS specimens 46
7.6 Overview of the MCLS specimens testing phase 47

8.1 Physical and mechanical properties of the uni-directional pre-preg HexPly® 8552/IM7 at ambient conditions (dry, 25°C) [86] 52
8.2 CNC milling parameters used for creating the scarf edge in all the manufactured specimens 52
8.3 Comparison between the layup selected for the modified patch and the original one chosen for the parent laminates 57
8.4 Thickness and surface flushness of the different repair patch concepts (* quantified with respect to the flushest conventional patch, ** this second conventional patch is the plate that was later re-milled) 60

9.1 Overview of the EN6066 tensile static tests, median values for various relevant parameters 69
9.2 Parameters used for the fatigue tests of the EN6066 specimens 72
9.3 Overview of the EN6066 residual strength tensile static tests, median values for various relevant parameters 76
9.4 Comparison between the specimens statically tested after fatigue and the ones statically tested in pristine conditions (delta values calculated using the median values listed in Table 9.1 and Table 9.3) 76

11.1 Requirements for the repairs in the functional material 86
11.2 Goal and scope of the second part of the thesis, aimed at investigating functional repairs 87

12.1 Adhesive, additive and fibre content for all the tested compounds intended to repair damages in the functional material 90
12.2 Parameters used for the centrifugal tensile tests 94
12.3 Summary of the tensile centrifugal tests, listing all the tested specimens 95

A.1 Parameters and test results for all the EN6066 specimens statically tested (a and b represent, respectively, the thickness and the width of the specimens measured along the scarf) 125

C.1 Parameters and test results for all the EN6066 specimens residual strength tests (a and b represent, respectively, the thickness and the width of the specimens measured along the scarf) 130
C.2 Comparison between the specimens statically tested after fatigue and the ones statically tested in pristine conditions (the reference values are the medians listed in Table 9.1) 130

1 Introduction

This introductory chapter describes the relevance of this thesis' topic, in order to motivate the need for this investigation. The relevant work previously completed at Airbus Defence and Space GmbH is then briefly recalled, in order to highlight the novelty of this project and its intended outcome. At last, the structure of this document is outlined.

1.1. Relevance

Composite materials gained popularity in many engineering applications due to their superior specific properties. Among the others, the aerospace industry makes wide use of such materials, given the necessity for lightweight designs able to achieve high structural performance.
Composites with carbon reinforcement were first introduced in the defence sector during the '60s. Then, their adoption gained traction because of their ability to be tailored to exact load cases and to allow for large integral structures — on top of their high specific properties, superior corrosion resistance and fatigue tolerance. If initially their application on aircraft was limited to certain components, composites are nowadays largely used for both primary and secondary load-carrying structures, both in civil and military applications (as visible in Figure 1.1). For example, composites account for around 50% in terms of weight in the latest generation of wide-body airliners (i.e. the Airbus A350 XWB and the Boeing 787), which boasts composite wings and fuselage — among the other components [1]. Similar observations can be made for military aircraft: for instance, composites make up for roughly 80% of the outer surface (and achieve a share of around 40% by weight) in the Eurofighter Typhoon [2], which has — for example — a composite monocoque and wing skin.

With that being said, it must be also mentioned that composites bring many new challenges. For example, their damage behaviour is inherently complex, due to their anisotropic and non-homogeneous nature. Stemming from this, an important aspect to be carefully considered is the repairability of composite structures.
As mentioned above, composites are becoming progressively widespread, and thus in-service damages are an increasingly frequent occurrence. Replacing entire components is often an unviable option, especially with large integral structures. Furthermore, even when possible, this option is expensive from both a financial and a down-time standpoint, and thus usually inconvenient. In addition, repair methods developed and certified for metallic structures over the past decades are not suitable for composites, due to their intrinsic differences. Therefore, investigating methods to effectively repair composite structures is clearly a pressing necessity.

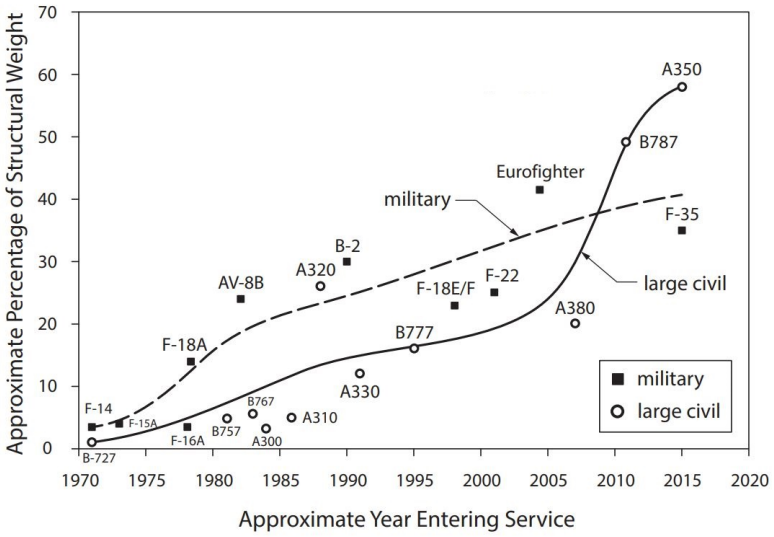

Figure 1.1: Percentage of composites in terms of weight adopted in various military and large civil aircraft over time (edited chart from [3])

There is the need to determine solid, reliable and repeatable procedures to fully restore the structural integrity of damaged components, especially when dealing with primary structures. Moreover, novel composite structures that include inserts manufactured out of functional materials are currently becoming more popular (consider for example the panels used on the nose of the F35-A, depicted in Figure 1.2). Such concepts pose additional challenges: on top of restoring the structural integrity of the component, it is also necessary to fully re-instate the functionality of the inserts, while ensuring a smooth and seamless repair.

Figure 1.2: Nose of the Lockheed-Martin F-35A, showcasing composite panels with functional material inserts on their edges

Figure from U.S. Air Force website: `www.af.mil`, visited on May 10, 2023

Motivated by this necessity of advancing the state-of-the-art in terms of composite repairability, this thesis tackles the topic with a specific focus on such composite aircraft structures that integrate functional inserts. Therefore, the goal of this thesis is to address the following high-level research question:

How to repair composite aircraft structures with microcomposite stealth functional inserts?

Based on the work previously completed at Airbus, as well as on the outcomes of a literature research performed as part of this thesis, the aforementioned high-level questions will be broken down into detailed sub-questions in a later chapter, in order to clearly define the specific objectives and scopes of this work.

1.2. Background

This thesis project was fully carried out at Airbus Defence and Space GmbH in Manching (Bavaria, Germany), the centre of competence for Airbus' military air systems activity in Germany. It therefore falls in the framework of currently ongoing research and design activities. Structures and components such as the one depicted in Figure 1.2 will be adopted in future aircraft by Airbus, which is therefore researching, implementing and testing such concepts. A relevant aspect that needs to be considered since the early design phases of such structural components is their repairability.

Research in this domain was initiated by D'Arduini [4], who identified several damage scenarios and some suitable repair procedures. Figure 1.3 depicts a computer-aided design (CAD) model of a component — which will be referred to as *"demonstrator structure/component*" throughout this document — similar to the one depicted in Figure 1.2. In more detail, this represents a section of an aircraft fuselage that comprises the removable hatch and the fixed side. As visible, both parts are made out of two different materials: a structural one used for the core, and a functional one that wraps only certain areas. It is worth noting that the previous work — as well as the current one — is focused on the removable hatch, despite certain considerations and findings may be applicable to the other side too. As depicted in Figure 1.3b, three distinct damage scenarios were identified: a) damages fully located in the structural part of the component, b) damages fully located in the functional part of the component, and c) damages expanding on both sides. D'Arduini [4] applied conventional bonded scarf repairs in the first scenario, and concluded that the remaining two require bespoke solutions.
Also, the investigation conducted by Scholz [5] in the domain of scarf repairs is relevant for the topic of this thesis. In fact, as aforementioned, scarf repairs are suitable to address certain damages in the demonstrator structure considered here, and can still be significantly improved despite being already used in various cases. Scholz [5] researched several ways to improve the surface flushness of scarf repairs, since this is a very relevant aspect for stealth reasons (and also from an aerodynamic standpoint, in certain specific applications).

This thesis continued the work initiated in both of the above-mentioned studies: methods to address the different damage scenarios were further explored, and ways to optimise scarf repairs with respect to flushness were further investigated. This thesis mainly focused on the damages fully located either in the structural part or in the functional one (referring once again to Figure 1.3). Nevertheless, also the damages affecting both materials were briefly — and only conceptually — addressed as well.

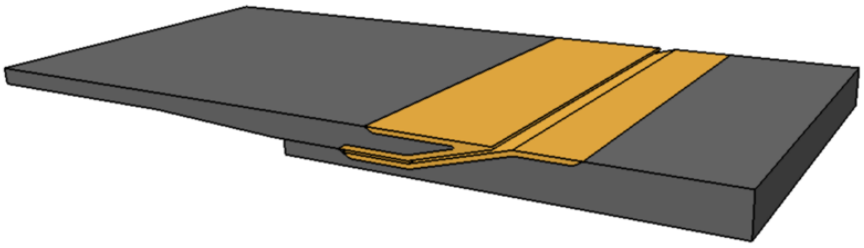

(a) Demonstrator structure considered in this project, similar to the panels depicted in Figure 1.2

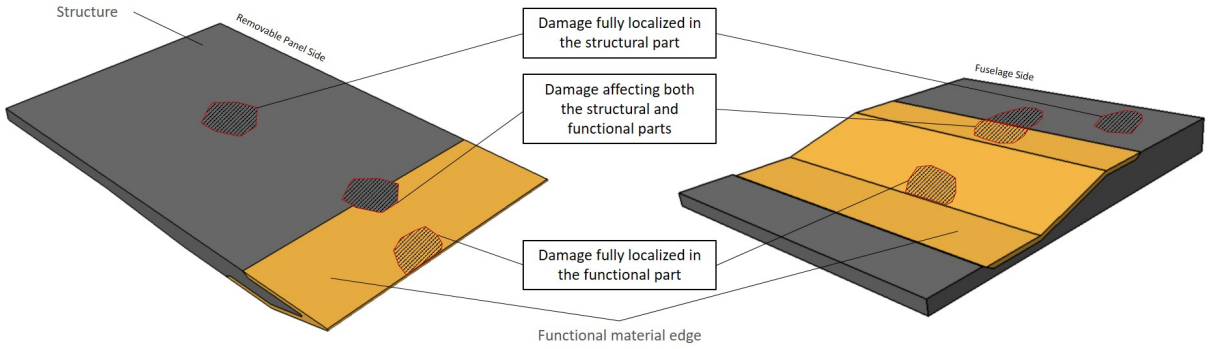

(b) Damage scenarios for a composite structure with functional inserts

Figure 1.3: Graphic representation of a composite structure with functional inserts, demonstrator structure considered during this master project [4]

1.3. Thesis structure

This thesis is organized according to the following structure, which is also schematically outlined in Figure 1.4.
Part I contains a summary of the literature review (chapter 2, 3 and 4) conducted as part of this thesis project, as well as the research sub-questions (chapter 5) — formulated based on the findings of the review and of the previous research performed at Airbus. A more extensive discussion about existing literature can be found in the literature study document drawn up at the beginning of this project [6].
Then, Part II deals with the repairs aimed at addressing damages located in the structural material of the considered structure, whereas Part III covers the repairs intended to tackle damages in the functional material. Part II is organized as follows: first, based on the research questions, different repair concepts are defined and the tests to be performed are determined in chapter 6. The specimens' production and analysis is then documented in chapter 7 and 8, right before presenting the tests results in chapter 9. Next, such outcomes are discussed, and conclusions are drawn in chapter 10. Similarly, Part III starts with defining the concepts and the tests to be performed (chapter 11). Then, the considered repair procedures are further detailed, analysed, eventually tested and implemented in chapter 12 and 13. Next, the discussion of the outcomes and the associated conclusions are covered in chapter 14.
Finally, Part IV concludes the thesis: the general conclusions are collected in chapter 16, which also provides the answers for the research questions. The recommendations are then presented in chapter 17.

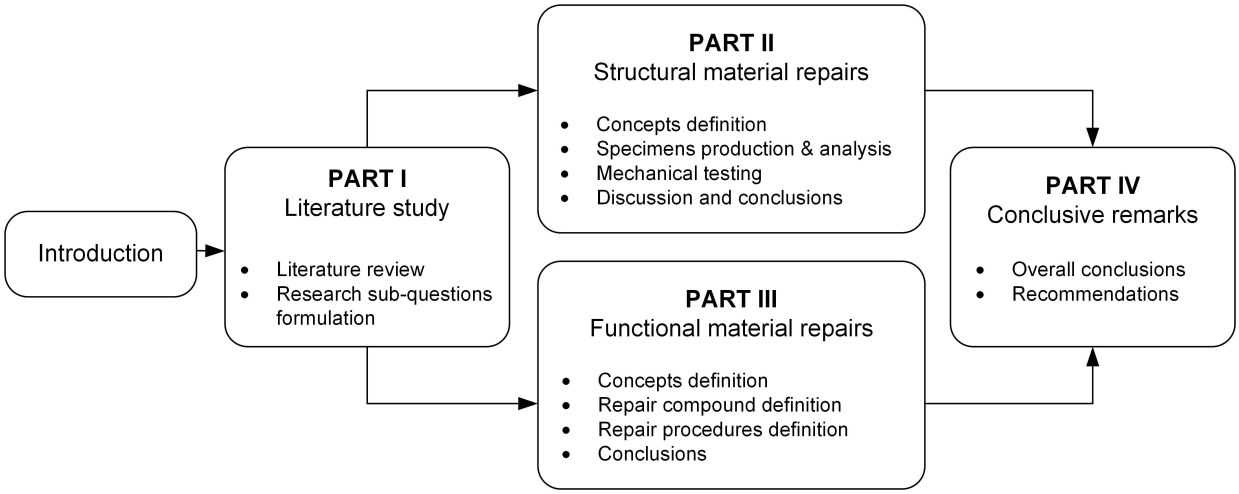

Figure 1.4: Flowchart outlining the overall structure of this thesis

I

Literature Study

2

Damages and repairs overview

Aircraft structures might undergo various kind of damages during their lifetime. Depending on the nature and severity of such damages, as well as on the typology of the damaged structure, different repair options might be suitable. This chapter is structured as follows: first, the main damage types are listed and briefly explained; second, the different sources of damage are introduced. Then, a brief, yet exhaustive, overview of the currently available repair methods is presented. In addition, the theories of adhesion and adhesive failure modes are also briefly reported, given that bonded repairs are particularly suited to composite structures.

2.1. Damage types

This section briefly outlines the various types of damage that a given composite structure may undergo during its lifetime [7], [8].

First, some damages — illustrated in Figure 2.1 — are material-related, and can be extended either at lamina-scale or at laminate-scale.
To begin with, **matrix imperfections** and **matrix cracks** (Figure 2.1a) can decrease some mechanical properties, especially compression stiffness, interlaminar shear strength — or, in general, all those ones that rely on the fiber-resin interface or the resin itself. Nonetheless, unless widespread, matrix imperfections do not drastically compromise the structure, albeit they might progress into larger damages over time.
Fiber breakage or fracture constitutes another damage type (Figure 2.1a): it is usually limited to the region of impact contact; however it is critical given that aerospace composites are mostly fiber dominant and thus their properties might be significantly affected. The combination of matrix cracks and fiber breakage generates **cracks** (Figure 2.1b), which are fractures along the thickness of the composite. They are usually originated by impacts, but they may also generate due to excessive local loads.
Delaminations (Figure 2.1a) originate at the interface between plies (or between the skin and the core, in case of sandwich structures). They can be caused by low-energy impacts, processing non-adhesion or under multiple loads. Delaminations may originate from cracks or other smaller imperfections, which then grow under the loading cycles.

Second, other types of damage can be identified at structural-scale, although they may include or lead to the damages at lamina- and/or laminate-scale presented in the previous paragraph. **Gouges**, **scratches** and **nicks** represent a non-dangerous damage type if limited to the outer layer of the matrix only. If the reinforcement is also affected, they should be regarded as cracks.

Dents are mostly generated by low-energy impacts, which may cause more extensive damage deeper in the composites such as matrix cracks, fiber breakage and delaminations. **Punctures** consist of penetration of the laminate, they are also generated by impacts and may cause further damage deeper in the affected laminates.

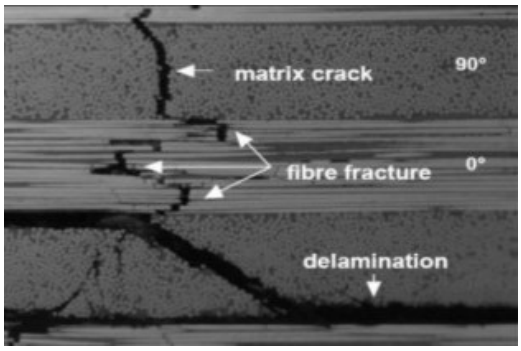

(a) Crack (fibre fracture and matrix crack) and delamination [9]

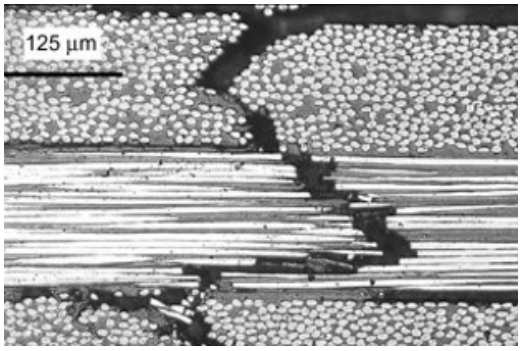

(b) Crack: combination of fibre breakage and matrix cracks [10]

Figure 2.1: Micrographic pictures of some damages in a composite material at lamina and laminate level

It is worth mentioning that certain events may lead to multiple damage types simultaneously. Especially when dealing with impact events, a combination of damage types is highly likely. The full extent of the damage is often not immediately recognizable, even though visual signs might be a clear indication. It is evident that rather small damages might progress into much more critical ones over time and ultimately to failure. Hence, it is important to identify them in a timely manner (relying on a variety of NDI techniques), and address them appropriately to prevent more severe consequences.
Lastly, it is also important to highlight that composites are particularly vulnerable to low-velocity impact damages — which may happen during production, service or maintenance. Such events can lead to delaminations deeper in the laminate, while showing only dents on the surface or no visible signs at all. The residual compression strength is particularly affected by these impacts, especially in presence of a fastening hole.

2.2. Damage sources

This section briefly outlines the various sources that can generate damage in a composite structure during its lifetime [7], [8].

First, **irregularities during processing** (i.e., manufacturing, handling and assembly) may cause damage to the final structure. Albeit such anomalies are usually identified during quality control procedures, some of them might go unnoticed — and eventually be spotted during regular inspections and maintenance. For example, inaccuracies in the curing phase might lead to voids, porosity and delaminations. Errors or negligence in handling, machining or assembly might lead to scratches, dents or even delaminations.
Second, **environmental conditions** or particular events can also represent a source of damage, consider the following examples. Hail can generate dents, and delaminations might originate deeper in the material as a consequence of such impacts. Lighting strikes can also cause damage to composites, surface layers or even entire laminate portions can be burnt once exposed. In addition, composites may enable lightning current to flow into onboard devices, especially in absence of proper shielding. UV radiation can cause epoxy degradation, with a subsequent

detrimental effect on the structural integrity of the composite. Moisture absorption, possibly allowed by impact damages or paint cracking — among the others — can reduce the mechanical properties of the composite.
Third, **ground and flight operations** constitute an additional source of damage. For instance, the following are possible occurrences in the lifetime of an aircraft: dropped tools or parts, incorrectly installed removable parts, debris thrown up during landing and take-off, bird-strikes or (severe) impacts with ground vehicles. Such sources can cause damage ranging from insignificant to critical for flight safety.

It is also worth mentioning that — regardless the peculiarities of each above-mentioned damage type — international aviation authorities propose a detectability-based classification in different categories, which are detailed in the relevant regulatory documentation [11], [12].

2.3. Repair classification

Repairs can be generally classified in two categories — namely, structural and cosmetic — based on the size of the damage that they address.
Structural repairs are necessary whenever the structural integrity of a component is affected by the damage in a significant extent. In such cases, the repair needs to first of all restore the original load-carrying capability of the component.
On the other hand, minor or **cosmetic repairs** are necessary in the presence of damages that are not structurally significant (e.g. small scratches and dents limited to the surface), they are thus intended to mainly restore the surface smoothness.
Regardless this distinction, the majority of repair techniques applied for composites relies on adhesive bonding, given that mechanical fastener techniques — largely adopted in metal structures — are not ideally suited to composite materials' characteristics.

2.4. Repair techniques

This section briefly summarizes the most commonly adopted composite repair techniques, presenting their features and limitations [7], [8].

Scarf repairs are widely adopted to address damage in primary and secondary structures. Such repair technique requires to remove parent material from one side of the damaged laminate, in order to generate a cavity with a given scarf angle and a small hole in the center. The optimal scarf angle is dependent on numerous factors; nonetheless, the tapered slope usually ranges between 1:20 and 1:50 (thickness:length). The scarfed area is then filled with either a dry hard-patch (later secondary-bonded) or a wet-soft patch (subsequently co-cured), which follows the parent material layup.
Machining the damaged area to create the scarf profile may require a high degree of accuracy, therefore scarf repairs tend to be more complicated to implement compared to other techniques. Scarf repairs are especially difficult to implement on thin laminates, since it becomes increasingly complex to achieve a precise scarfing as the thickness decreases.
Scarf repairs are the most suitable option to obtain a flush surface finish, they are thus often selected to repair external surfaces serving an aerodynamic purpose. Due to their relevance, scarf repairs are further discussed in the coming chapter to a comprehensive extent.

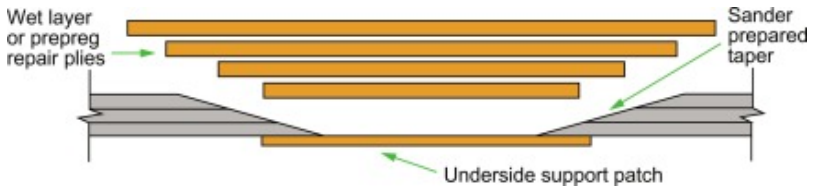

Figure 2.2: Schematic representation of a scarf repair [7]

External patch repairs are also rather common: they require creating a hole in the damaged region of the parent laminate, which is then filled with resin. Composite patches are then bonded on the outer surfaces of the parent laminate with additional adhesive. This technique is applicable regardless of the laminate thickness, it is easier to implement and more cost-effective too compared to the previous one. Such repairs are also easily implementable on site, given that the preparation phase is not complex, however they do not allow for a flush surface finish.

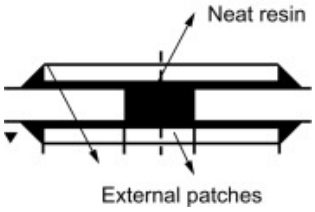

Figure 2.3: Schematic representation of an external patch repair [7]

Resin infusion or **injection repairs** restore the damaged area via a vacuum-aided adhesive infusion process [13]. The injected adhesive, once cured, re-joins together the damaged surfaces, allowing to almost re-instate the design shear and compressive strength fully. This technique is used to address delaminations, if rather limited in size, thus preventing their progression into more severe damages. Surface preparation is only needed in the presence of contamination, and eventually consists of flushing the damaged region with a cleaning agent before injecting the adhesive. Similar procedures can also be applied to correct assembly errors, such as improper hole size or alignment in secondary load carrying structures. In these cases, it is possible to fill the region of interest with a chopped-fiber-reinforced resin that, upon curing, enables to re-drill the correct hole.
Recalling the goal of this master project and Figure 1.3b, such repair procedures may be particularly suitable to address damages located in the functional inserts of advanced structures, they will thus be further explored in a later chapter.

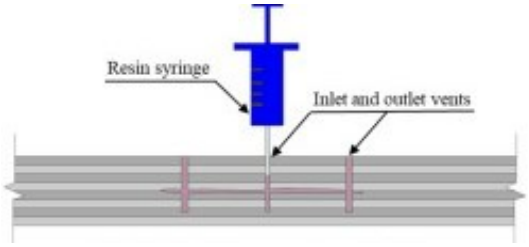

Figure 2.4: Schematic representation of a resin injection repair [13]

Filling repairs consists of filling the damaged area with an adhesive or resin, applied manually and then cured. This procedure is suitable for minor cosmetic damages, e.g. surface scratches

or dents. Such repair procedure is also potentially applicable to address damaged functional materials, and is thus further discussed at a later stage.

Mechanically fastened repairs constitute another option, which consists of bolting an external patch on top of the damaged area. Such repairs do not address the actual damage, but they rather create an alternative load path around it. In addition, they can induce stress concentrations and do not allow to achieve a flush surface finish. Fastened repairs are generally not preferable for composites, whose material characteristics better match the features of adhesive bonds. Nonetheless, they may be selected especially for heavily loaded composite laminates.

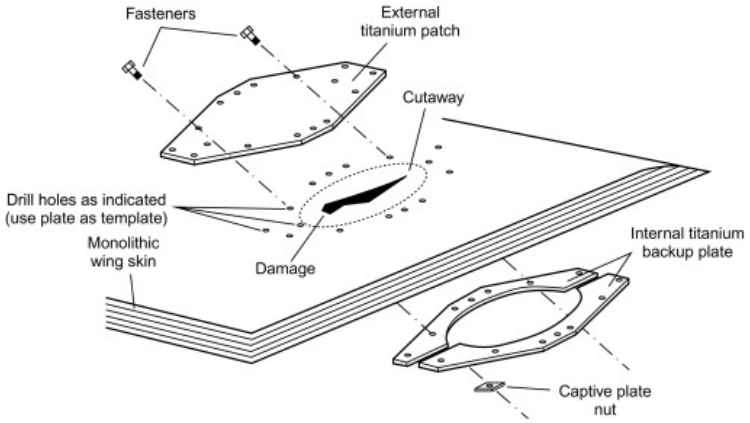

Figure 2.5: Schematic representation of a mechanically fastened repair [7]

Plug repairs consist of placing a plug in a machined hole covered with an adhesive layer, patches are then usually applied on the outer surfaces of the damaged component. Such repairs are simple to implement and also cost-effective, however they provide a limited mechanical strength.

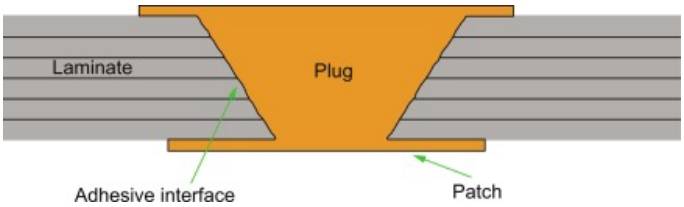

Figure 2.6: Schematic representation of a plug repair [7]

2.5. Adhesive bonding

Considering the large use of adhesives in composite repairs, this section briefly treats the topic of adhesive bonding from a more general standpoint. Adhesion theories are first briefly introduced, failure modes in adhesive joints are then presented.

2.5.1. Adhesion mechanisms

It is generally accepted that adhesion can take place through four basic mechanisms (or theories of adhesion) [14], which are briefly introduced hereafter.
First, **mechanical interlocking** takes place when the adhesive penetrates into the adherend

surfaces thanks to their roughness and/or porosity. In such way, the adherend and the adhesive results to be mechanically interlocked.
Second, **diffusion** takes place when the molecules of two different surfaces mutually interdiffuse, in such a way that their initial interface boundary is replaced with a new interdiffusional one. In order to achieve a strong adhesion, the adherends' molecules need to be compatible, mobile and miscible.
Third, **absorption** or **chemical bonding** entails the formation of intermolecular bonding caused by forces of attraction between the adhesive's and adherends' molecules. Such forces of attraction have various nature, namely: primary bonds (i.e. covalent, ionic or metallic), secondary bonds (i.e. van der Waals and hydrogen bonds) and donor–acceptor interactions (e.g. Brønsted acid–base interactions).
Finally, **electrostatic** adhesion takes place when a transfer of electrons between two contacting surfaces occurs. Attraction forces are thus introduced by the difference in polarity between the surfaces.

2.5.2. Adhesive joints failure modes

Adhesive joints may fail according to different failure modes, namely: adhesive failure, cohesive failure, thin-layer cohesive failure, fiber-tear failure, light-fiber-tear failure, stock-break failure, and mixed failure. All these failure modes are schematically represented in Figure 2.7, and more comprehensively discussed in the relevant ASTM standard [15].

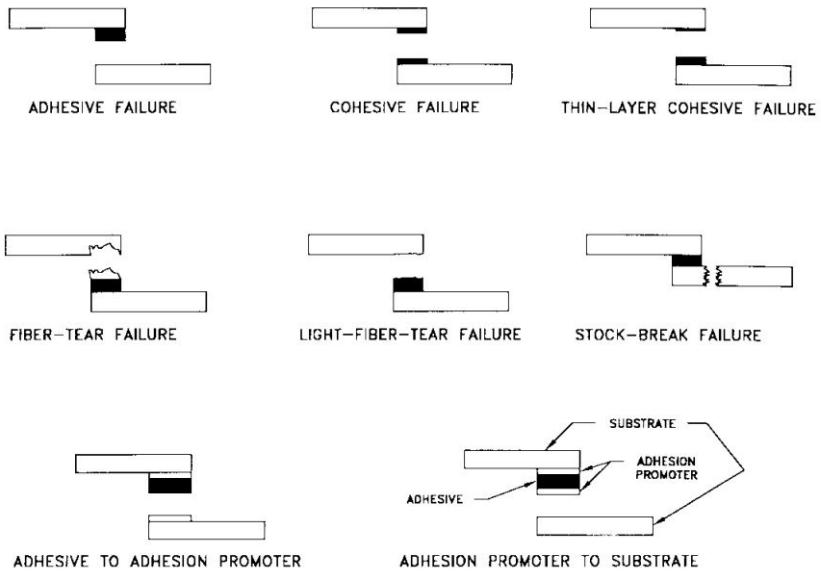

Figure 2.7: Schematic representation of various adhesive joint failure modes [15]

It must be also mentioned that joints often fail in combined modes, where multiple failure modes (among the ones depicted in Figure 2.7) occur simultaneously, as highlighted in several studies such as [16] and [17]. This is because cracks can initiate in both the adhesive and the adherends concurrently, and it is also possible that a single crack changes its medium while propagating. At last, it is worth pointing out that — according to regulations [11], [12] — adhesion failures are not acceptable for bonds in aircraft.

3

Structural Material Repairs

As mentioned in the previous chapter, scarf repairs are commonly adopted for primary and secondary structures, in order to restore the structural integrity while also ensuring a smooth surface finish. They are therefore the option of choice when dealing with structural repairs. This is for example evident considering the previous work performed at Airbus, which also highlighted certain aspects to be further investigated. It is thus appropriate to analyse in more detail scarf repairs, given the framework of this thesis project. This chapter is fully dedicated to such repairs: first, the features of scarf joints are presented. Then, the various parameters that characterise a scarf repair are listed and their effects are analysed. Finally, additional aspects related to this repair method are explored.

3.1. Scarf joints

Scarf repairs can be modelled in a two-dimensional way — along a given load direction — as a scarf joint (Figure 3.1), as evidently shown in Figure 3.2. Therefore, many aspects, considerations and studies related to scarf joints are also relevant and applicable to scarf repairs.

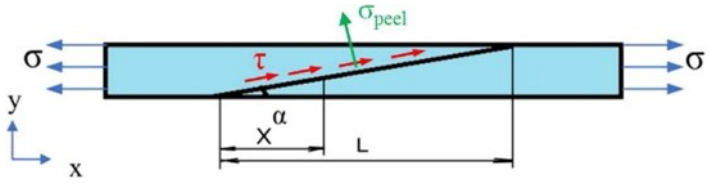

Figure 3.1: Schematic representation of a scarf joint under tensile load [18]

Scarf joints were introduced well before the dawn of aviation, they have been widely used in carpentry and can be found in many historical buildings [19]. Scarf joints are regarded as an efficient way of transferring loads: indeed, the adherends' thickness decreases as the load is transferred to the adhesive, thus allowing for a constant strain distribution along the bondline. Contrary to other types of joints — namely, single lap and double lap joints — scarf joints allow for flush surfaces, which can be an essential requirement in certain repair scenarios. In addition, their geometry does not generate secondary bending, and also stress concentrations are significantly reduced compared to other joints' configurations. Due to these reasons, as already mentioned in the previous chapter, scarf bonded repairs are the preferred option when restoring the surface smoothness is an essential requirement.

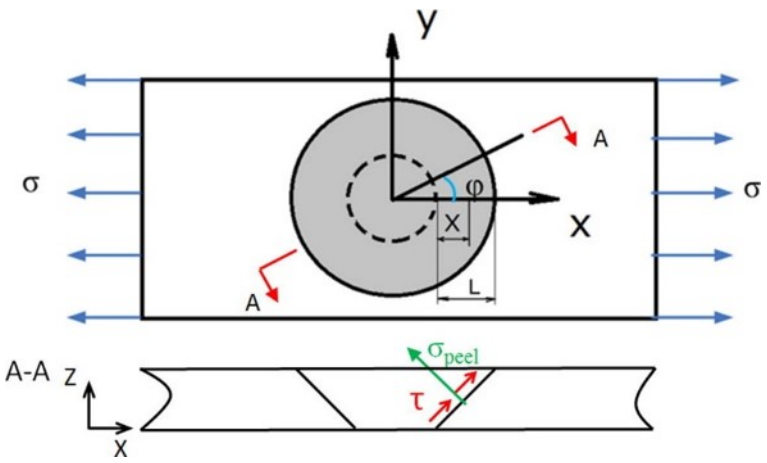

Figure 3.2: Top and side views of a scarf repair under tensile load [18]

Figure 3.3 depicts the shear stress and peel stress distributions along the scarf line for a 2D scarf joint (red lines) and for a 3D scarf repair (blue lines) with composite adherends. For the 3D scarf repair, three different loading directions φ — i.e. 0°, 30° and 45° — are plotted. The stresses vary along the bondline due to the difference in stiffness of the different plies.

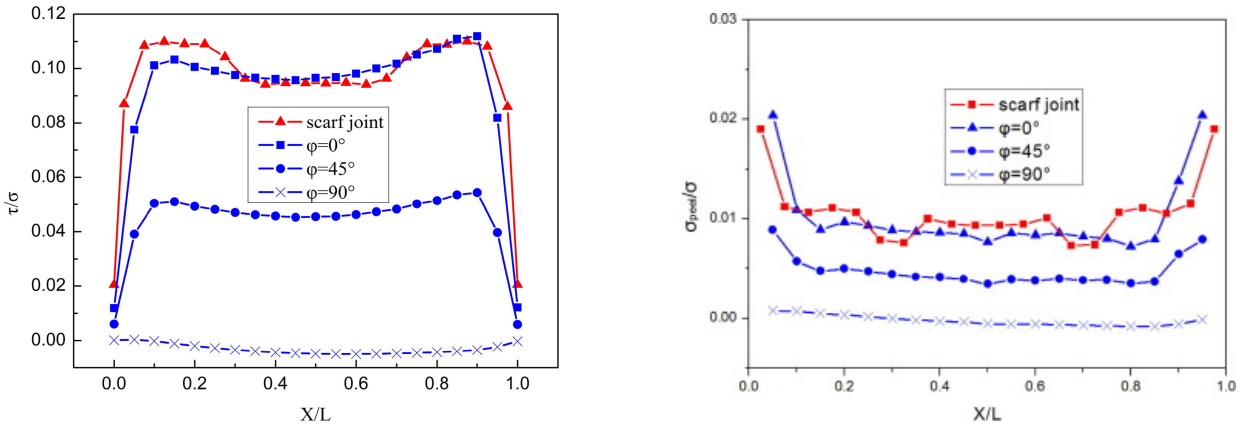

(a) Shear stress

(b) Peel stress

Figure 3.3: Normalized shear and peel stress distribution along the scarf length L of a 2D scarf joint (red lines) and a 3D scarf repair (blue lines). For the latter, the stresses are plotted along three distinct loading directions φ (refer to Figure 3.2 for a graphical definition of φ) [18]

3.2. General repair procedure

This section briefly describes the general procedure to be followed in order to obtain a scarf repair on a composite structure [20], [21]. Figure 3.4 provides a graphic overview of the entire process. It is worth mentioning that many variations of scarf repair are possible, nonetheless all of them require the same basic steps — which are presented in the following subsections — namely: damage identification and assessment, material removal, surface treatment, adhesive and repair patch application.

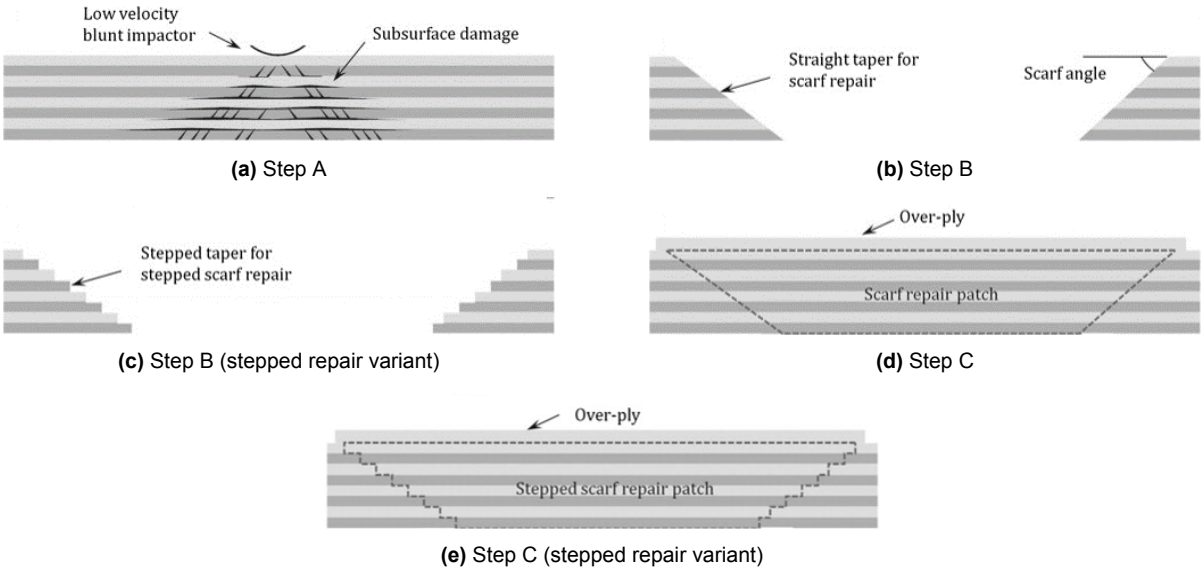

(a) Step A

(b) Step B

(c) Step B (stepped repair variant)

(d) Step C

(e) Step C (stepped repair variant)

Figure 3.4: Schematics of the necessary steps to implement a scarf repair in a composite structure [22]

3.2.1. Damage identification and assessment

First and foremost, the damage needs to be identified and assessed, since this will determine the size of the repair. As already mentioned previously, damages might be widespread deep into composites, possibly without showing any evident sign. Therefore, the area where the damage is expected to be located needs to be thoroughly examined. It is important to clearly identify the type of damage and its extension. Such assessment process relies on various NDI techniques, namely: visual inspection, dye penetrant method, ultrasonic inspection, radiography or X-ray, infrared/thermography or laser shearography. A highly detailed explanation of these techniques — including their working principles, common applications, advantages and limitations — is provided by Jefferson *et al.* [20].

3.2.2. Material removal

Once the damaged area has been identified, parent material is removed in order to form the scarf cavity that will accommodate the repair patch. This procedure is standardly performed via conventional machining, although alternative techniques — namely, laser and waterjet machining — are currently also being explored and tested. This is because — despite being the conventional approach — machining composites remains a non-ideal solution, considering that the applied machining forces and the tool-generated heat can introduce material damage [22]. Only the conventional technique is described here, since it was later used in the thesis. Whereas the alternative options are presented in the literature study [6].

Conventional machining (milling and grinding in this case) is the most commonly adopted material removal procedure. It can be carried either manually by qualified technicians or relying on CNC machines. The latter obviously ensures superior accuracy, and it is therefore preferred for critical repairs.
Despite being currently the conventional approach, it must be mentioned that milling composites is complex, due to their heterogeneity, anisotropy, thermal conductivity, high abrasiveness, and low heat sensitivity [23]. In fact, the contrasting response to milling of the polymer matrix and the fibres

causes intermittent microfractures: damages such as delaminations may consequently initiate. Nonetheless, a proper tuning of milling parameters (e.g. tool geometry, feed rate and speed) can ensure a good surface quality and minimize the risk of introducing (or initiating) damage.

It is worth noticing that the material removal method does not seem to have a crucial impact on the properties of the final repair. As part of their work — for instance — Psarras *et al.* [24] produced and tested two identical scarf repairs, exception made for the material removal phase: a specimen was milled, and the other one laser machined. Both the recovered strength and stiffness of the two specimens were extremely similar, with a maximum difference quantifiable at three percentage points. Such small discrepancy cannot be surely tracked back to the material removal phase, considering the high number of other parameters involved.

3.2.3. Surface treatment

Once the scarf cavity has been created, the surface needs to be treated so that the adhesive can be applied [20], [21]. The goal of the surface pre-treatment phase is to promote the adhesion mechanisms. The following aspects should be ensured in order to achieve a solid and durable joint: removal of all contaminants (such as dusts, lubricants or micro-organisms) from the surfaces, good surface wettability, as well as good activation of the material surfaces to be bonded.
Do note that this step might not be necessary in certain cases. For instance, if the material removal has been performed via laser machining, given that such process can have a two-fold purpose (i.e. material removal and surface treatment).
Many surface treatment methods exist, an overview is provided in Table 3.1. Only the ones actually used in this thesis are described here, a more thorough discussion can be found in the literature study [6].

Sanding is a widely used and cost-effective surface treatment procedure, consisting of abrading the adherend surfaces by hand or by polishing tools, using sandpaper materials. An additional cleaning step is then required in order to remove debris. Sanding is strongly dependent on the selection of abrasive materials and grit size, the sanding direction and duration, and the post-sanding treatment, on top of the technician skills. Nonetheless, if properly performed, it is one of the most effective procedures. In fact, it allows to achieve good roughness and to enhance the mechanical performance of the joints, albeit heterogeneous morphology or non-uniform roughness may be introduced.
Milling can also be applied as a surface pre-treatment, as shown by Freese *et al.* [25]. The bond strength is however lower than that achievable via sanding; in addition, the process causes surface damages and generate particles residues.
Similarly, **plasma treatment** bombards the adherends with plasma-generated particles; it can be performed both in open or closed chambers (contrary to corona discharge that is usually performed in open spaces only). Plasma treatment removes contaminants, modifies the surface morphology (introducing an ablation effect that evaporates the matrix phase) and surface chemistry (substituting the atoms of the surface layer with chemical groups from the plasma).
Laser treatment creates a heat affected zone and ablates the treated surfaces, thus modifying their chemical elements. As already mentioned above, this procedure can be used both as a material removal process and/or as a surface treatment one, by tuning the various process parameters accordingly. Laser treatment affects both mechanical interlocking and chemical bonding. For instance, ALYousef *et al.* [26] proved that laser ablation with an optimal laser fluence improves bond strength, which on the other hand results to be decreased if the same parameter

is set too high.
Solvent cleaning is regarded as a finishing treatment to support other treatments. This is because it cannot improve the joint strength or toughness, but only allows to dissolve and wipe off some contaminants.

Table 3.1: Overview of surface treatment techniques (edited from [20])

Mechanical	Chemical	Energetic
Abrasion (sanding, milling)	Detergent wash	Corona discharge
Peel ply	Solvent cleaning	Plasma
Blasting	Etching	Flame
		Laser

3.2.4. Adhesive application

Once the adherend(s) surface has been properly treated, the adhesive can be applied. Adhesives can be applied in different forms, namely: film, paste, tape, pellets, bead, drops or coating. Film adhesives are the standard option for scarf repairs, given that such form is particularly suited to the repair procedure. Many types of adhesives exist and can be classified in different ways, for instance based on their chemistry or field of application. Epoxy adhesives are the most widely used for composites — including repairs — since they can ensure good shear and tensile strength, good chemical resistance, high rigidity, good creep resistance and good tolerance to elevated temperatures. Such adhesives comprise two components, a resin and a curing agent, plus eventual additives.

3.2.5. Repair patch application

Once the scarf cavity has been created, the surface appropriately treated and the adhesive applied, the repair patch can be positioned. Two types of patches are currently available, namely soft patches (also referred to as wet patches in literature) and hard patches (also called dry patches) [22], [27].

First, **soft patches** are assembled ply by ply with pre-preg directly inside the scarf cavity. Once the layup is completed, the patch is cured and thus bonded to the parent material via a co-bonding process. The patch usually cures under vacuum, at controlled temperature but generally out-of-autoclave.
This approach is currently the mainstream one, mainly due to its rather simple manufacturing and cost-effectiveness. Nonetheless, it also presents some drawbacks: first, the patch does not generally match the parent material properties (e.g. fibre content) given that curing happens at different conditions (and often the matrix material differs from the parent laminate's one). Second, ply distortion and wrinkles are a quite common occurrence considering the manual work required. Third, it might be difficult to carry out such procedure in certain components due to accessibility reasons (e.g. vertically-mounted components). At last, soft patches cannot be inspected before being permanently bonded.

Second, **hard patches** are manufactured before-hand and then bonded in the scarf cavity via a secondary bonding process. Hard patches can be fabricated in two different ways: either in a

mold that matches the repair cavity or — alternatively — CNC machined from solid following the contour of the scarf cavity (this last option allows to manufacture patches out of metal alloys as well, should this be desirable for certain applications).
This approach allows to obtain patches with properties matching the parent material's ones and also allows for inspection prior to bonding. On the other hand, it is lengthier, more complicated to implement and thus less cost-effective compared to the soft patch approach. In addition — as already mentioned above — machining is not the most suitable procedure for composites.
The hard patch approach is currently not widely adopted, although it is worth further exploring considering the possibility to obtain patches better matching the parent laminate properties, and also to achieve higher degrees of accuracy thanks to the aid of automation.

The two patch options presented above are briefly compared in Table 3.2, which highlights the various advantages and disadvantages.

Table 3.2: Advantages and disadvantages of different repair patch configurations

Type	Advantages	Disadvantages
Soft-patch	Simple manufacturing process	Properties not matching parent laminate ones (fibre content volume and voids)
	Ideal shape conformity	Prone to ply distortion and wrinkles during curing due to shrinkage
	No mould required	No pre-inspection possible
		Difficult to apply in many orientations of the component
Molded hard-patch	Matches parent laminate's properties	Mold required
	Minimal plies' distortion	Longer processing time
	Prior NDI possible	Higher cost
		Possible local warping
Machined hard-patch	Matches parent laminate's properties	Machining-related issues
	Minimal plies' distortion	Higher cost
	Prior NDI possible	

3.3. Repair parameters

This section presents and briefly discusses the various parameters that characterize a scarf repair, with a focus on their influence on the repair properties and performance.

3.3.1. Scarf angle and geometry

The scarf angle is a crucial parameter for a scarf repair, given that it directly influences the strength, stress distributions along the joint and fatigue life, among the others. As mentioned above, a scarf repair can be modelled as a scarf joint: based on simple theory, it can be thus deduced that the maximum allowable scarf angle for a given joint is determined by Equation 3.1 (valid for small angles) [27], [28]:

$$\alpha < \frac{\tau_p}{E\varepsilon_u} \quad [rad] \tag{3.1}$$

where α is the scarf angle, τ_p the laminate design ultimate stress, E the laminate Young's modulus and ε_u the allowable laminate strain.
Figure 3.5 depicts the behaviour of relative shear and peel bond stresses as function of the scarf angle. Generally, a scarf angle lower than 3° is required to repair composite structures [27]. However, it must be mentioned that low angles require long scarfs, which are complex to manufacture and imply to remove large portions of undamaged parent laminate. In addition, the extension of the removable area may be also constrained by the presence of features (e.g. hatches) that cannot be affected in the immediate vicinity of the damage. Therefore, the optimal scarf angle is a trade-off between the ideal mechanical performance and various practical constraints.

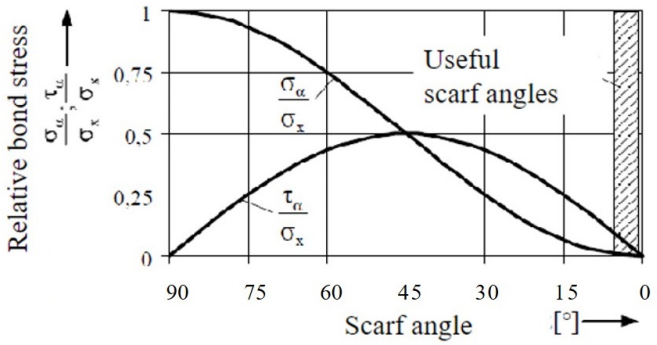

Figure 3.5: Relative bond stress (shear and peel) as function of the scarf angle (edited from [29])

Numerous studies performed in the past assessed the influence of the scarf angle on various properties of scarf joints (e.g. [30]–[32]), which is thus well known and documented. Consider again Figure 3.1 for a graphical definition of the parameters (namely, α, x and L) discussed in the following. Gunnion and Herszberg [31] analysed the influence of scarf angle on the distribution of stresses along the bond line via finite element (FE) modelling, proving how both shear and peel stresses increase as the scarf angle gets larger. The behaviour of the stresses along the bondline is function of the laminate layup, given that different plies with different orientations have different stiffness values. The same trend is described in the paper of Sonat and Özerinç [32], who performed a similar analysis with different scarf angles and laminate parameters.

Li *et al.* [33] proved that, as the scarf angle gets larger, the ultimate failure load decreases, while the lap shear strength increases (both with a progressively slowing rate). The same relation between failure load and scarf angle was also observed in other studies, such as the one of Yoo *et al.* [30]. This trend is explained considering that larger scarf angles imply smaller scarf (bond) surfaces, and that the lap shear strength is defined as the ratio between ultimate failing load and the bond area.
Lower scarf angles are also beneficial from a fatigue standpoint, as highlighted in several studies such as [30] or [34]. This can be explained considering that low scarf angles lead to lower peel stresses as well as to larger bond areas, which in turn imply increased resistance to shear stress.

Regarding the repair geometry — which, as a matter of fact, also consists of a design parameter — the continuous tapered scarf is the most widely adopted option. Nonetheless, it is also possible

to consider a stepped geometry, which is easier and less time-consuming to produce. Some studies showed that stress concentrations in stepped joints tend to be higher than in scarf joints of equivalent angle, thus making them more prone to earlier failure initiation. However, an optimal choice of design parameters can reduce peak stresses, ultimately making the two options comparable [35], [36]. In any case, most studies focus on either of the two options, and therefore not many sources comparing their performance directly (especially experimentally) seem to be available.

3.3.2. Adhesive thickness

The thickness of the adhesive layer is another important parameter. Gunnion and Herszberg [31] — among the others — analysed its influence on the bondline stresses via FE modelling, by varying the adhesive thickness to ply thickness ratio. Their results clearly show a high sensitivity of the stresses to this parameter. Both the peak peel and peak shear stresses increase significantly as the adhesive gets thicker. The same trend was observed in other studies, also experimentally (e.g. [34] and [30]).
It was also noted that the stress-apparent strain curves for scarf joints with thinner adhesive bondlines are almost linear, while the ones for thicker adhesive bondlines deviate from linearity at a given stress level (in agreement with the curves of bulk adhesives). This is because crack initiation at the joint overlap edges — and subsequent reduction in stiffness — is more pronounced for thicker adhesive bondlines [30].
Overall, increasing adhesive thickness leads to a decreasing adhesive shear strength and failure strength [37].

3.3.3. Laminate thickness & stacking sequence

The laminate thickness is also an influential parameter for a scarf joint: increasing the number of plies (and thus the overall laminate thickness) causes the peak stresses near the ends of the bondline to decrease, thus approaching the levels recorded away from the free surfaces [31]. The same trend is also identified in other studies, such as the work of Wang and Gunnion [38].
The stacking sequence also affects the peak stresses. For a given loaded scarf joint, most of the load will be carried by the plies with the higher stiffness in the loading direction. Therefore, increasing the number of such plies in the laminate results in lower peak stresses (since the proportion of load carried by each of such plies progressively decreases as their number is increased). Additionally, the peak peel stress tends to increase if 0° plies are placed on the outer surfaces [31].
Increasing the laminate thickness also leads to higher values for the ultimate failure load, as shown in the work of Li *et al.* [33]. This behaviour can be potentially explained considering that the bond surface — as well as the intralaminar stiffness — increases as the laminate is thickened. On the other hand, the lap shear strength seems to slightly decrease as the laminate thickness is increased.

3.3.4. Plies mismatch

Conventionally, it is common practice to match the layup of the repair with the one of the parent laminate in order to restore the original stiffness. Nonetheless, it has been proven that such parameter has little effect on the peak stresses along the bondline. Gunnion and Herszberg

[31] performed several FE simulations flipping the ply orientation by 90° across the scarf joint, also varying the number of plies. It was shown that — when compared to repairs with patches matching the parent laminate sequence — peak peel and shear stresses were mostly unaffected, albeit the shape of the distribution obviously changed.
Breitzman *et al.* [39] also performed FE analyses, concluding that mismatching plies might even reduce von Mises stress in the bondline compared to a conventional matching patch; an optimised patch was also simulated and exhibited superior performance, nonetheless its non-symmetric layup would most likely be disadvantageous in real-case scenarios due to the induced tension-bending interaction and higher manufacturing complexity.

3.3.5. Overply

Once a repair patch has been placed, it is rather standard to apply an additional ply on top (and eventually on the bottom side as well), referred to as overply, cover ply, external ply or over-laminate (in case few plies are added instead of a single one). This additional layer covers part of the surrounding parent laminate, thus sealing the bondline and the entire repaired region. The overply is beneficial in reducing peak stresses near the free edges, thus increasing the overall repair strength, as proven in several studies (e.g. [31], [39]). The overply orientation does not seem to have any significant effect on the peak stress reduction, while its length influences the failure mode. Yoo *et al.* [30] observed that short overplies tend to disbond contrary to longer ones.
The application of an overply has another major advantage: it avoids direct exposure of the adhesive bondline to moisture (and thus decelerates its absorption), which would significantly decrease the properties of the adhesive. This phenomenon is examined in detail in the work of Zhang *et al.* [40], who modelled the effect of the overply on the moisture absorption behavior of composite scarf repairs.
On the other hand, it must be mentioned that overplies generate a thickness offset between the parent laminate and the repaired area. This is clearly not acceptable in all those repair scenarios where obtaining a fully flush surface finish is required.

3.4. Failure modes

Being effectively adhesive bonded joints, scarf repairs fail according to the modes presented in subsection 2.5.2 — and primarily as a combination of such mechanisms. Some common failure modes typical of scarf repairs are depicted in Figure 3.6. As summarised by Orsatelli *et al.* [41], the scarf angle has an influence on the failure mode.
In case of repair failure under tension loads — which is the most studied scenario, e.g. in [42]–[44] — steep scarf angles lead to cohesive failure, while for lower angles a combination of cohesive, intralaminar and interlaminar failure is observed. Cohesive failure usually occurs in the proximity of 0° plies, while matrix cracking initiates near 90° plies and then extends near 45° plies as the ultimate load of the specimen is approached. In general, the failure is adhesive-dominated with steep angles whereas it becomes composite-dominated as the angle gets smaller. For extremely low scarf angles, failure tends to occur in the repair patch or in the parent laminate, leaving the bondline even completely unaffected by the failure path. This highlights how the actual repaired region is not always the weakest and most critical area.
In case of repair failure under compression loads [45]–[47], steep scarf angles predominantly lead to cohesive failure — as in the tensile load case. In presence of lower angles, mixed cohesive and matrix failure takes place; alternatively, local buckling of the composite without debonding

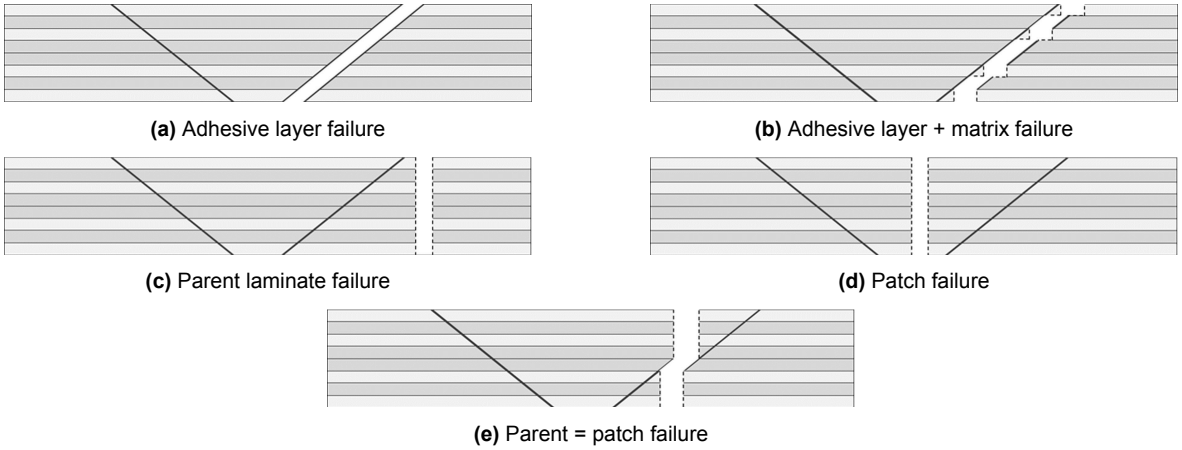

Figure 3.6: Schematic representation of common tensile failure modes for scarf repairs [41]

occurs if Euler buckling is prevented.
Despite most of the studies performed in this domain considered UD CFRP laminates, it was proven that woven fabric CFRP exhibit the same failure behaviour [32]. In addition, stepped repairs also show a similar behaviour, with failure transitioning from patch debonding to patch or laminate fracture as the number of steps increases [41].

The failure modes presented above are drawn from studies performed at specimen level. The limited amount of work performed on scarf-repaired panels seems in accordance with such conclusions. More experimental investigation with full components is thus needed in order to define to what extent the results for 2D scarf joints are actually applicable to full scarf repairs.

3.5. Repair flushness

As already mentioned, scarf repairs are the option of choice whenever restoring surface flushness is a crucial requirement. Often scarf repairs and flush repairs are even used interchangeably in literature. Nonetheless, it must be noted that reaching a fully seamless repair (i.e. with a thickness offset between the parent laminate and the patch in the order of few tenths of a millimeter) is extremely complicated, especially considering that overplies are often applied due their benefits on stress distributions.

Having a certain thickness mismatch is usually considered acceptable, therefore extensive investigations on the causes and details of such aspect are lacking in literature.
Considering the studies of Scholz [5] and Keil [48], it seems clear that the layup procedure of the patch affects its flushness. This is evident observing Figure 3.7: two possible layup configurations are schematically shown, and both clearly generate a certain surface irregularity. Moreover, composites are known to deform during processing [49], in such an extent that these phenomena are compensated during the design phase. Such process-induced deformations may play a role also in scarf repairs and thus affect their flushness. In particular, resins tend to undergo a volumetric shrinkage while curing [50]: this could cause the patch to deform in a non-negligible extent, thus negatively affecting the surface flushness. These curing related issues are eliminated if hard patches are used. However, in this case, different variables are introduced: the repair flushness is determined by the patch alignment and the thickness of the adhesive layer. In addition, upon loading, repair patches — regardless of their type — may deform, as highlighted

by Breitzman *et al.* [51]. Eventual distortions in the vertical direction may thus negatively affect the surface flushness.
Generally speaking, all the above-mentioned aspects need to be further investigated in detail, in order to better understand the mechanisms and the parameters that affect surface flushness.

(a) "Ply-match" configuration **(b)** "Full overlap" configuration

Figure 3.7: Schematic section views of possible soft-patch scarf repair configurations [48]

As mentioned above, a certain thickness mismatch is usually acceptable for most applications, and therefore also investigations on possible ways to minimize it are very limited. Nevertheless, in those demanding scenarios where stealth or aerodynamic performance is a priority, eliminating — or at least reducing as much as possible — such thickness offset is highly important. Therefore, there is still the need to further explore this aspect.
This necessity was for instance addressed in the work of Scholz [5]: some concepts to implement fully flush repairs (i.e. with a thickness mismatch in the order of few tenths of a millimeter) were defined and tested at coupon level. Similar test samples were also produced and tested by D'Arduini [4]. Re-milling the repaired surface via a CNC process was overall identified as a viable and promising solution, although the need for further investigations was highlighted in order to better understand its effects, improve the accuracy, optimise the procedure and possibly standardize it. Additionally, testing was limited at specimen level and a limited number of repair patch concepts. Therefore, it would be advisable to consider more patch designs, and eventually to extend such activities to repaired panels (or higher-level coupons) in order to assess the re-milling effects on a full patch. Other than re-milling the repaired surface, alternative solutions to achieve a fully flush surface finish should be explored. For example, repair patches may be designed in the first place to address this issue; however, such approach has not been researched — or at least published in literature — so far.
In general, more investigation seems to be required to tackle this specific aspect.

3.6. Innovative configurations

In order to improve (flush) repairs, certain studies went beyond tuning the parameters of traditional scarf repairs: novel repair configurations were designed and eventually tested. Some examples of such are presented in this section.

Wang and Gunnion [52] developed an algorithm to optimize the patch shape for scarf repairs under bi-axial loading. It was indeed shown that the circular shape is not ideal under non equi-bi-axial stress, as it requires removing more pristine material than needed. Therefore, it was proposed to vary the scarf angle all around the repair, while maintaining it constant in each radial slice. This results in an innovative elliptical shape patch, able to spare a significant amount of unaffected material. Similar developments have been proposed and implemented at industrial level, for example at Airbus and WIWeB [21].

Niedernhuber *et al.* [53] designed a modified stepped repair (depicted in Figure 3.8a), where the overlap length for the plies aligned in the direction of the load is increased (while it is reduced

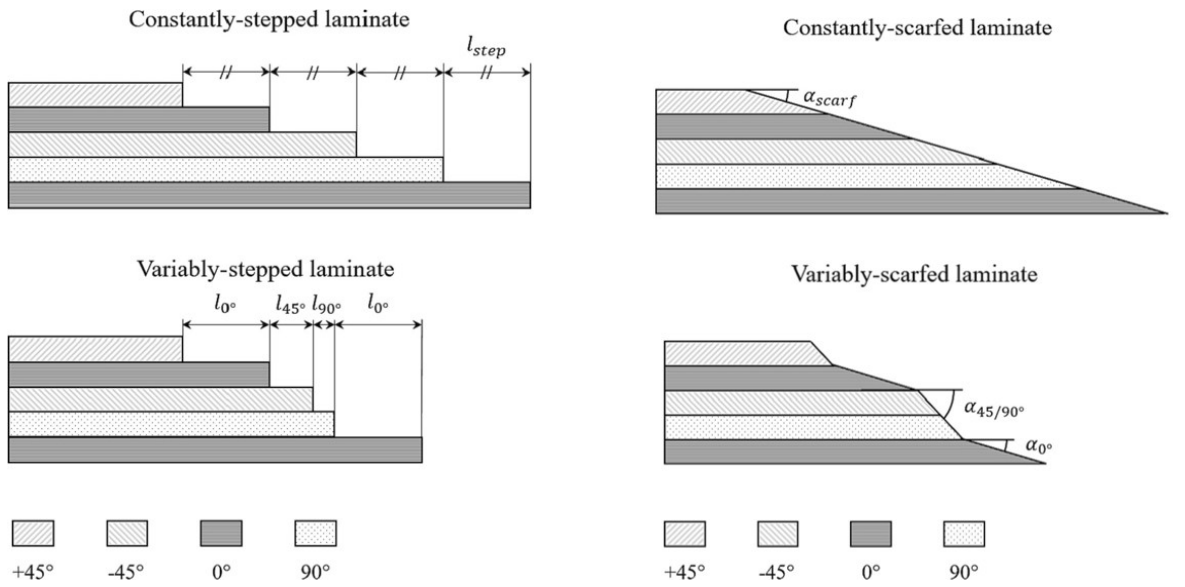

(a) Schematic representation of the variable step design proposed by Niedernhuber *et al.* [53]

(b) Schematic representation of the variable scarf angle design proposed by Pitanga *et al.* [56]

Figure 3.8: Schematic representation of some innovative repair designs [41]

for the other plies), since they take up most of it and thus experience the highest stresses. Experimental activities demonstrated that such design can reduce the repair length by almost 40%, while retaining the same tensile strength of a traditional scarf repair. However, Pierce and Falzon [54] argued that more tests with steeper scarf angles should be performed in order to further assess such benefits, given that their 3D FEM simulations showed marginal differences between normal step and fibre-oriented step joints in different ranges of angle. Damghani *et al.* [55] proposed design similar to the one of Niedernhuber *et al.* [53], and demonstrated via mechanical testing how their concept could restore 64% of the pristine laminate strength, compared to the 77% achieved by a traditional scarf repair.

Pitanga *et al.* [56] proposed a new design showcasing a variable scarf angle throughout the thickness (Figure 3.8b), in order to reduce the extension of the repair area. Scarf repairs with piece-wise linear scarf joints were produced: taper ratios of 1:30 and 1:20 were applied to the 0° plies, while a ratio of 1:2 was adopted for the 45° and 90° plies. After testing, it was concluded that the proposed 1:30/1:2 piece-wise linear scarf can achieve 75% of the tensile strength while reducing the repair-affected area by 60%, when compared to 1:20 straight scarf.
Similar scarf geometries were also investigated in the work of Scholz [5] (later resumed by D'Arduini [4]), experiments at specimen level were performed and variable scarf designs were compared with the traditional one. The tensile strength of the traditional scarf repair was found to be about 5% higher than that of the best performing variable scarf concept. In this case, it was thus concluded that the traditional scarf repair still remains the preferable option, mainly due to the easier and quicker manufacturing procedure (on top of the slightly superior performance).
Overall, variable scarf repairs can achieve performances close to the standard scarf ones, they are generally more complicated to produce but potentially allow to significantly reduce the repair-affected area. Therefore, provided that an optimal selection of parameters should lead to very small performance differences, the choice between the two is mainly driven by ease of manufacture and eventual constraints on the extension of the repair area.

A more unique and inventive solution was defined in the work of Sun *et al.* [57], who proposed

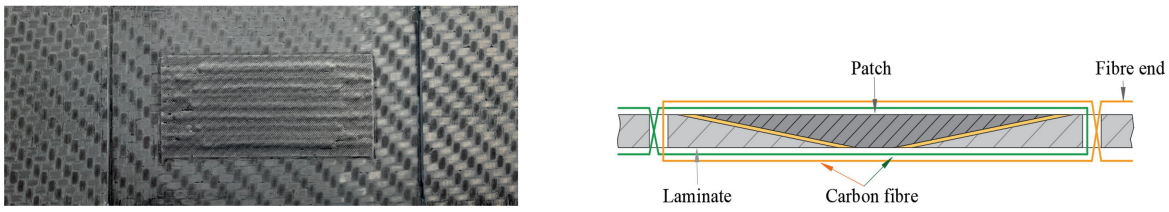

(a) Sample repair once cured

(b) Schematic section view

Figure 3.9: Photograph and schematic representation of the stitched scarf repair concept [57]

a stitched scarf repair concept. The scarf patch was hand-stitched to the parent laminate via pre-drilled holes, which were then resin-infused and cured, thus bonding the patch. The influence of holes' diameter and scarf angle on the load-carrying capacity of the repaired laminates was investigated. It was observed that the ultimate tensile strength of stitched repaired laminates was up to 45% higher compared to traditional repaired laminates with the same scarf angle.

All in all, many different alternative options have been proposed and tested over the years. Nonetheless, it seems that none have been widely adopted in real-case scenarios. In fact — as also demonstrated by the work of Scholz [5] — standard and simpler concepts (e.g. the conventional scarf joint) seem to still be preferred in industrial settings, prioritizing well-proofed and easier-to-produce designs, while possibly marginally sacrificing on other aspects. In other words, it often seems that the benefits theoretically allowed by certain tailored and sophisticated solutions are not enough to outweigh their increased complexity, required time and eventual cost.

3.7. Certification

Certification is another extremely relevant aspect to be at least briefly discussed when dealing with bonded repairs. Airworthiness certification is indeed required whenever bonded repairs are applied to primary structure in presence of damage that has reduced — or could potentially reduce — the residual strength below the design ultimate threshold.
The requirements that need to be met in case of composite repairs are outlined by the competent authorities in several documents [11], [12], [58]. In principle, it is necessary to prove the ultimate load capacity for a given repair. As mentioned by Baker *et al.* [59], in summary, two aspects are of key importance: first, the integrity and durability of the adhesive bondline must be ensured; second, it is necessary to satisfy and prove the compliance with all the relevant structural performance requirements.
The most challenging aspect is currently proving the integrity of the bondline, given that this is not possible with existing technologies or their straightforward evolution. In addition, the potentially brittle and sudden failure of bonded joints, and their limited crack-arresting capability are also sources of concern. Therefore, for the time being, these aspects significantly limit the applicability of bonded repairs for primary structures. In fact, current state-of-the-art applications include additional rivets on top of the bondline, which partially undermine the advantages of bonded joints [60]. Alternatively, bonded repairs are limited to scenarios where the structure is still capable of withstanding its ultimate load in case of repair failure.
A significant amount of research effort is therefore devoted to tackle this current issue, with the goal of increasing the applicability of bonded joints (and so repairs) on primary load-bearing structures. Exploring this domain in detail goes beyond the scope of this study and thesis project.

3.8. Additional aspects

This section briefly touches upon some other relevant aspects that are worth at least addressing when dealing with scarf repairs. As highlighted in the review work of Orsatelli *et al.* [41], it is important to consider the effect of eventual impacts, fatigue and environmental agents on scarf repairs, since they will be subjected to these events throughout their lifetime.

The effects of in-service impacts on scarf repairs have been previously investigated. For example, Kumari *et al.* [61] performed numerical simulations and concluded that the area most vulnerable to impact is the bond edge: impact loads in this location are found to cause more severe damages. Cheng *et al.* [62] analysed the influence of the patch's layup and orientation via 3D modelling; it was observed that aligning the patch with the parent laminate (±3°) allows to achieve impact properties close to the pristine ones, and that the patch layup is less influential.

Composites with bonded repairs are more vulnerable to fatigue compared to pristine structures. Research is therefore being performed in order to better understand the long-term behaviour of scarf repairs. For example, Yoo *et al.* [30] performed tensile fatigue tests of scarf-repaired specimens with different scarf ratios. It was observed that the fatigue strength recovery rate is on average around 46%, with shallow angles proving to be also beneficial from this standpoint. On the other hand, the recovery rates for static strength are generally higher, ranging between roughly 50% and over 100%, with the highest values obtained with low scarf angles (according to several studies [24], [30], [32], [63]).

The issue of environmental durability for scarf repairs was widely reviewed in the work of Budhe *et al.* [64]. It was acknowledged that the main parameters to consider are temperature and moisture, whose combined effects on bonded repairs are not as well-known as their influence on composites' properties in general. Moisture is detrimental for the repair strength and thus its absorption needs to be prevented. In addition, many parameters — such as adhesive type and its curing method — are found to be influential for the fracture toughness. In general, more investigation in this domain seems to be needed.

As mentioned in the previous section, according to regulations, repairs are supposed to meet the design ultimate load in the eventual presence of disbonds. In order to address this aspect, several studies considered a damage-tolerant approach, and so analysed scarf joints that already include initial defects in their bondline. Many of such studies have been reviewed in the work of Orsatelli *et al.* [41]. Also in this regard, there seem to be a lack of studies and experimental investigations on repaired panels, which would definitely be beneficial to better understand the effect of flaws in multi-axial loading cases.

4

Functional Material Repairs

This chapter deals with the repair methods intended to address damages located in functional materials (or in functional inserts of hybrid components, recalling the demonstrator structure shown in Figure 1.3). Within this domain of application, such functional materials usually serve the purpose of enhancing the stealth features of an aircraft, and thus possess electromagnetic interference (EMI) shielding and absorption properties. Nonetheless, functional materials intended to serve other purposes do also exist. Limited literature is available in this domain — in particular about repairs — due to the novelty of such structures, and also the fact that their application is rather limited to the defence industry. D'Arduini [4] defined a preliminary repair concept, based on the use of hard patches to be secondary-bonded after removing the damaged section. Nonetheless, it was concluded that such option would be uneconomical and unpractical in case of small, localised, cosmetic damage. Therefore, there is the need to define additional repair procedures in order to specifically address such minor damages.
The aim of this chapter is thus to cover various aspects relevant and useful to further investigate the above-mentioned topic. This chapter is structured as follows: first, the principles of stealth technology are introduced, the radar absorption mechanisms and available absorbing materials are presented. Then, considering the framework of this thesis project, the focus is shifted towards radar-absorbent microcomposite materials, and so some relevant aspects are discussed. At last, some of the currently available repair procedures that may be applicable to address damages in functional materials are discussed.

4.1. Stealth technology

Low observability (more commonly referred to as *stealth*) technology comprises a series of techniques aimed at making an object more difficult to identify by various detection methods (in different emission spectra, e.g. microwave, thermal or acoustic).
In the case of military aircraft, it is often desired to reduce their radar cross section, in such a way that they become harder to detect with such technology. In order to achieve this goal, aircraft are designed in such a way that the amount of radar signal power reflected back to the transmitting radar is significantly reduced.
Fundamentally, there are two viable ways to reduce the reflected energy: either absorb the radar signal with functional materials (often applied as coatings), or deflect it away from the radar transmitter by carefully designing the shape and the contours of the aircraft. Various radar absorbent materials are currently available, and they will be presented in more detail in the following section. For what concerns the shape, stealth aircraft predominately adopt convex

surfaces due to their ability to scatter the radar signals in various directions, ultimately reducing the amount of energy reflected back directly to the transmitter [65]. Other than these two approaches, modern aircraft are also equipped with electronic radar jamming systems: interfering signals are generated and transmitted in order to make detection more complex.

4.2. Microwave absorbing materials

Radar absorbing materials — or, more generally, microwave absorbing materials (MAMs) — were first introduced in the defence industry to hinder radar detection in the first half of the 20th century. Nowadays, such materials are rather common in many other applications as well, given the necessity to prevent and/or mitigate electromagnetic radiation, interference and pollution. This section briefly explains the basic microwave absorption mechanisms, and then presents the currently available absorbent materials [66], [67].

4.2.1. Absorption mechanisms

When materials are exposed to electromagnetic waves, they can either transmit, reflect or absorb such radiation. Absorbent materials are capable of converting waves into other forms of energy (mainly heat) via different mechanisms, namely: magnetic loss, dielectric loss and conductive loss. Microwaves can be essentially considered as a magnetic field and an electric field that propagate simultaneously in the same direction. In order to absorb such waves, MAMs thus need to be capable of interacting with these fields (either of them or both). Therefore, radar absorbent material are desired to have favourable dielectric and conductive properties. A combination of both is normally desired, in order to maximise absorption.

4.2.2. Materials

This subsection presents an overview of some MAMs used for stealth applications in the defence industry, where radar's frequencies range between 2 and 18 GHz [66]. First, **alloys** absorbents are widely used (e.g. traditional alloys, high entropy alloys and composite alloy materials), they attenuate waves via magnetic loss, Eddy current loss and resonance. Second, **conducting polymers** absorb electromagnetic radiation via dielectric loss; in addition, their composition and microstructure are highly controllable, thus enabling to tune their properties. Third, **carbon materials** (e.g. fibre, graphene or nanotubes) are widely adopted, they absorb electromagnetic waves mainly via conductive loss, due to their high electrical conductivity. Currently, research focuses on mixing carbon materials with dielectric or magnetic materials, in order to decrease wave reflection tendency, allow to absorb via the magnetic loss mechanism and improve permeability. Then, **ceramic materials** are currently being studied and deemed as a viable option too, since modifying their morphology and structure allows to control their conductivity and dielectric properties. Additionally, combinations of different materials (e.g. epoxies or GFRP mixed with various metallic particles) are also being researched and adopted, since this allows for the integration or improvement of absorption mechanisms while retaining a high level of tailorability [66]. Composites tailored with various particles to integrate stealth capabilities are especially interesting, considering that many new aircraft feature an increasingly large number of composite components. Furthermore, the functional material considered in this thesis also belongs to this category. Therefore, the discussion in the coming sections is specifically related to this type of MAMs.

4.3. Particles dispersion in polymer composites

This section briefly addresses dispersion, which is a crucial aspect when adding various kinds of microparticles and/or nanoparticles to polymer composites. Achieving a good, uniform dispersion is not straightforward, yet of primary importance to obtain superior and consistent properties. Incorporating particles in polymer composites has been an emerging research trend in recent years, across different industries [68], [69]. The goal is to enhance the material properties, or to equip additional functionalities. In the aerospace industry specifically, the addition of carbon nanotubes (which are the most researched nanoparticles) is being investigated in order to mainly improve the mechanical properties, while — recalling the aim of this chapter — other types of particles are considered to give, for example, stealth capabilities.
In any case, regardless of the exact nature of the particles, mixing them with polymer composites brings a series of challenges. For the time being, one of the key issues is to prevent particles agglomeration, thus ensuring a good and uniform dispersion within the materials [70]. Failing to achieve such uniformity, may lead to inconsistent properties across the structure and ultimately to a deterioration of its overall performance. Another relevant aspect is the interfacial interaction between the particles and the polymer matrix. Being such a relevant aspect, agglomeration — and its effects — have been thoroughly investigated. For example, Zare [71] concluded that increasing particles content — as well as decreasing their size — leads to a larger degree of agglomeration. In addition, increasing agglomeration progressively decreases the effective particles volume fraction, ultimately reducing their effectiveness and affecting the properties of the overall structure. A similar conclusion was also reached by Ma *et al.* [72], who focused on the influence of agglomeration on the Young's modulus of the composite. The available techniques to disperse particles are listed in Table 4.1, and extensively described by Ma *et al.* [70].

Table 4.1: Comparison of different techniques to incorporate particles in polymer composites

Technique	Suitability	Parameters
Ultrasonication	Low-viscous, soluble	Mode of sonication, power, processing time
Calendering	Liquid, low-viscous	Rolls' rotation speed, distance between rolls
Stirring	Low-viscous, soluble	Mixing speed and time, propeller shape and size
Extrusion	Thermoplastics	Configuration of the screw, processing temperature

4.4. Applicable repair methods

This section briefly presents some existing repair methods, whose applicability to functional materials might be explored.

4.4.1. Filling repairs

Filling repairs are not largely investigated in academic literature. Nonetheless, aircraft manufacturers adopt such kind of procedures to address certain minor types of damage, and therefore discuss them in the relevant maintenance documentation. For example, the filling repair procedures applicable to Eurofighters are defined by the involved manufacturers in a dedicated repair document [73].
In any case, regardless of the type of aircraft, filling repairs are generally accepted to treat imperfections such as surface scratches or minor defects. In principle, this type of repair is

always carried out via the following steps, using paste adhesives or resins (potentially mixed with chopped fibers) as filling materials. First, the damaged area is identified, eventual sharp edges and the repair surface in general are smoothened via sanding. Second, the repair surface is cleaned and eventually further treated in order to promote adhesion. Third, the adhesive (or resin) is mixed and manually applied, usually with a spatula (or other similar spreading tools), trying to match the original shape of the structure as much as possible. The adhesive/resin is then cured, either at ambient conditions or at a pre-defined temperature and/or pressure, depending on the type of filling material used. Finally, once the filling compound has fully cured, excess material is eventually removed via sanding to fully match the original surface contour. In certain cases, in presence of slightly larger damages, it is also acceptable to apply glass fibre cloth pieces in combination with a adhesive/resin, in order to provide additional support.

4.4.2. Injection repairs

As already mentioned in chapter 2, injection repairs are adopted to address small delaminations or minor damages located somewhat deep in the structure. Injection repairs allow to stop damage propagation and restore matrix-dominated properties [7], [22]. This repair technique is potentially applicable to tackle the kind of repairs discussed in this chapter.
A main parameter to be carefully considered is the viscosity of the resin/adhesive/compound selected for the repair, considering that it needs to be easily injected. The following consists of some of the other required properties: short cure time, low shrinkage upon curing, good wettability, and glass transition above service temperature of the structure [13], [74].
The effectiveness of the repair is mainly driven by the ability of the repair compound to flow within the structure, thus filling the cracks and imperfections generated by the damage. In order to facilitate such process, injection repairs are usually vacuum-assisted, and vent holes can also be drilled for the same reason [75]. The benefits of such venting holes are evident, nonetheless their drawbacks should not be disregarded. Despite their effects have not been largely investigated by many studies so far, the work of Lai *et al.* [76] showed how venting holes are detrimental for the mechanical properties of the laminate, since the drilling process tends to induce (or initiate) additional delaminations in the previously undamaged parent material.
Injection repairs are carried out according to the following procedure [13]. First, the damage-affected region is blasted and rinsed, to remove any fragments and/or residues [77]. Second, the repair material is injected, this can be done in different ways, namely: manual injection [78], injection under pressure and vacuum, injection under vacuum, and through-thickness vacuum assisted injection [79]. Each of these methods is explained in more detail by Omairey *et al.* [13]. Third, the repair material needs to be cured. Depending on the selected repair compound, this process might differ significantly, given that different resin systems require different curing cycles (temperature, pressure and time).

4.4.3. Other methods

On top of the standard techniques briefly presented in the previous subsections, other repair approaches might also be suitable to tackle damages in functional materials. For example, D'Arduini [4] proposed a concept based on the use of hard patches: the damaged area is removed from the structure and replaced with a matching, pre-cured patch that is then secondary-bonded. This procedure was identified as suitable to tackle rather large damages and thus inconvenient to repair minor, localised defects. Nonetheless, the need to improve the repair procedure in order to achieve higher quality repairs was highlighted.

5

Research questions

As previously mentioned in the introduction, the focus of this thesis is on repair methodologies for composite structures that include functional inserts. The following consists of the main research question that was addressed during the thesis:

How to repair composite aircraft structures with microcomposite stealth functional inserts?

Based on the review work reported in the previous chapter, a series of sub-questions was defined, in order to determine in more detail the scope of this project. The process of defining such questions, together with the questions themselves, are presented hereafter.

First, regarding damages located in the structural part of the component, it is evident that — if their size is significant — they need to be addressed with scarf repairs. As highlighted in the previous chapter, making such repairs as flush as possible is still an open issue, not largely investigated. Additionally, overplies are often applied on top of the repair area — to seal it off and reduce peel stresses — thus increasing even further the thickness mismatch with the parent laminate. Such uneven surface finish is detrimental from a stealth and aerodynamic standpoint: avoiding it is thus desirable. The work performed by Scholz [5] at Airbus Defence and Space GmbH, tackled this issue proposing to re-mill the repaired surface; the concept was deemed promising, albeit the need for more investigation was highlighted in order to further refine and eventually qualify this procedure. No further work has been performed and alternative concepts to achieve a fully flush surface finish have not been investigated in literature. Therefore, this gap drove the definition of the first two sub-questions, SQ1.1 and SQ1.2, namely:

SQ1.1 *How to manufacture a fully flush, bonded scarf repair by re-milling the repaired area?*
SQ1.2 *How to optimize the repair patch layup in order to achieve a fully flush, bonded scarf repair while minimizing further surface post-processing?*

Second, regarding damages located in the functional part of the component, it was concluded that no standard repair procedure is currently in place to address this scenario. In addition, due to the topic sensitivity and limited field of application, available literature is not abundant. Considering the work performed by D'Arduini [4] at Airbus Defence and Space GmbH, the need to define a repair procedure to fix minor, localized damages — most likely based on the filling repair method — is evident. In addition, stemming from the same work, further exploring the option of using hard patches to restore larger damages seems to be beneficial. Overall, these open issues led to the definition of sub-questions SQ2.1, SQ2.2 and SQ2.3.

SQ2.1 *What are the suitable procedures to repair localized, small, cosmetic damages using a filler compound?*
SQ2.2 *How to define the optimal functional material filler compound to repair localized, small, cosmetic damages?*
SQ3.3 *How to improve the repair process using hard patches to tackle larger damages?*

Third, regarding damages extending on both the structural and functional parts of the component, no previous work is available. A variation of the concept defined by D'Arduini [4] for repairs in the functional material might be applicable, however more investigations are necessary. Therefore, based on this gap, the research sub-question SQ3.1 was defined.

SQ3.1 *What are the suitable procedures to repair damages affecting both the structural and the functional parts?*

Table 5.1 provides an overview of all the research questions derived above and considered in this thesis.

Table 5.1: Overview of the research questions considered in this thesis

Main research question	
RQ	How to repair composite aircraft structures with microcomposite stealth functional inserts?
Repairs localised in the structural part	
SQ1.1	How to manufacture a fully flush, bonded scarf repair by re-milling the repaired area?
SQ1.2	How to optimize the repair patch layup in order to achieve a fully flush, bonded scarf repair while minimizing further surface post-processing?
Repairs localised in the functional part	
SQ2.1	What are the suitable procedures to repair localized, small, cosmetic damages using a filler compound?
SQ2.2	How to define the optimal functional material filler compound to repair localized, small, cosmetic damages?
SQ2.3	How to improve the repair process using hard patches to tackle larger damages?
Repairs affecting both parts	
SQ3.1	What are the suitable procedures to repair damages affecting both the structural and the functional parts?

II

Structural Material Repairs

6

Problem statement

This part of the thesis deals with the repairs localised in the structural part of the considered component, i.e. the demonstrator structure already introduced and depicted in Figure 1.3. This chapter serves as a sort of introduction for the work performed in this phase of the thesis. At first, the background and the previous work performed at Airbus are presented, together with the connection with the research questions that were answered in this phase. Then, the adopted approach is introduced: the considered concepts and the performed tests are discussed. At last, all the steps completed in this phase are summarised, and a graphical workflow is presented.

6.1. Background and approach

As mentioned in the previous chapter, scarf repairs are standardly adopted to repair structural damages. Despite such repair procedure is already deployed in different scenarios, there are still aspects that could be improved. The most relevant one — as already introduced — is how to better the surface finish of the repaired area in order to make it as flush as possible.
A superior surface smoothness is beneficial for both stealth and aerodynamic reasons, and is especially sought for in high-performance applications. From a low observability (LO) standpoint, it is important to avoid any sharp edge, sudden change in thickness or small mismatch between exterior parts. These may indeed reflect radar waves in an undesired direction, thus compromising the stealth capability of the aircraft. Minimizing such mismatches is so crucial that some of the most advanced stealth aircraft rely on high-precision CNC machining, to make sure that certain composite parts can be snugly assembled [80]. From an aerodynamic standpoint, having a flush surface is generally beneficial in terms of efficiency. However, extremely smooth surfaces — in the order of magnitude sought for in this thesis — are most likely required only in very few applications, or eventually when laminar wing concepts might be implemented in the future.
Currently, certified scarf repairs can achieve a surface mismatch between the undamaged and the repaired area up to a few millimeters — also due to the frequent application of an oversized overply on top of the repaired area in order to seal it off and reduce peel stresses. The goal of this investigation is to reduce such mismatch well below half a millimeter.

This aspect has been previously researched at Airbus, being applicable to several current and future aircraft. The most relevant and recent work was performed by Scholz [5], who defined, manufactured and tested at specimen level different scarf repair configurations aimed at improving surface flushness. The cross sections of the various geometries that were tested

and compared to the conventional one (Figure 6.1a) are shown in Figure 6.1b, 6.1c, 6.1d and 6.1e. A key aspect that was investigated in this work for the first time is the post-processing of the repaired surface via CNC milling, in order to eliminate the thickness offset generated by the repair. This investigation concluded that — among the considered options — the re-milled variant (Figure 6.1b) is the optimal one, due to the relative simplicity in terms of manufacturing and good mechanical performance (i.e. comparable to the original, undamaged material). Nonetheless, it was highlighted how the re-milling procedure — despite being promising — needs to be further investigated and refined. Indeed, a fully flush surface could not be achieved after milling, which still left a thickness difference quantifiable at around 0.2 mm.

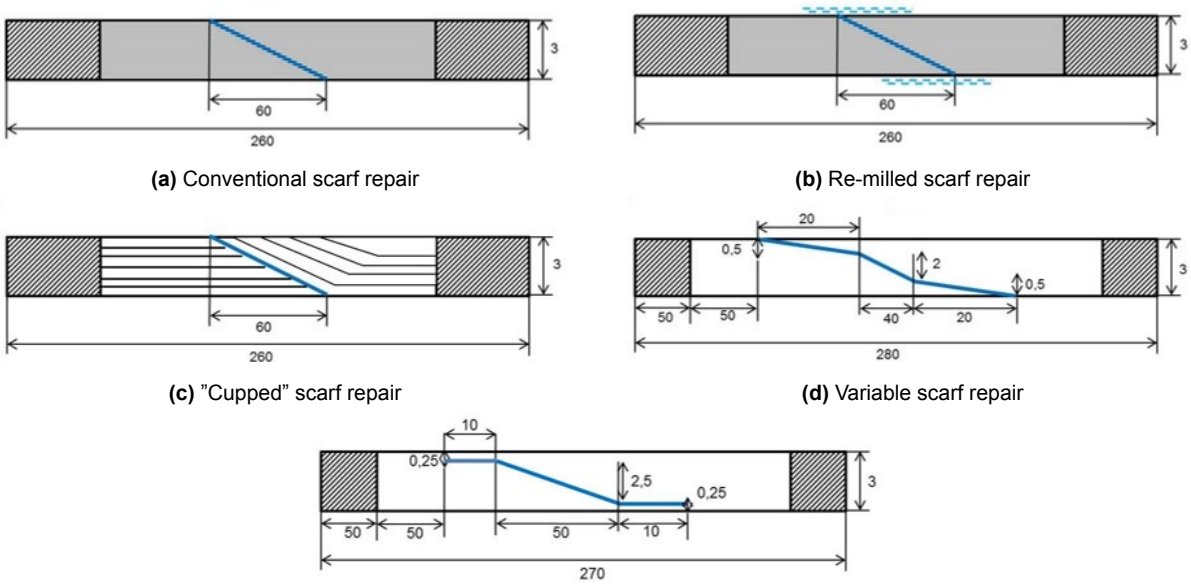

(a) Conventional scarf repair

(b) Re-milled scarf repair

(c) ”Cupped” scarf repair

(d) Variable scarf repair

(e) Countersunk, stepped scarf repair

Figure 6.1: Flush scarf repair geometries previously tested at Airbus (dimensions in mm) [5]

This part of the thesis picked up the open point left by the previous work, on top of exploring additional possibilities, always with the ultimate goal of improving repair flushness. The option of post-processing the repaired surface to improve its flushness was further investigated: such concept was implemented once again at specimen level and the milling processing parameters were re-evaluated to improve the final results. This allowed to tackle and answer research question SQ1.1 (Table 5.1). In addition, a novel idea to ideally achieve the same purpose was explored: a repair patch was re-designed with a lower number of plies. Once properly aligned, this allowed to minimize the thickness offset between the parent laminate and the patch, reducing the need for further post-processing. This allowed to address the second research question (SQ1.2, Table 5.1) related to structural repairs.
It is also important to point out that, while the previous works implemented soft patch repairs, only hard patch repairs were manufactured and tested in this thesis. The advantages and disadvantages of both concepts have already been discussed in subsection 3.2.5. A comparison between the hard patch results obtained in this thesis and soft patch ones taken from previous Airbus studies will be proposed in a later chapter.

6.2. Concepts definition

Three different scarf repair concepts were manufactured (using hard, secondary-bonded patches), tested and compared in this phase of the thesis. First, the conventional scarf repair concept was considered (Figure 6.2a): this served as a reference for the other options. Second, building up on previous Airbus work, the option of re-milling the repaired region was further investigated (Figure 6.2b), aiming at optimizing the milling procedure. Third, the novel idea of using a thinner repair patch (obtained with a lower number of plies) was explored (Figure 6.2c). For the last option, a rigorous design process (explained in detail in a later chapter) was followed in order to define the new, thinner layup, with the goal of minimizing the differences with the parent material.

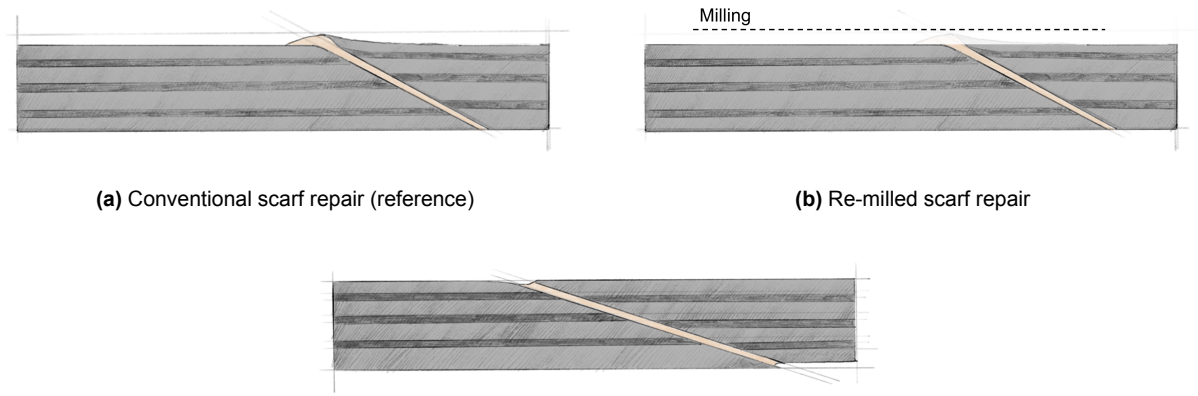

(a) Conventional scarf repair (reference)

(b) Re-milled scarf repair

(c) Re-designed patch scarf repair (modified patch)

Figure 6.2: Cross sections of the flush scarf repair concepts considered in this thesis

6.3. Specimen and tests selection

This section briefly describes the specimen type used in this analysis: its characteristics and selected parameters are first introduced, then the performed mechanical tests are presented.

The EN6066 specimen [81] (whose geometry and dimensions are depicted in Figure 6.3) was selected to test the various repair concepts defined in this phase of the thesis. This type of specimen is particularly suitable to test different scarf repair geometries, considering that — as already mentioned in section 3.1 — full repairs can be modelled in 2D as scarf joints. Additionally, it was already used in previous investigations at Airbus (e.g. [4], [5]), therefore adopting it once again allowed to generate comparable experimental data.

Some relevant characteristics of the selected specimen are listed in Table 6.1. The material was selected being the one currently adopted for several Airbus projects and aircraft. The quasi-isotropic layup is the same one used in several other previous investigations. The same reasoning applies to the scarf ratio of 1:20. Testing different scarf ratios was deemed not necessary, given that the influence of such parameter is already well known and understood, as already mentioned in subsection 3.3.1. These characteristics match the ones selected in the previous work of Scholz [5] and D'Arduini [4], so that experimental results can be eventually compared: this was useful to assess the difference between the hard patch repairs implemented in this thesis and the soft patch repairs manufactured in the previous studies.

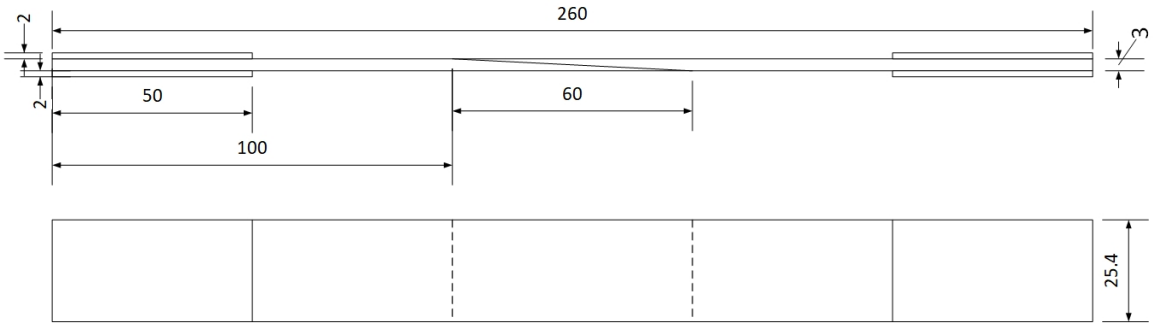

Figure 6.3: EN6066 specimen geometry, side and top view (dimensions in mm)

Table 6.1: Parameters and characteristics of the EN6066 specimens

Parameter	Value
Material	HexPly® 8552/IM7
Layup	$[\ 45, 135, 0, 0, 45, 135, 90, 90, 45, 0, 135, 90\ ]_s$
Scarf ratio	1:20

The specimens were tested both quasi-statically and dynamically, in such a way that both the ultimate strength and fatigue life of the different repair concepts could be assessed. For the sake of comparison, also the test parameters were the same as the ones used in previous studies [4], [5], [48]. For each repair concepts, 5 specimens were tested quasi-statically and 5 specimens dynamically. Therefore, 30 specimens were intended to be tested in total, but a slightly higher number was manufactured to account for eventual defects or any other aspect that might cause a specimen to be unusable. The specimens' nomenclature is defined as follows:

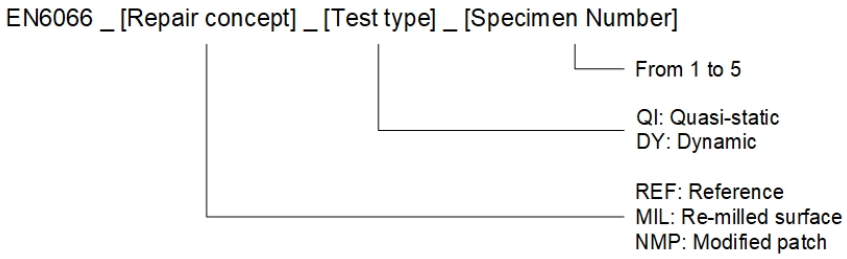

6.4. Workflow

Figure 6.4 provides an overview of all the steps that were performed in this phase of the thesis, with the aim of investigating flush scarf repairs and thus answering the related research questions. The starting point of this phase is represented by the definition of the repair concepts that were assessed, which have already been introduced in a previous section. The adhesive to manufacture such concepts with EN6066 specimens, was first of all selected via dedicated tests. Currently, two different adhesives are being investigated for this sort of procedures at Airbus, the selection process is covered in detail in chapter 7. Next, the EN6066 specimens were manufactured and tested, as described in chapter 8 and chapter 9, respectively. Finally, the test results were evaluated and compared, and the conclusions related to this phase of the thesis

are drawn in chapter 10.

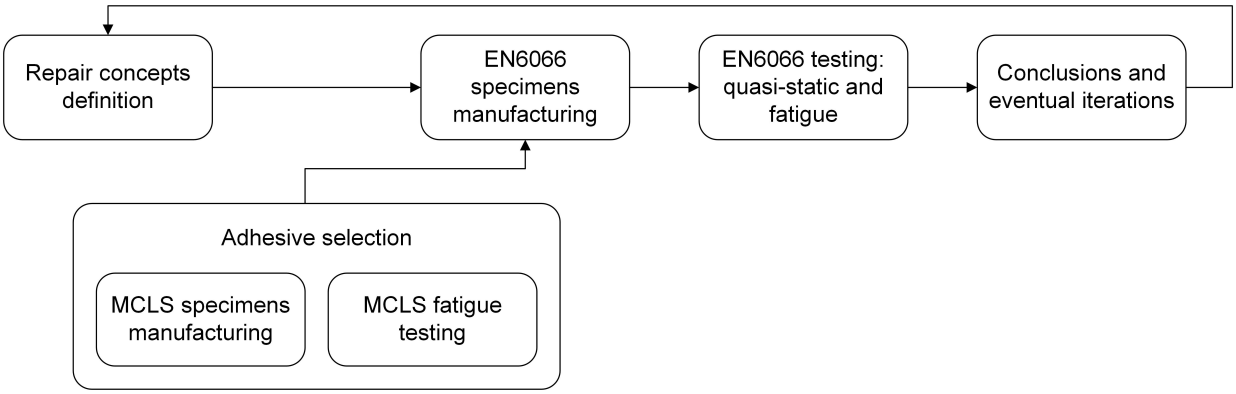

Figure 6.4: Flowchart depicting the steps performed to tackle the research questions related to the repairs localised in the structural part of the demonstrator structure

To summarise and clarify the aim and the content of this first part of the thesis, its goal and its scopes are stated in Table 6.2.

Table 6.2: Goal and scope of the first part of the thesis, aimed at investigating structural repairs

Goal	
	Investigate how to achieve fully flush scarf structural repairs in CFRP aircraft structures
Scope	
1	Evaluate different hard patch concepts for flush repairs
	1.1 Compare their mechanical performance (static & fatigue)
	1.2 Assess their manufacturing feasibility
2	Compare the performance of hard patches vs soft patches (relying on existing data for soft patches, generated in previous investigations)

7

Adhesive selection

This chapter describes the selection procedure to define the adhesive for the EN6066 specimens. The choice was between two options, namely: the Loctite EA9695 AERO, and the Solvay Aeropaste 1006. The former is a film adhesive, already widely adopted at industrial level; the latter is a newly-developed paste adhesive, whose applicability in different domains is currently under research. This chapter is structured as follows: first, the selected specimens and its manufacturing steps are presented. Second, the test results are shown and discussed, before finally selecting the adhesive for the EN6066 specimens.

7.1. Specimen characteristics

The specimen chosen for the adhesive selection is the Modified Crack Lap Shear (MCLS), whose geometry was defined — combining the crack lap shear (CLS) [82] and the EN6066 specimen [81] — by Hamberger [83] at Airbus Defence and Space. Such specimen was designed with the specific objective of allowing for the observation of a steady crack propagation along the bondline of composite scarf joints. The geometry and the dimensions of the MCLS specimen are depicted in Figure 7.1.

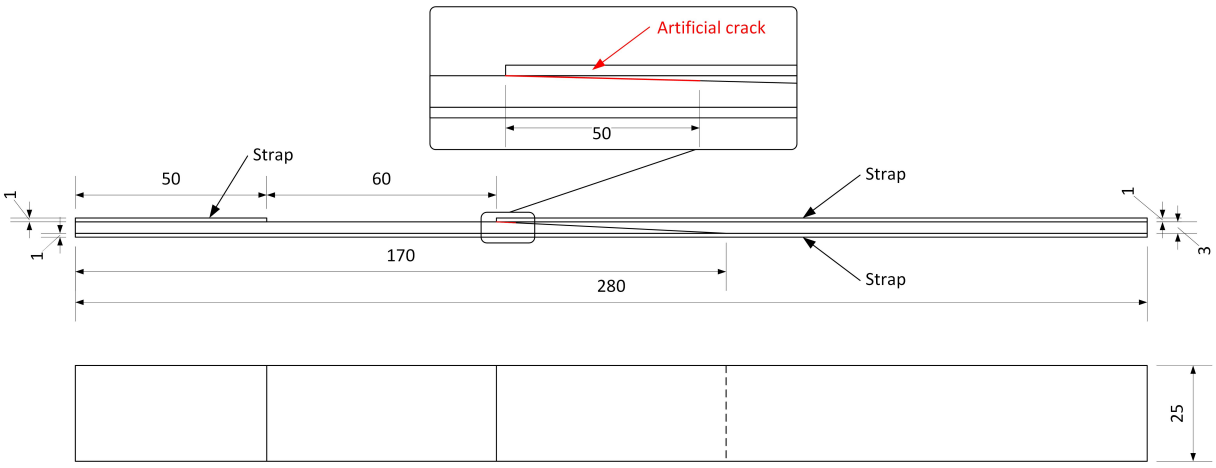

Figure 7.1: Modified Crack Lap Shear (MCLS) specimen geometry, side and top view (dimensions in mm)

A distinctive feature of these specimens is that a ≈5 mm crack along the adhesive bondline is artificially initiated by inserting a release film in the very first part of the scarf, thus preventing

the two adherends from bonding. In this way, the crack propagation is observable in shorter time frames, since the initiation period — which is generally rather long — is basically eliminated. Furthermore, it is ensured that the crack propagates primarily along the bondline, thus allowing to observe the adhesive behaviour.
The strap on the top side is intended to generate a stress concentration around the beginning of the scarf bond, thus promoting the propagation of the artificial crack. On the other hand, the strap on the bottom side prevents the specimen from breaking and splitting abruptly once failure is reached.

The layup and other characteristics of the MCLS specimens manufactured and tested in this work are listed in Table 7.1. It is worth mentioning that such parameters match the ones used in previous investigations by Hamberger [83] and Preisz [84], in order to generate comparable experimental data.
It must be however noted that, in this investigation, the two adherends are secondary bonded to create the scarf joint. On the other hand, the specimens manufactured in previous studies adopted a co-bonding procedure: the first adherend was cured and scarfed, then the second one was hand-laid up on the scarf area, in accordance with the conventional scarf repair procedure.

Table 7.1: Parameters and characteristics of the MCLS specimens

Parameter	Value
Material	HexPly® 8552/IM7
Main layup	$[\ 45, 135, 0, 0, 45, 135, 90, 90, 45, 0, 135, 90\ ]_s$
Layup straps	$[\ 45, 135, 0, 90\ ]_s$
Scarf ratio	1:20

In total, 10 specimens were manufactured and tested: 5 using the film adhesive and the remaining 5 using the paste one. The specimens' nomenclature was defined as follows:

7.2. Specimen production

This section briefly describes the production of the MCLS specimens. First, the manufacturing procedure is outlined, second — and most importantly — the quality of the specimens is assessed focusing on the thickness of the adhesive bondline.

7.2.1. Manufacturing

Figure 7.2 provides a graphical overview of the steps necessary to manufacture the MCLS specimens. More information about the laminate production and the used material will be provided at a later stage in section 8.1, when the EN6066 specimens production will be described

— being the two types of specimens manufactured from the same laminates. The same applies for the CNC scarfing procedure and the scarf surface treatment. This section only provides some key, worth-mentioning aspects peculiar of the MCLS specimens manufacturing.

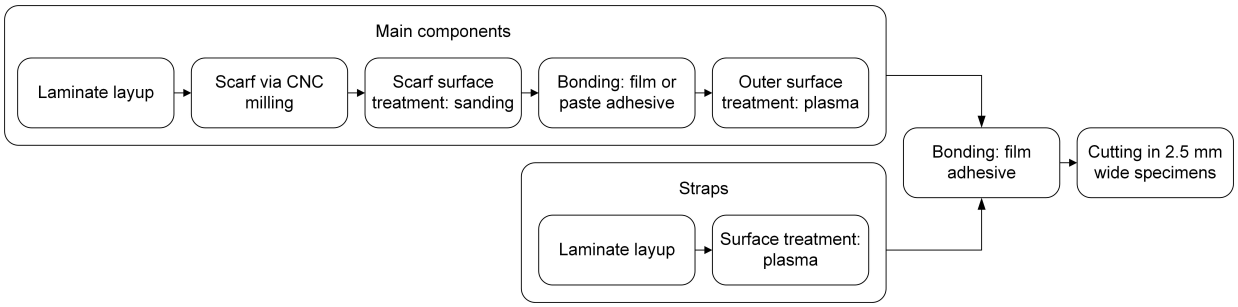

Figure 7.2: Flowchart depicting the manufacturing steps of the MCLS specimens

Some of the manufacturing steps are shown Figure 7.3 and Figure 7.4, for the film and paste adhesive specimens, respectively. Do note the presence of the jagged release film acting as crack initiator (Figure 7.3a, 7.3b, 7.4b and 7.4c), distinctive feature of this specimen type. Based on the observations from a previous investigation [83], the jagged film was positioned in such a way that no spikes were located inside the 0° layers, as this proved to prevent premature crack propagation.

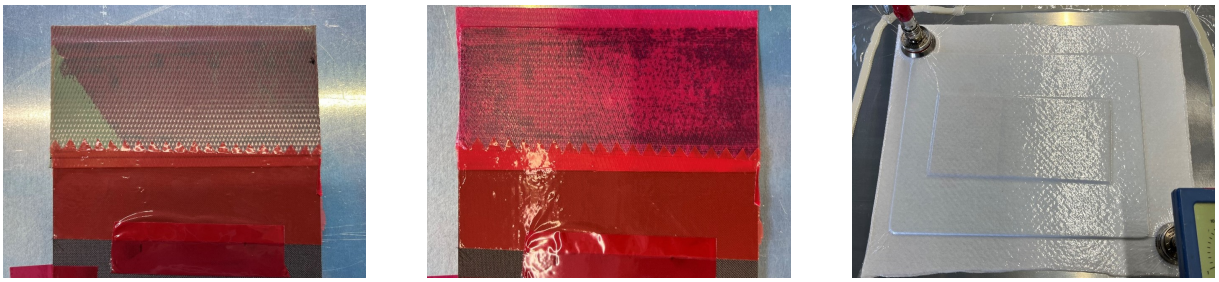

(a) Adhesive application **(b)** Adhesive compaction **(c)** Curing under vacuum

Figure 7.3: Manufacturing steps for the MCLS specimens with the film adhesive

For the specimens with paste adhesive — as shown in Figure 7.4b — the bondline thickness was controlled by gluing four metallic shims on the corners of the bond area and a strip in the middle (instant glue was used for this purpose, eventual excess was immediately removed from the bond surface). The shims were then cut out once the panel was later trimmed, and the strip had been aligned with a cut between two single specimens, so that it was also later removed.
It is also worth mentioning that — as depicted in Figure 7.4e — the adhesive was compacted under vacuum for roughly 10 minutes using a pressure plate. Excess adhesive was then removed and then curing took place in an oven, under an amount of weight corresponding to the pressure indicated by the manufacturer — in absence of a press.

Table 7.2 provides the relevant information about the curing cycles of the two different adhesives, selected based on the manufacturers' guidelines as well as on Airbus internal composite manufacturing procedures.

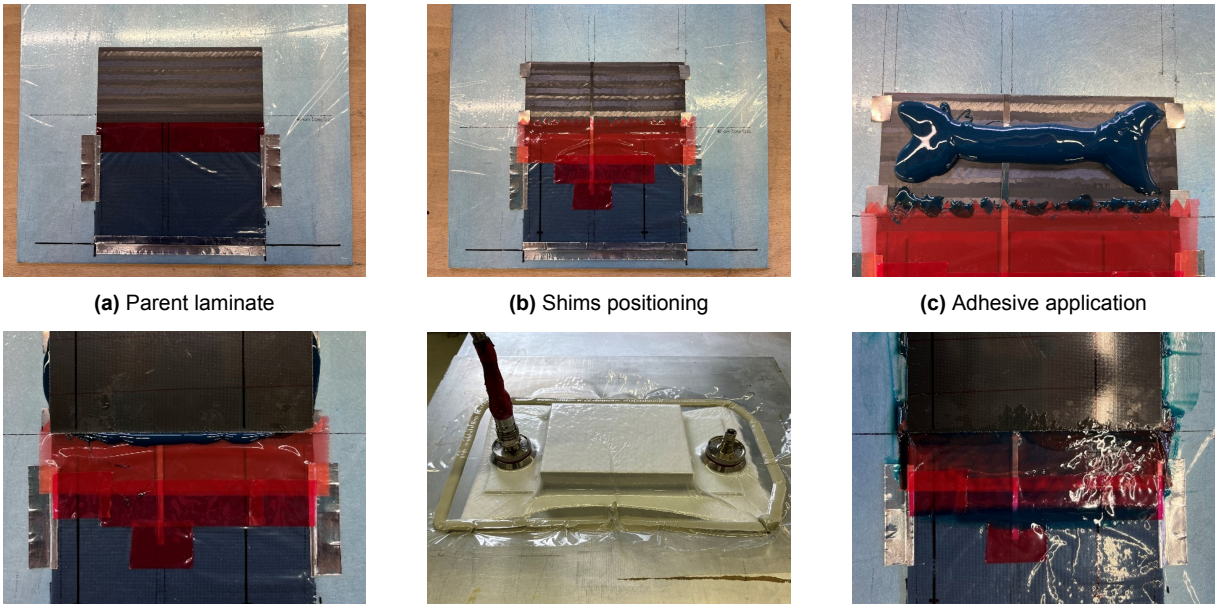

(a) Parent laminate **(b)** Shims positioning **(c)** Adhesive application

(d) Patch alignment **(e)** Compaction **(f)** Cured repair

Figure 7.4: Manufacturing steps for the MCLS specimens with the paste adhesive

Table 7.2: Curing conditions of the two adhesives used for the MCLS specimens

Adhesive	**Curing T** [°C]	**Curing t** [min]	**Heating/cooling rate** [°C/min]	**Pressure**
Film, EA9695 AERO	121	120	1.5	Vacuum
Paste, Aeropaste 1006	93	120	1.5	0.025 MPa

Prior to the bonding of the straps, both surfaces (i.e. the straps' surface and the ones of the core laminate) were plasma treated. The process parameters are listed in Table 7.3, and the bonding was then completed within 45 minutes from the treatment, in accordance with applicable Airbus guidelines. The straps were bonded in place using the film adhesive Loctite EA9695 AERO for all the specimens.

Table 7.3: Parameters used for the surface treatment of the MCLS specimens and their straps

Parameter	**Value**	**Unit**
Nozzle type	Rotating	[-]
Feed rate	100	[mm/s]
Distance from CFRP surface	10	[mm]
Offset	5	[mm]

At last, the specimens were cut out from the laminate with a diamond blade, the speckle pattern was then manually applied with a airbrush.

7.2.2. Quality control

The bondline thickness was measured in three different locations (shown in Figure 7.7) along the scarf for all the specimens, via analysis of images taken with a digital microscope (two examples of such images are depicted in Figure 7.5). The measurements are listed in Table 7.4 and graphically shown in Figure 7.6. Do note that the specimen MCLS_FA_1, due to manufacturing complications, did not meet the dimensional specifications and was therefore discarded.

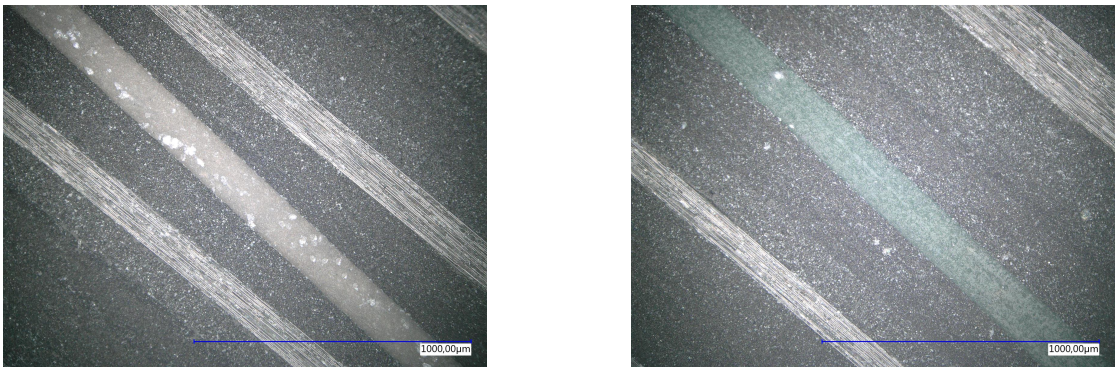

(a) Film adhesive **(b)** Paste adhesive

Figure 7.5: Micrographs showing the bondline of the MCLS specimens

Table 7.4: Measurements of the bondline thickness for the MCLS specimens

Specimen #	**Bondline thickness** [µm]			
	Location 1	Location 2	Location 3	Average
MCLS_FA_1	-	-	-	-
MCLS_FA_2	144.69	94.96	57.92	99.19
MCLS_FA_3	239.70	140.42	61.19	147.10
MCLS_FA_4	243.10	155.99	54.73	151.27
MCLS_FA_5	175.77	96.23	44.82	105.61
MCLS_PA_1	118.87	102.86	124.12	115.28
MCLS_PA_2	167.16	165.03	137.56	156.58
MCLS_PA_3	222.51	205.79	176.41	201.57
MCLS_PA_4	223.91	204.58	165.30	197.93
MCLS_PA_5	236.82	203.88	134.63	191.78

In Figure 7.6, the bars represent the average of the measurements, while the error bars the minimum and maximum measured values. As one can notice, the bondline thickness is generally lower for the film adhesive specimens compared to the paste adhesive ones, although there is more variation along its length.

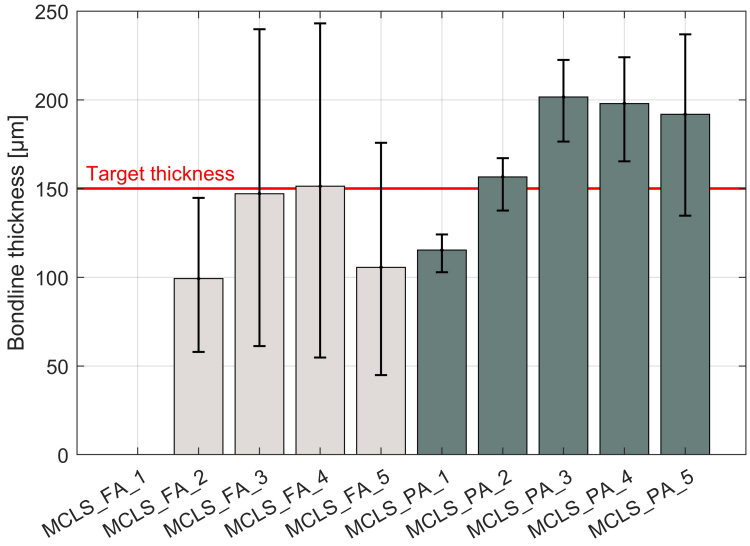

Figure 7.6: Adhesive bondline thickness of the MCLS specimens, both with film and paste adhesive

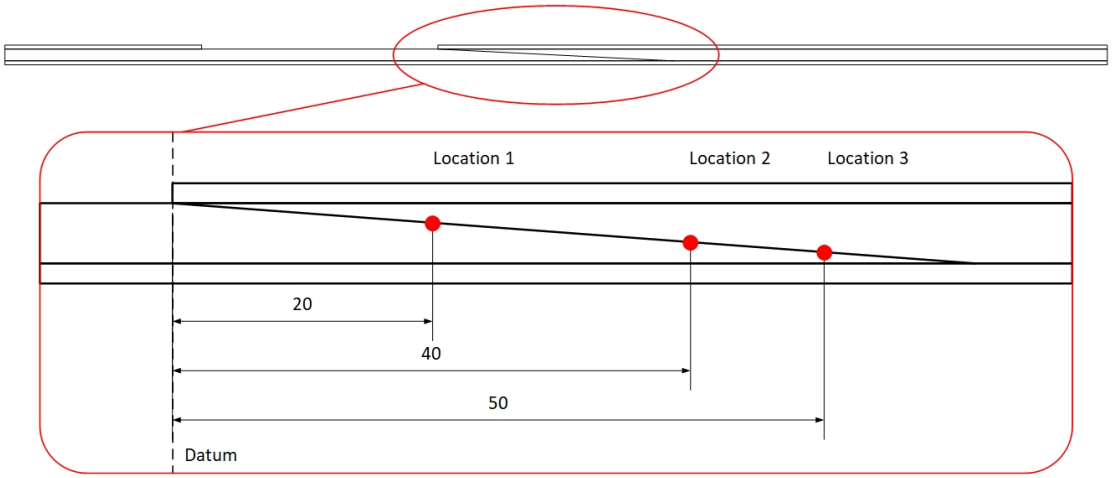

Figure 7.7: Locations along the bondline of the adhesive thickness measurements (dimensions in mm)

7.3. Testing

This section provides some details about the fatigue tests performed with the MCLS specimens. First, information about the test set-up is provided, then the selected testing conditions are presented.

7.3.1. Test set-up

The fatigue tests were performed with a servo-hydraulic machine (from MTS Systems Corporation, Eden Prairie, Minnesota, United States) with a 100 kN load cell and hydraulic jaws, equipped with a two-dimensional DIC set-up (Q-400-2D system from Limess GmbH, Krefeld, Germany and Istra4D 4.4.6 software from Dantec Dynamics GmbH, Ulm, Germany). The image acquisition was synchronized with the periodic analog signal generated by the test rig. In this way, images could be taken once the maximum force level of a cycle was reached, whereas the

image acquisition rate was set independently.

The crack length — and thus the crack growth — could be then determined in post-processing, following the same procedure adopted by Thäsler *et al.* [85]. This is possible by finding in advance the strain distribution at the crack tip, which is a peculiar property of each different adhesive. The software then analyses each image, and identifies the crack tip location — and so its length — by comparing the characteristic, critical crack tip strain with the strain levels recorded along an approximate, user-defined crack path. If the strain level along such line exceeds the given critical threshold, this position is marked as part of the crack.

For the film adhesive, the critical strain level at the crack tip was already known in advance, since such adhesive had already been extensively tested in the past. Such value was quantified at 1.15% in the work of Hamberger [83].
On the other hand, this critical strain level had to be determined for the paste adhesive, since it had never been previously tested and analysed with this set-up. It had been originally planned to find this value with a bespoke batch of five Single Lap Shear (SLS) specimens, which were thus manufactured. However, due to time reasons and complications with the set-up, it was ultimately decided to use one of the MCLS specimens to define this critical value. Therefore, the specimen MCLS_PA_5 was tested for 15000 cycles, in such a way that crack propagation could be observed, but no failure occurred. The specimen was then removed from the rig, cut in sections, polished and analysed via microscopy to identify the actual crack tip location (depicted in Figure 7.8a). Once such position (i.e. its coordinates) was known, its corresponding strain value was found in the last DIC image (shown in Figure 7.8b). In conclusion, the critical strain level at the crack tip for the paste adhesive was quantified at 1.3%.

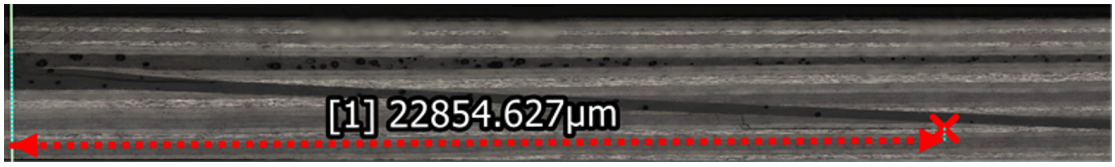

(a) Laser microscope picture showing the crack tip location

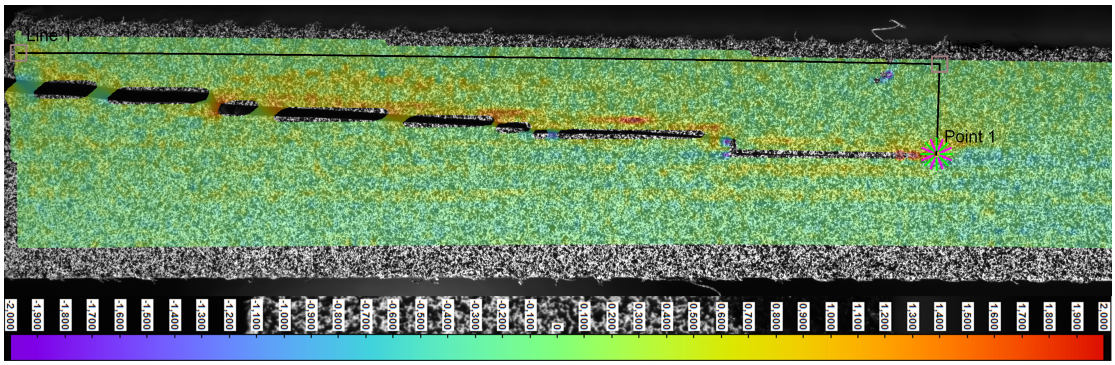

(b) DIC image showing the crack tip location

Figure 7.8: Crack tip location in the specimen MCLS_PA_5, used to identify the critical strain level corresponding to the crack front for the paste adhesive

It must be mentioned that the analysis method used here was developed for a slightly different application, and therefore is not ideal for this specific testing conditions. Nonetheless, since the goal here is to compare the two adhesives, rather than precisely defining the crack growth rate for each of them, it is considered acceptable and able to yield the desired outcome.

The method was initially developed to study crack propagation in isotropic mediums, and not specifically on scarf joints. Hence why it was decided to adopt a user-defined line element, and compare strains along this with the critical value. The shortcoming of this approach — once applied to the tests performed here — is that the crack path is not linear, but presents many steps and irregularities (as clearly visible in Figure 7.8b). Therefore, it is rather hard to define a line element able to precisely follow the path. As a consequence, it is not trivial to make sure that the local strains labelled as part of the crack actually belong to it.
In order to overcome this issue, it would be necessary to develop an alternative analysis script, for example able to compare strains within a user-defined area rather than along a single line. Or, eventually, even slicing the area vertically and comparing the strains stripe by stripe may be a suitable approach. Overall, it is advised to reconsider this aspect if in the future it is required to precisely study the crack growth rate within the bondline of composite scarf joints.

7.3.2. Test conditions

The fatigue tests were performed under load control with a sinusoidal waveform. The conditions selected for the two different adhesives are listed in Table 7.5, while the process that led to their definition is briefly explained thereafter.

Table 7.5: Fatigue testing conditions for the MCLS specimens

Adhesive	f [Hz]	**R** [-]	**Max load** [kN]
Film, EA9695 AERO	8	0.1	54000 cycles at 10 kN, then 13.1 kN
Paste, Aeropaste 1006	8	0.1	10 kN

The testing parameters were selected with the main goal of allowing for a steady, observable crack propagation, while not requiring excessive testing time (primarily due to the availability of the testing machine). The parameters chosen in the studies of Hamberger [83] and Preisz [84] were considered as a starting point.
The load was initially set at 10 kN, however, this load level allowed to observe hardly any crack propagation in the film adhesive specimens, even after several hundred thousand cycles. Therefore, the load was progressively increased up to 13.1 kN, at which the film adhesive specimens could reach failure within a reasonable time frame. However, such load level proved to be too high for the paste adhesive specimens, which failed prematurely (below 2000 cycles), thus not allowing to observe and record any crack growth. Therefore, based on these observations — and recalling the main goal mentioned above — it was decided to test the remaining paste adhesive specimens at 10 kN; whereas, the film adhesive ones were tested at 10 kN for 54000 cycles[1], after which the load was increased up to 13.1 kN until failure was reached. In this way, it was possible to collect crack propagation data at the same conditions for both adhesives (since for the first 54000 cycles the conditions are identical), while not requiring excessive testing time.

[1] This value is conventionally used as threshold for fatigue testing with this type of specimens, for this applications at Airbus Defence and Space

7.4. Results and discussion

This section presents the results of the MCLS tests. First, the specimens' performance in terms of crack growth over number of cycles is described. Second, the failure modes and pattern are shown. At last, such results are discussed and the adhesive to be used for the EN6066 specimens is selected.
Originally, as mentioned above, it was intended to test 5 specimens for each adhesive type, so 10 in total. However — for various reasons — this could not be achieved: only three specimens for each adhesive type generated useful experimental data, as summarised in Table 7.6.

Table 7.6: Overview of the MCLS specimens testing phase

Specimen	Comment
MCLS_FA_1	Scrapped, out-of-spec
MCLS_FA_2	Used to define optimal testing parameters
MCLS_FA_3	Successfully tested (10 kN for 55k cycles, then 13.1 kN until failure)
MCLS_FA_4	Successfully tested (10 kN for 55k cycles, then 13.1 kN until failure)
MCLS_FA_5	Successfully tested (10 kN for 500k cycles, then 13.1 kN until failure)
MCLS_PA_1	Successfully tested (10 kN until failure)
MCLS_PA_2	Used to define optimal testing parameters
MCLS_PA_3	Successfully tested (10 kN until failure)
MCLS_PA_4	Successfully tested (10 kN until failure)
MCLS_PA_5	Used to define DIC correlation value

7.4.1. Failure cycles

Figure 7.9 plots the crack growth over time (expressed as number of cycles) for the specimens with the film adhesive. In more detail, Figure 7.9a shows all the specimens at once, while Figure 7.9b only depicts the two specimens with a more similar timescale. The results for the specimen with the paste adhesive are plotted in Figure 7.10. Do note the difference in order of magnitude between the specimens with the film adhesive and the one with the paste one.

7.4.2. Fracture surfaces

This section shows the fracture surfaces and presents the failure modes of the MCLS specimens. Since the specimens showed very similar fracture surfaces, only a few representative pictures are presented in Figure 7.11. Figure 7.11a and 7.11b depict the fracture surfaces of two specimens with the film adhesive, while Figure 7.11c shows the fracture surface of a specimen with the paste adhesive.
In the case of the film adhesive, a combination of pure cohesive failure, mixed cohesive/adhesive failure and adherend failure is observed. In the case of Figure 7.11a, towards the top of the bond area, the mixed cohesive/adhesive failure is mainly adhesive, while this cannot be observed in the same region of Figure 7.11b. Adherend failure occurred around the 45°/135°/90° plies, while cohesive/adhesive failure around the 0° plies°. This can be explained considering the specimens' load case: failure occurred in the adherend around the plies not aligned with the load (45°/135°/90°), while around the main load-bearing plies (0°) the adhesive failed.

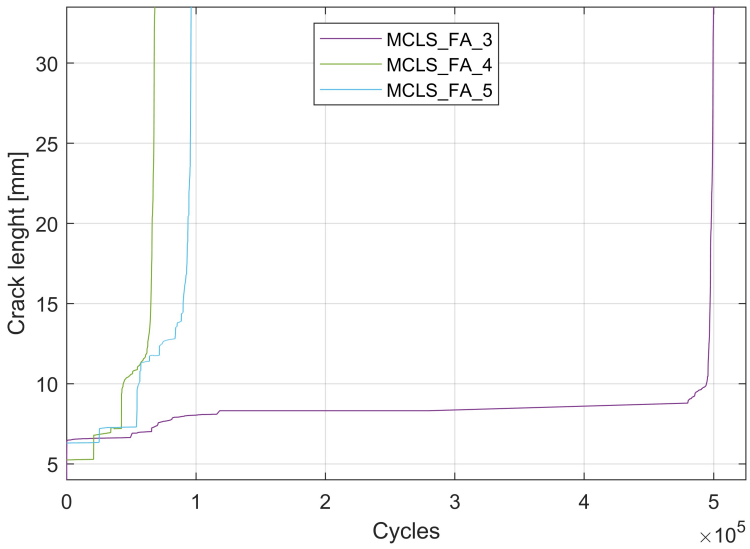

(a) Overview of all the specimens with the film adhesive

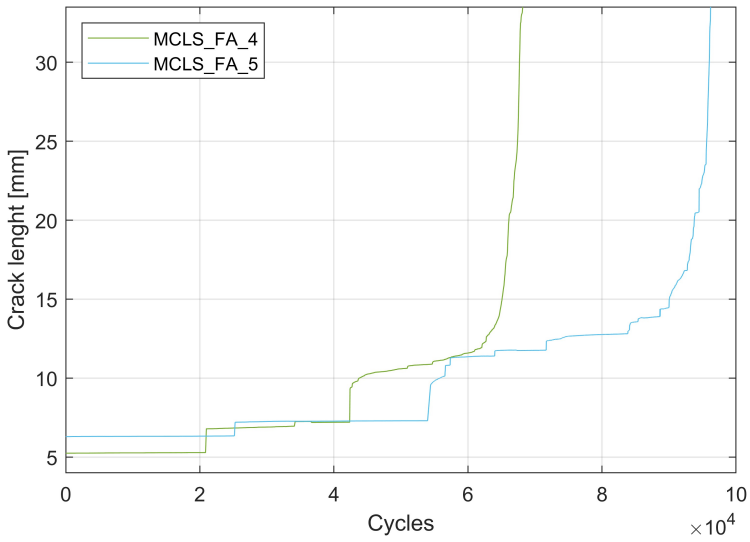

(b) Focus on the two specimens with similar performance

Figure 7.9: Crack growth as function of the number of cycles for the MCLS specimens with the film adhesive

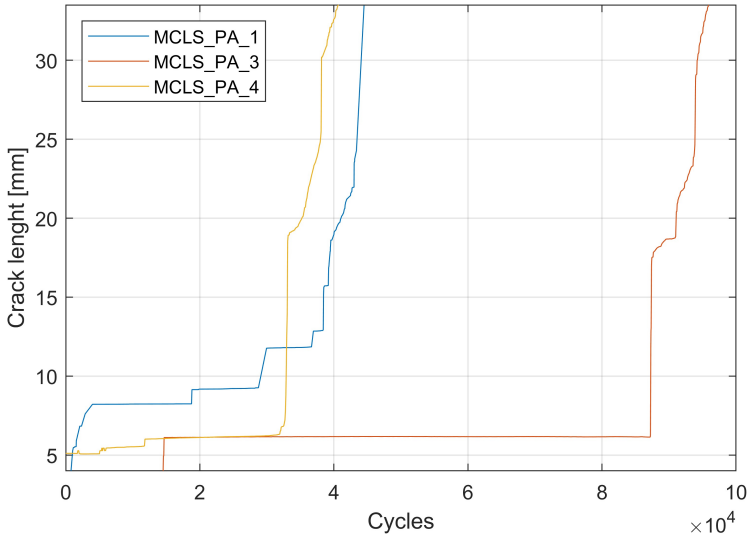

Figure 7.10: Crack growth as function of the number of cycles for the MCLS specimens with the paste adhesive

In the case of the paste adhesive, a combination of pure adhesive failure and adherend failure is observed, as clearly visible in Figure 7.11c. As for the film adhesive, failure occurred in the adherend around the plies not aligned with the load (45°/135°/90°), while around the main load-bearing plies (0°) the adhesive failed.

7.4.3. Adhesive selection

Considering the results presented in subsection 7.4.1, it is evident that the film adhesive demonstrated a superior performance, allowing for a significantly slower crack propagation. When tested at a maximum load of 10 kN, the film adhesive specimens hardly showed any crack propagation (even after hundreds of thousands of cycles), while the paste adhesive specimens allowed cracks to propagate and lead to failure in a rather limited time frame. Additionally, when tested at 13.1 kN, the film adhesive specimens showed a steady crack propagation behaviour (at least below ≈60000 cycles), while the paste adhesive specimen quickly failed — in an abrupt manner, without allowing to observe any steady crack propagation — after a few thousands of cycles. Do note that MCLS_FA_5 and MCLS_PA_3 had a comparable end-of-life. However, the film adhesive specimens were fully tested at 13.1 kN; whereas, for the paste adhesive specimens, the maximum load was ≈30% lower for roughly half of the testing time.

Considering the results presented in subsection 7.4.2, the paste adhesive specimens also showed a less preferable failure behaviour. In fact, pure adhesive failure was observed, and this is far from ideal considering that — as already mentioned in subsection 2.5.2 — this failure mode is not allowed by the applicable regulations.

The difference between the two adhesives can be most likely explained by the different nature of the two materials, and thus their different response to fatigue. In addition, the film adhesive embeds a thermoplastic fabric, which allows for the adhesive to be applied in film form and should also ensure a constant adhesive thickness (although it does not seem very effective in this regard, considering Figure 7.6). This feature may contribute to significantly slowing down crack propagation.
Nonetheless, it is worth pointing out some additional aspects that might have had a minor

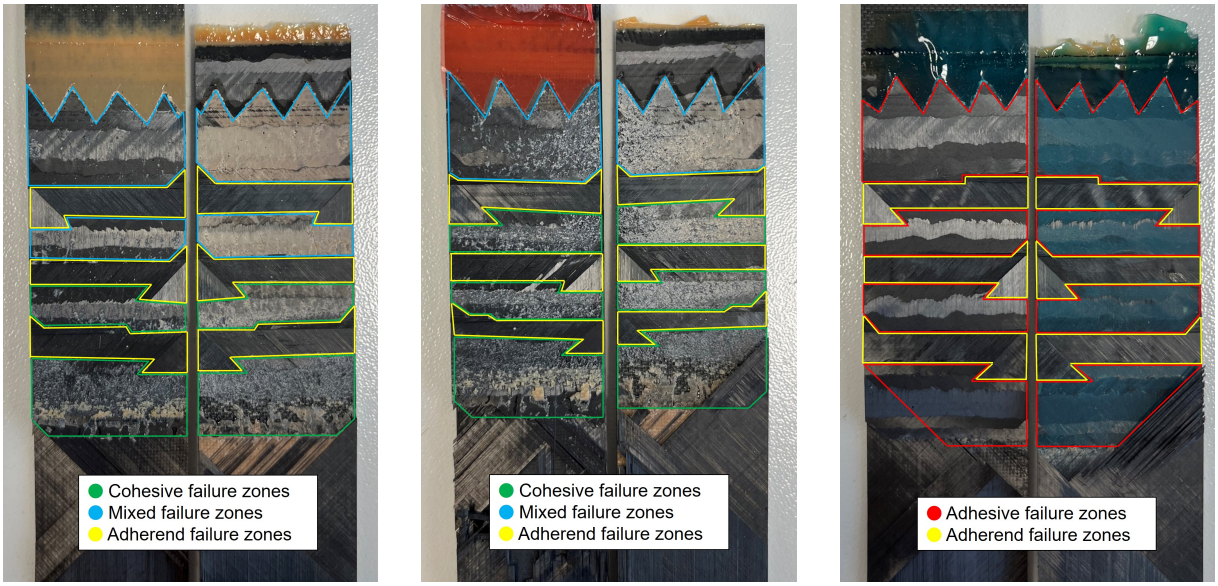

(a) Film adhesive **(b)** Film adhesive **(c)** Paste adhesive

Figure 7.11: Fracture surfaces and failure modes for the MCLS specimens with film and paste adhesive

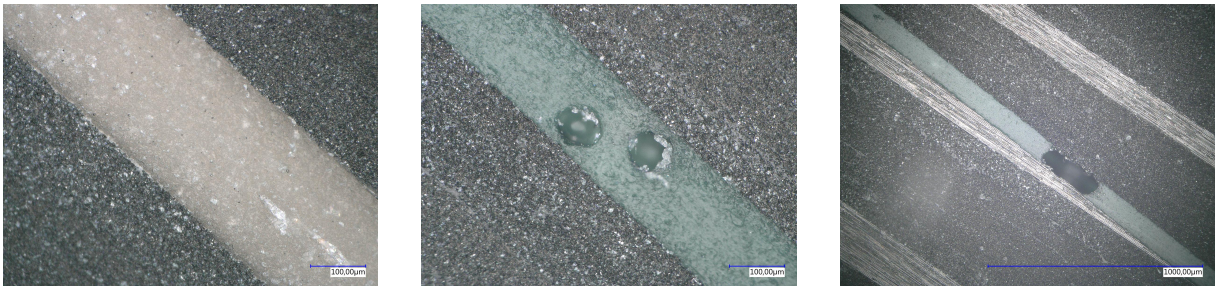

(a) Film adhesive **(b)** Paste adhesive, bubbles **(c)** Paste adhesive, void

Figure 7.12: Micrographs depicting imperfections — or the lack of — in the bondline of the MCLS specimens

influence on the results, despite none of these seem capable on its own — or even combined — to justify the major discrepancy. First, as shown in Figure 7.6, the paste adhesive bondline was generally thicker in all the specimens, albeit more consistent along its length. Second, a higher number of voids/imperfections was observed in the paste adhesive specimens while analysing their sides with the optical microscope (few sample images are shown in Figure 7.12). The void content was not properly estimated, and the bond areas were not inspected in their entirety. Nonetheless — based on what was observed on the sides — it is reasonable to assume that the paste adhesive specimens had a higher void content than the film adhesive ones. Third, the tabs were glued to the specimens with an adhesive that was cured at 121°C, which happens to be right below the glass transition temperature of the paste adhesive (122°C – 124°C). This means that the paste adhesive is likely to have entered its glass transition phase while the tabs were being bonded. Since the paste adhesive was not subjected to any mechanical load during this phase, this most likely did not have any consequence. Nevertheless, a deeper analysis should be performed in order to confirm this assumption.

Based on the results and considerations presented in this section, the film adhesive was selected and thus used for the EN6066 specimens, whose production and testing is discussed in the upcoming chapters.

8

Specimens production and analysis

This chapter is dedicated to the production and analysis of the EN6066 specimens. Given that manufacturing aspects may strongly influence the flushness of a scarf repair, it is worth presenting some details of this phase. First, the key manufacturing details are covered; then, the quality of the final specimens is discussed, with a special regard for their surface finish and level of flushness.
Figure 8.1 provides an overview of the EN6066 specimens manufacturing steps, some of which are then further presented in this chapter. Do note that section 8.1 applies to the MCLS specimens as well, being the two types of specimens manufactured with the same laminates.

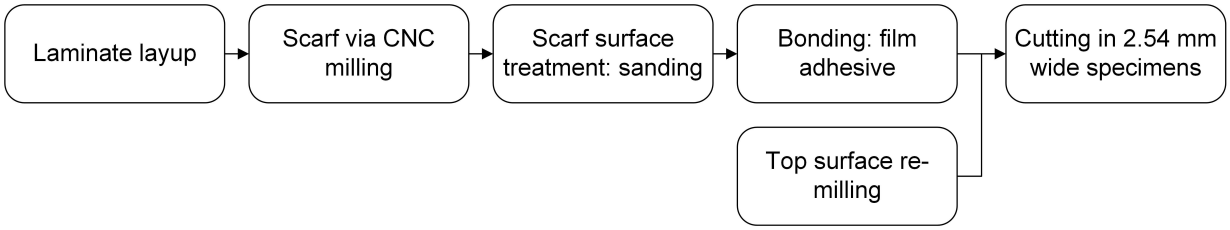

Figure 8.1: Flowchart depicting the manufacturing steps of the EN6066 specimens

8.1. Laminate production

This section briefly describes the manufacturing phase of the laminates, including the scarfing procedure and its surface treatment. Only the most relevant details and parameters are presented, nonetheless the applicable documents that detail the followed procedures are referenced.

8.1.1. Layup

As already mentioned, the specimens were manufactured with 8552/IM7 matrix-fibre combination, which is available — among the others — as uni-directional pre-preg in the form of 7.5 cm wide tapes (HexPly® 8552/IM7 12k UD from Hexcel Corporation, Stamford, Connecticut, United States [86]). The physical and mechanical properties of the pre-preg are listed in Table 8.1. The laminates were hand-laid up following the applicable Airbus procedure [87].

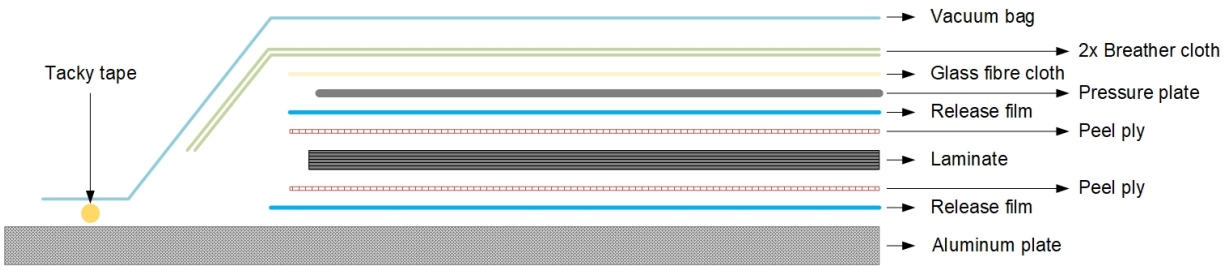

Figure 8.2: Vacuum lay-up followed for the produced laminates (thicknesses not to scale)

Table 8.1: Physical and mechanical properties of the uni-directional pre-preg HexPly® 8552/IM7 at ambient conditions (dry, 25°C) [86]

Property	Value	Unit
Physical properties		
Fibre density	1.77	[g/cm³]
Resin density	0.30	[g/cm³]
Nominal fibre volume	5%	[-]
Mechanical properties		
0°Tensile strength	2724	[MPa]
90°Tensile strength	64	[MPa]
0°Tensile modulus	164	[GPa]
90°Tensile modulus	12	[GPa]
0°Tensile strength	1690	[MPa]
0°Tensile modulus	150	[GPa]
In-plane shear strength	120	[MPa]

8.1.2. Curing

The used vacuum build up is depicted in Figure 8.2, once again in accordance with the applicable Airbus procedures. The curing cycle is shown in Figure 8.3, this is based on the manufacturer's data sheet and on applicable Airbus procedures [86], [87].

8.1.3. Scarf

The scarf was created using CNC milling system comprising a 6-axis robot (KR 6 R900 sixx from Kuka AG, Augusburg, Germany) equipped with a high-frequency milling head, a force/torque control and a laser scanner. The adopted milling parameters are shown in Table 8.2

Table 8.2: CNC milling parameters used for creating the scarf edge in all the manufactured specimens

Parameter	Value	Unit
Milling tool diameter	8	[mm]
Path offset	0.5	[mm]

Revolutions	12000	[rpm]
Feed rate	2	[m/min]
Lubrication	None	[-]

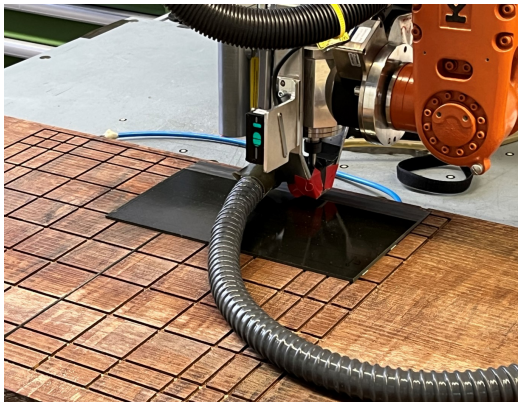

(a) Milling head on the robot arm

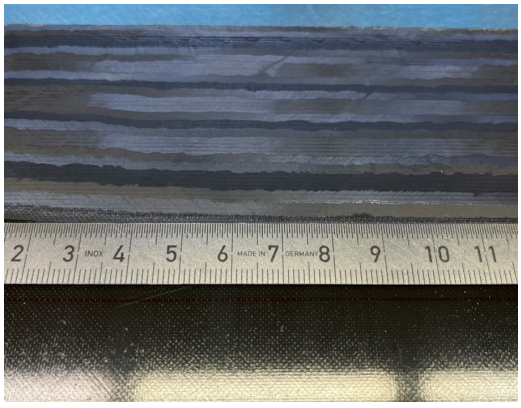

(b) Top view of a scarf surface

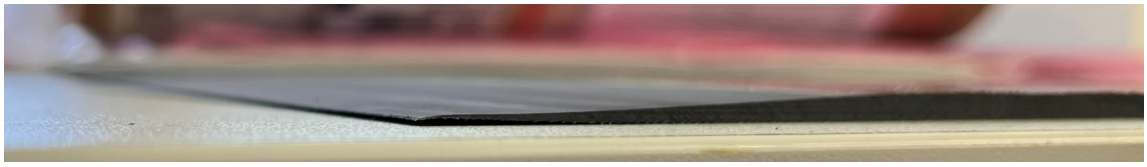

(c) Curvature of the scarf edge of a laminate

Figure 8.4: Creation of the scarf surface via a CNC milling procedure

It is worth noticing that — as evidently depicted in Figure 8.4c — the laminates tend to distort towards their edge. This is due to the fact that milling causes the laminates to lose their symmetry and balance.

8.1.4. Surface treatment

The scarf bonding area was treated via a manual sanding process using Scotch-Brite™ pads from 3M Company (Saint Paul, Minnesota, United States) as abrasive material, in accordance with a qualified Airbus procedure [88].
This method was selected for two main reasons. First, because of its proven effectiveness in removing surface micro-cracks and imperfections — originated by the milling procedure — that may act as damage initiators. Second, the specimens manufactured in previous studies underwent this surface treatment. Therefore — for the sake of test data comparability — it was reasonable to stick to the same method. The other option taken into consideration was atmospheric plasma treatment, which is especially appealing due to the absence of required manual work and thus the superior repeatability. This advantage was however outweighed by the two reasons mentioned above, especially considering that carefully following the relevant procedures allows to obtain consistent results, despite the involvement of manual work.

The scarf surfaces were treated according to the following steps. First, they were thoroughly cleaned with acetone and virtually divided into strips with an approximate width of 10 cm, as shown in Figure 8.5. Then, ensuring that both the surface and the abrasive pad were constantly

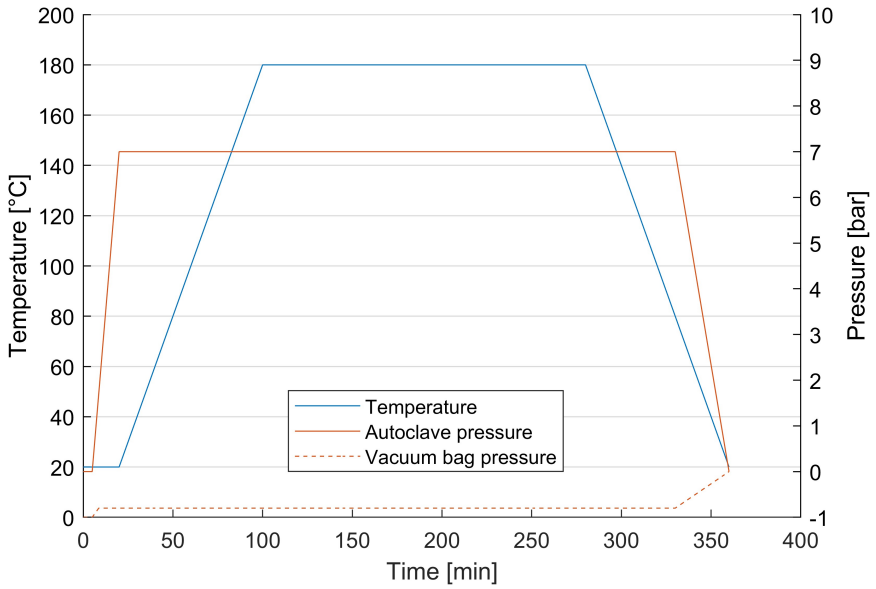

Figure 8.3: Autoclave curing cycle for the 8552/IM7 laminates [86], [87]

wet with deionized water, each stripe was abraded moving the pad 15 times back and forth — without lifting it from the surface and without applying pressure — and then rinsed with deionized water. Next, in the same fashion, the total area was abraded moving the pad 30 times back and forth. These steps were performed in four different directions; the first one (0°) is shown in Figure 8.5, the remaining ones are 90° and ±45°. The surface was then cleaned with isopropanol, deionized water and then left to dry for 45 minutes before applying the adhesive.

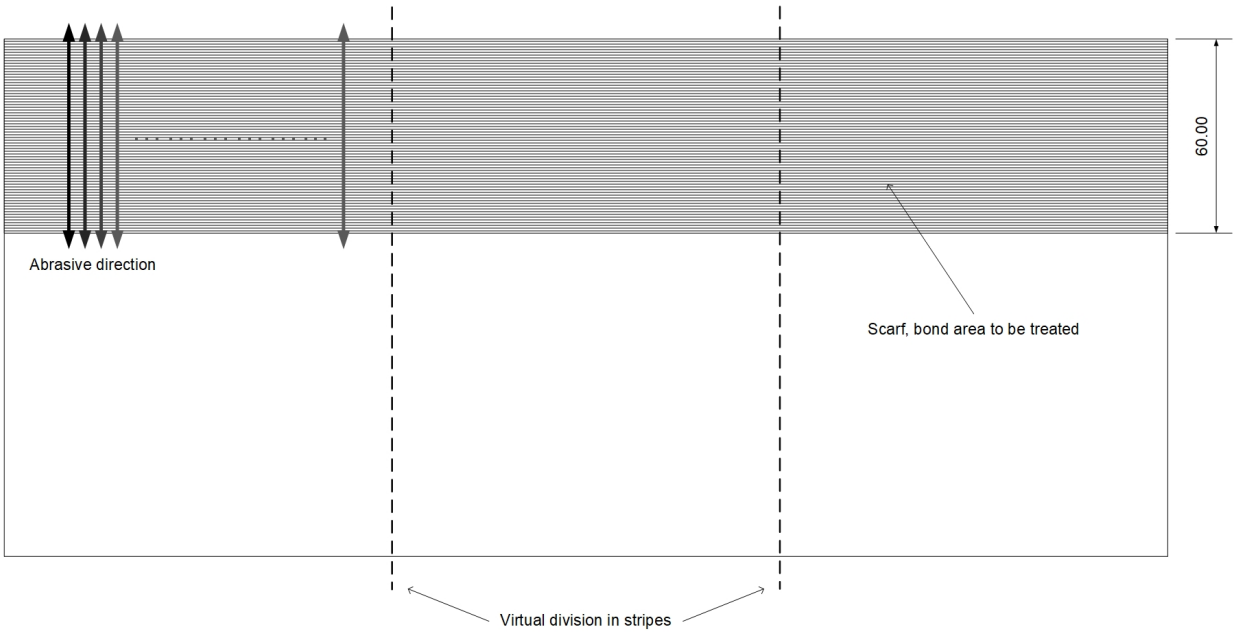

Figure 8.5: Division into strips and first sanding direction for the surface treatment (dimensions in mm)

8.2. Repair concepts implementation

This section describes the relevant manufacturing aspects for the different repair concepts. For the re-designed, thinner patch, also the design process that led to the definition of the layup is presented.

8.2.1. Conventional patch specimens

Figure 8.8 represents two steps in the manufacturing of scarf repairs with the conventional patch: Figure 8.6a shows the positioning of the adhesive layer while Figure 8.6b depicts the alignment of the repair patch. The adhesive is then cured under vacuum in an oven at 121°C for 120 minutes, with a heating and cooling rate of 1.5 °C/min (in accordance with the manufacturer's and Airbus' guideline).

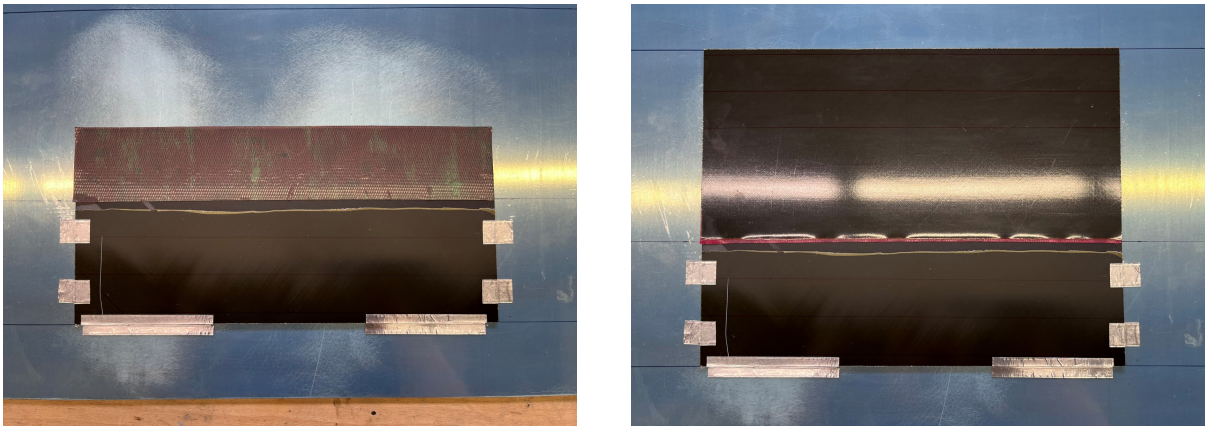

(a) Positioning of the adhesive film

(b) Alignment of the patch

Figure 8.6: Manufacturing of the scarf repair with the conventional patch

In order to obtain the best possible outcome in terms of surface flushness, the edge of the patch was precisely aligned with the beginning of the scarf area in the parent laminate (i.e. 6 cm from the parent laminate edge). A series of lines were marked on the support aluminum plate in order to guide and ease the positioning of the patch, as visible both in Figure 8.6a and 8.6b.

8.2.2. Re-milled patch specimens

The re-milled specimens are assembled like the conventional ones shown above (i.e. via the following steps: adhesive placement, patch positioning and alignment, and adhesive curing), their surface is then milled. Figure 8.7 shows two stages of the manufacturing procedure: Figure 8.7a depicts the repaired plate prior to re-milling, while Figure 8.7b shows the plate after this post-processing procedure (once already cut into single specimens).

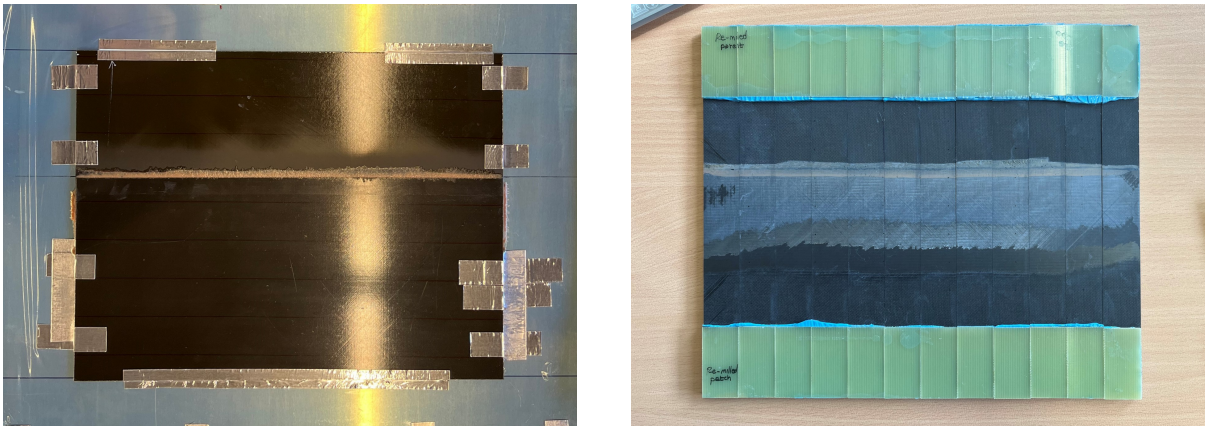

(a) Repaired laminate before re-milling

(b) Specimens after re-milling

Figure 8.7: Manufacturing of the scarf repair with the re-milled patch

The following procedure was adopted to re-mill the repaired surface. First, only the region where the parent laminate and the patch overlap were milled, in order to remove most of the excess material. Second, the complete plate was milled over to eventually remove any other remaining imperfection.
The robot arm was programmed to constantly maintain the vertical coordinate, which was set equal to the thickness of the parent laminate far away from the repaired region. The same set-up and milling parameters mentioned in subsection 8.1.3 were used. Compared to the previous work where the same procedure was implemented [5], the following was changed: first, the panel was positioned as close as possible to the robot, so that the arm did not have to extend significantly: this is relevant given that the stiffness of the robot arm — and so its accuracy — tends to decrease as the arm is extended further away. For the same purpose, the milling path was also changed (the robot arm was closing in rather than stretching out) so that the repaired region was within the area where the robot accuracy is maximum. Also, the robot elasticity was compensated relying on the force/torque control unit throughout the entire procedure. At last, a new milling tool was used to maximise the precision.

8.2.3. Re-designed patch specimens

This section discusses the design process followed to define the layup of the modified patch, as well as some relevant manufacturing-related aspects.

8.2.3.1. Patch design

This design process followed to define the layup of the thinner, modified patch is presented hereafter. The goal is to determine the plies' orientation in such a way that the resulting laminate behaves as closely as possible to the original one. Therefore, it is intended to minimize the stiffness difference, as well as to preserve similarity in terms of other characteristics. It is also important to mention that the original layup is taken as a starting point: this means that the layup of the modified patch is obtained by removing some plies from the original one. Therefore, the new layup is not defined from scratch. The design process simply comes down to selecting which plies need to be removed from the original layup.

To begin with, it is necessary to define how thinner the modified patch shall be compared to the

original laminate, or — in other terms — how many plies should be removed from the original layup. This is determined analysing the thickness mismatch between the repair region and the unaffected area of the laminate in the previously joined panels. Such measurements are obtained via ultrasonic inspection: the thickness of the components is measured in multiple locations, and the mismatch is determined subtracting the thickness of the unaffected laminate from the one of the repaired area (as later explained in section 8.3).
Based on this analysis, it is determined that the conventional scarf repairs generate a surface unevenness quantifiable at approximately 0.5 mm. Recalling that the thickness of a single ply is 0.125 mm, one can deduce that the number of plies shall be reduced by 4. Therefore, the re-designed patch needs to be built up with 20 plies for a total thickness of 2.5 mm, compared to the 24 plies for a thickness of 3 mm of the parent laminate.
Overall, this number of plies drove the definition of the modified patch layup, together with the aim of achieving the highest possible level of similarity with the parent laminate in terms of mechanical properties. The proposed design procedure mainly relies on the Classical Laminate Theory (CLT), although some qualitative considerations and aspects are also taken into account.
The final layup and its properties are listed in Table 8.3, which also provides a comparison with the original layup chosen for the parent laminates (the removed plies are highlighted in red in the original layup). The complete design process is then described step by step in the following paragraphs.

Table 8.3: Comparison between the layup selected for the modified patch and the original one chosen for the parent laminates

Property	**Original layup, parent laminate**	**New layup, modified repair patch**	
Layup	[45, 135, 0, 0, 45, 135, 90, 90, 45, 0, 135, 90]$_s$	[45, 135, 0, 0, 45, 90, 90, 0, 135, 90]$_s$	
Thickness [mm]	3	2.5	(-16.67%)
E_x [GPa]	60.442	66.452	(+9.94%)
E_y [GPa]	60.442	66.452	(+9.94%)
G [GPa]	2.249	1.899	(-15.56%)

First, it was decided to consider only symmetric layups, thus allowing to de-couple forces and moments (in the frame of the CLT, this means that the B matrix is a zero matrix). Having this feature is generally preferred in composite design, furthermore the parent laminate also possesses this characteristic and it is thus reasonable to preserve it. Based on this assumption, all the possible options to reduce the original layup by 4 plies were defined. The order of the original plies was maintained, and all the possible combinations to remove 4 plies were determined. The number of possible combinations is given by the binomial coefficient, which is defined by Equation 8.1:

$$ {}_nC_k = \binom{n}{k} = \frac{n!}{(n-k)!k!} \tag{8.1} $$

where n represents the total number of plies in the original layup, and k the number of plies to be removed. Since only symmetric layups were considered, the combinations were found for half of the layup ($n = 12$ and $k = 2$). The full stacking sequence was then found by mirroring the half layup. This procedure generated 66 possible options, which were then reduced to 47 unique ones via the elimination of identical layups obtained removing a different combination of two plies.

Second, only quasi-isotropic layups were further considered, thus disregarding all the ones that do not meet this requirement. The rationale behind this design choice is the same as for the previous one: the parent laminate boasts this characteristic, it is thus convenient to maintain it in order to minimize the difference between the original material and the modified patch. This design choice significantly reduced the number of options from 47 to 19.

Third, it was decided to disregard all those options whose Young's Modulus in the load direction (and so in the transverse one as well, being all the remaining layups quasi-isotropic) is lower compared to the parent laminate. This choice is motivated by the load case of the specimens, which were tested in tension. Considering this scenario, it is more reasonable to have higher Young's Moduli and a lower shear modulus, rather than the other way around. This design decision reduced the number of options from 19 to 15.

Then, it was opted to consider only balanced layups, so all those options whose entries A_{16} and A_{26} of the A matrix are zero. This is generally a desirable feature in composite design, since it allows to avoid in-plane coupling. In addition, once again, the original laminate already possesses this characteristic, and it was thus logic to preserve it. This further reduced the number of options from 15 to 9.

At this point, it was decided to disregard all the layups where the plies in the direction of the load (so the 0° plies in this case) were located towards the extremities of the laminate. The reason behind this design choice has already been mentioned in subsection 3.3.3, as explained by Gunnion and Herszberg [31]. To reiterate, it is unfavourable to have the outer-most 0° plies on the extremities of the laminate, since this tends to increase the peak peel stress. In addition, the top/bottom ply might get damaged — although in principle they should not — while removing the peel ply: this constitutes another reason to avoid placing the plies aligned in the load direction on the extremities. This design consideration lowered the number of options from 9 to 4.

At last, the final layup was selected comparing the ABD matrices of the remaining options with the one of the parent laminate. The rationale behind this design choice is the following: since the ABD matrix basically relates the applied loads to the associated strains, two laminates with similar ABD matrices should behave similarly once loaded. The comparison was based on the Euclidian distance, which is defined by Equation 8.2, where — in this specific case — q_i and p_i represent corresponding entries of the two matrices to be compared, and n the total number of entries. This distance was calculated with respect to the original laminate's ABD matrix for each of the remaining option. The layup with the lowest Euclidian distance from the reference matrix was then selected and used for the modified patch.

$$d(p,q) = \sqrt{\sum_{n=1}^{n} (q_i - p_i)^2} \tag{8.2}$$

It must be noted that — at this stage — the A matrix is the same for all the remaining options, therefore the differences are determined by the D matrix (being the B matrix a zero matrix for quasi-isotropic laminates). For this reason, it had also been considered to look at each single entry of the D matrix, and weight them differently in the selection based on the specimens' load case, rather then resorting to a metric such as the Euclidian distance. However, this procedure had been deemed less appropriate since the D matrix is more relevant when dealing with bending or flexural behavior, and thus it does not directly influence the axial behaviour, which is primarily controlled by the A matrix. Therefore, it is not straightforward to understand which D entry plays a more dominant role in the considered loading scenario, and thus which should be given priority

in the selection. Therefore, using a metric such as the Euclidian distance, able to give a more comprehensive idea of the similarity between two matrices, seemed more appropriate.

8.2.3.2. Patch alignment

These specimens were manufactured according to the steps already mentioned in the previous two cases, i.e. adhesive placement, patch positioning and alignment, and adhesive curing. Figure 8.8 shows two stages of such procedure: Figure 8.8a depicts the patch alignment, while Figure 8.8b shows the adhesive's curing phase — which was performed under vacuum.

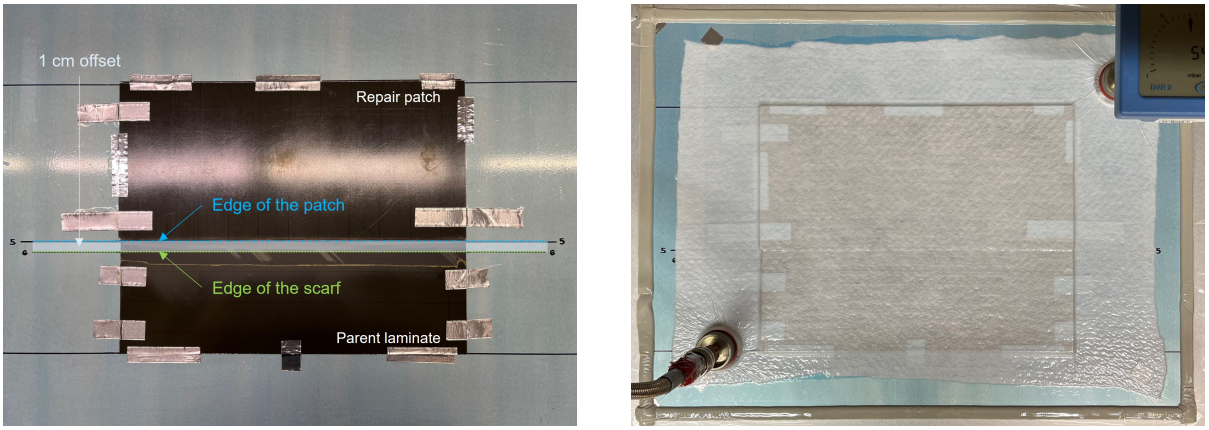

(a) Patch alignment

(b) Plate curing under vacuum

Figure 8.8: Manufacturing of the scarf repair with the re-designed patch

In order to obtain a flush surface finish with the re-designed patch, it is necessary to align it precisely. As clearly visible in Figure 8.8, several lines were marked in order to help precisely positioning the patch. It must be noted that — due to the lower thickness of 2.5 mm, compared to the 3.0 mm of the parent laminate — the length of the scarf area in the re-designed patch is 5 cm (the same feature is 6 cm in the parent laminate), since the scarf ratio remains 1:20. Therefore, as visible in Figure 8.8a, the edge of the patch needs to be aligned with an offset of 1 cm with respect to the edge of the scarf in the parent laminate. In this way, the parent laminate and the patch result levelled, while a small surface depression — whose size will be shown in subsection 8.3.3 — is present along the 1 cm offset.

8.3. Surface flushness

Being this phase of the thesis primarily focused on optimizing the surface finish of scarf repairs for flushness, this feature needed to be measured. This was done via ultrasonic analysis, with the pulse-echo method. The thickness of the bonded panels (prior to being cut into single specimens) was measured in multiple locations using a hand-held probe. In this way, it was possible to quantify the surface flushness, in terms of the thickness offset generated by the repair patch. Figure 8.9 marks the locations on the plates where the thickness was measured. During this procedure, it was also verified that no major porosities, voids or other kinds of imperfections were present in the bond area.

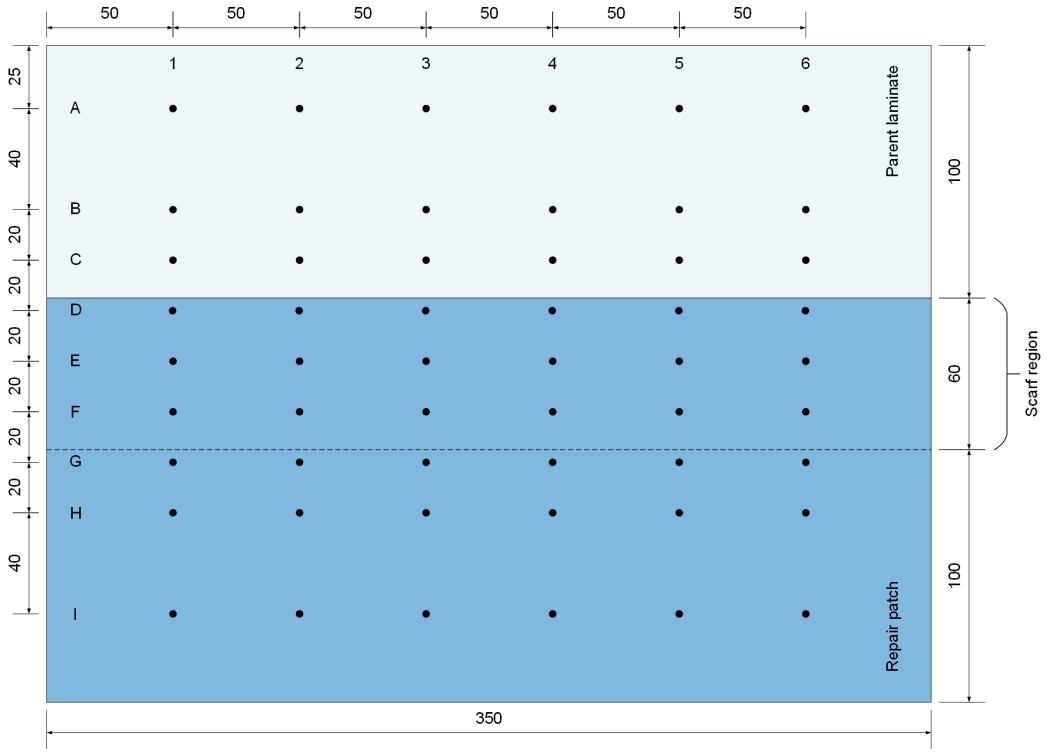

Figure 8.9: Location on the EN6066 plates where the thickness was measured via ultrasonic inspection (dimensions in mm)

The thickness offset generated by the scarf repair was then obtained subtracting the average thickness of the undamaged section (i.e. the average of measurements A1 to C6, referring again to Figure 8.9) from the average thickness of the repaired section (i.e. the average of measurements D1 to F6). Table 8.4 provides an overview of such values for the three different repair patch concepts considered in this work.

Table 8.4: Thickness and surface flushness of the different repair patch concepts (* quantified with respect to the flushest conventional patch, ** this second conventional patch is the plate that was later re-milled)

Patch concept	**Thickness** [mm]			**Improvement***
	Undamaged region	Repaired region	Offset	
Conventional	3.06	3.48	0.42	-
Conventional**	3.08	3.60	0.52	-
Re-milled	3.09	3.18	0.09	≈80%
Re-designed	3.11	3.08	-0.03	-

It must be noted that quantifying the repair flushness with this approach comes with a few limitations, which are listed hereafter. First, this approach is an indirect way of assessing the surface flushness and might thus result imprecise, especially considering that measurements are taken at discrete points and not continuously along the entire surface.
Second, this approach only measures the plates' thickness, implying that eventual voids originated by the alignment of the two hard plates on the bottom side — which would negatively affect the surface flushness — would not be identifiable.

Moreover, for stealth purposes it is important to have a continuously smooth surface, free of any sharp steps or edges. In other words, having an extremely consistent thickness is not so crucial as long as the change is progressive, and no sudden changes are present. The measurement approach adopted here does not allow to precisely measure this aspect, nonetheless it is clear that the re-milled patch is superior in this regard. The full surface is indeed re-worked and smoothed, while both the reference and modified patch showcase more abrupt transitions at the interface between the patch and the parent laminate. The same can not be said for the modified patch: the offset is negative because of a small concavity at the interface between the parent laminate and patch (depicted in Figure 8.10), generated by the different scarf length caused by the different layup (for this reason, no percentage improvement is given in the table).
In addition, the thickness of the plates is calculated based on the waves' time of flight in the laminates, and their propagation speed in the selected material (so, in this case, 8552/IM7). However, in this specific instance, the plates also contain an adhesive bondline, where the wave propagation speed is different from the one of the CFRP. This aspect is not accounted for in the determination of the thickness, which may thus be not fully accurate. However, this seems to have a negligible impact, since the ultrasonic measurements are in agreement with the ones manually taken with a caliper on the edges of the plates. Additionally, even if this aspect was not negligible, it would not affect the comparison of the different concepts — being a sort of systematic measurement error — but only the accuracy of the values in absolute terms.

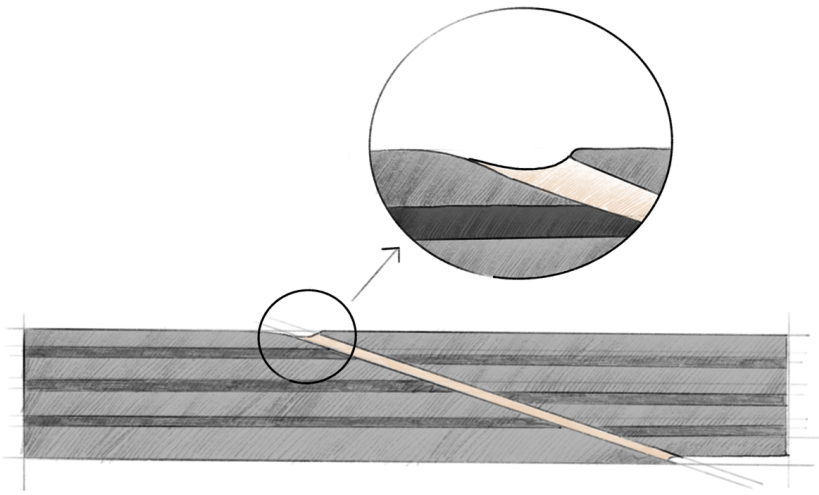

Figure 8.10: Sketch of the modified patch configuration, depicting the concavity at the interface between the parent laminate and the repair patch

8.3.1. Conventional patch specimens

Figure 8.11 plots the thickness measurement for the plate repaired with the conventional patch. These plots are obtained interpolating the individual measurements recorded at the locations depicted in Figure 8.9. In more detail, Figure 8.11a provides a top view of the plate, while a side view — clearly showing the profile of the surface — is depicted in Figure 8.11b.

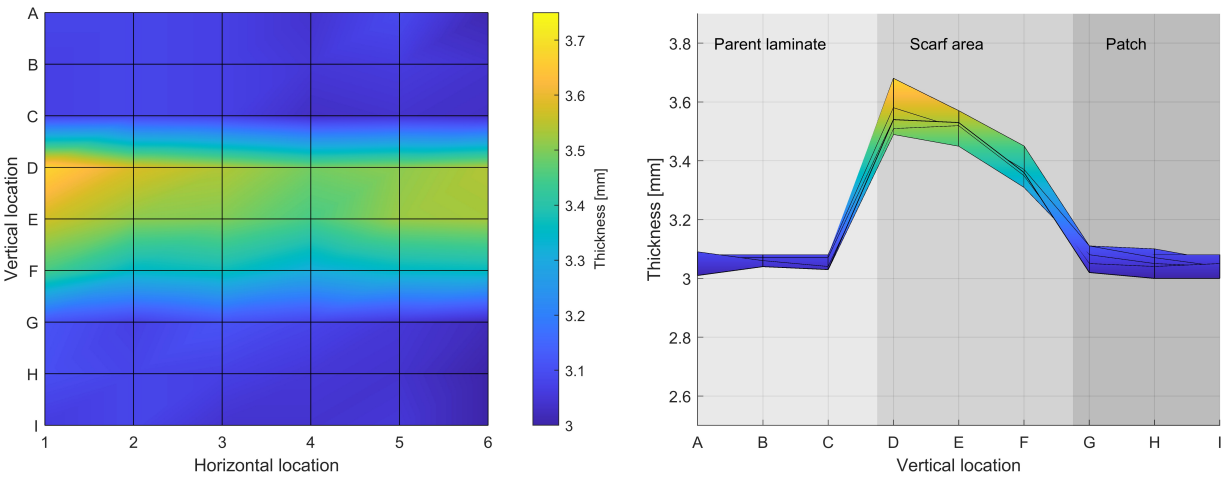

(a) Top view of the plate

(b) Side view of the plate

Figure 8.11: Surface flushness of the plate repaired with the conventional patch

It is clearly noticeable how the main surface thickness increase is located on the overlap between the parent laminate and the patch — especially at the very beginning — along the scarf surface. This can be also clearly noticed in Figure 8.12a, which shows a side view of the beginning of the scarf area. A portion (roughly 2x4 cm) of the top surface was 3D-scanned, the results are shown in Figure 8.12b and 8.12c.

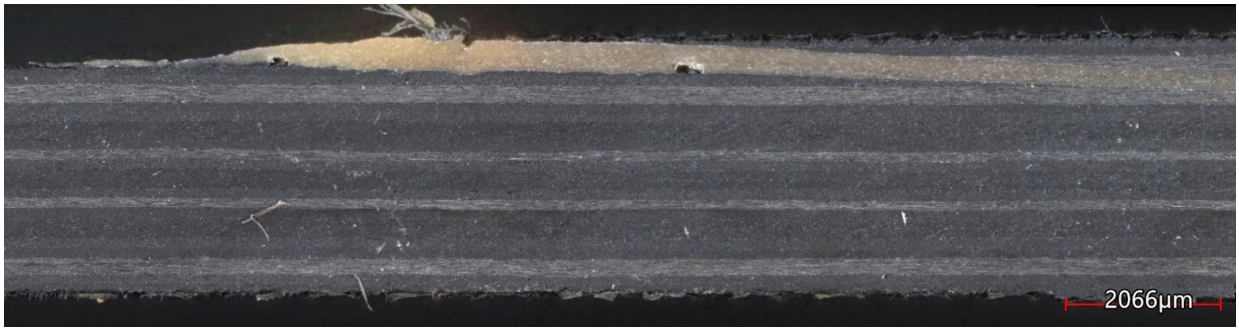

(a) Photomicrograph depicting a section view in the transition area between parent laminate and repair patch

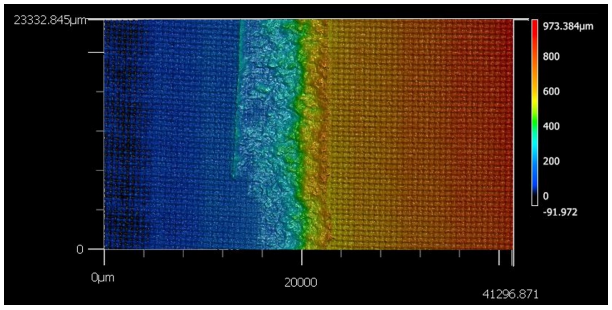

(b) 3D scan of a portion of the top surface in the transition area between parent laminate and repair patch

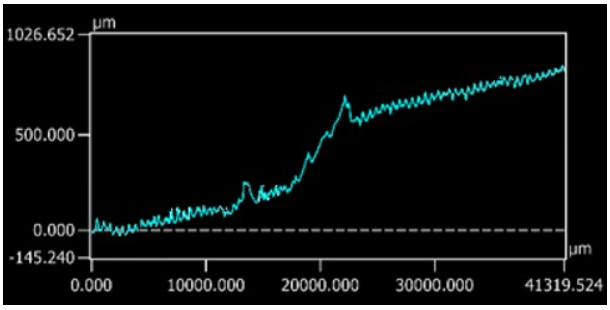

(c) Thickness of a portion of the top surface in the transition area between parent laminate and repair patch

Figure 8.12: Side view and top surface analysis of a conventional patch specimen, obtained with a laser microscope

This scan also provided an alternative measure for the mismatch between the parent laminate and the patch: while the order of magnitude matches the ultrasonic measurements, a certain

discrepancy is observable in terms of magnitude — which is generally higher. In this regard, the following considerations can be made. First, the laser scan can achieve a higher accuracy, measuring smaller features that cannot be caught with the ultrasonic setup used here. In addition, the laser scan continuously measured the entire scanned surface, while the ultrasonic scan measured the full plate but only in a limited number of discrete locations. However, the 3D scan was limited to a small region, while the ultrasonic analysis covered the entire plate, thus resulting overall more representative. In any case, a full laser scan of the entire surface would surely be more accurate and is thus recommended for future investigations.

8.3.2. Re-milled patch specimens

Figure 8.13 plots the thickness measurements for the plate allocated to be re-milled, before performing such procedure. Therefore, this figure represents fundamentally a plate repaired with a conventional patch, hence the similarity with Figure 8.11.

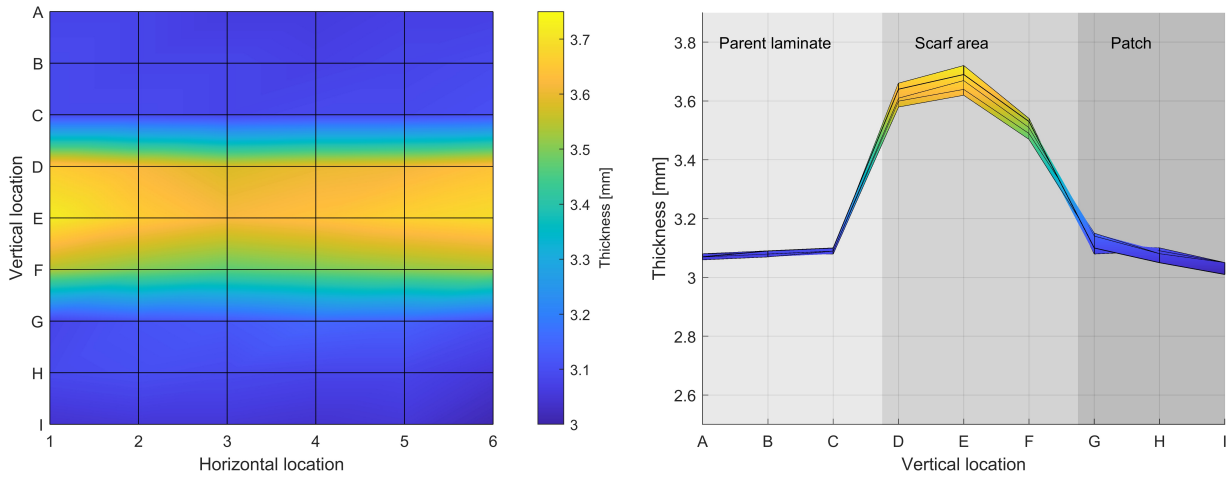

(a) Top view of the plate

(b) Side view of the plate

Figure 8.13: Surface flushness of the plate repaired with the re-milled patch, before re-milling

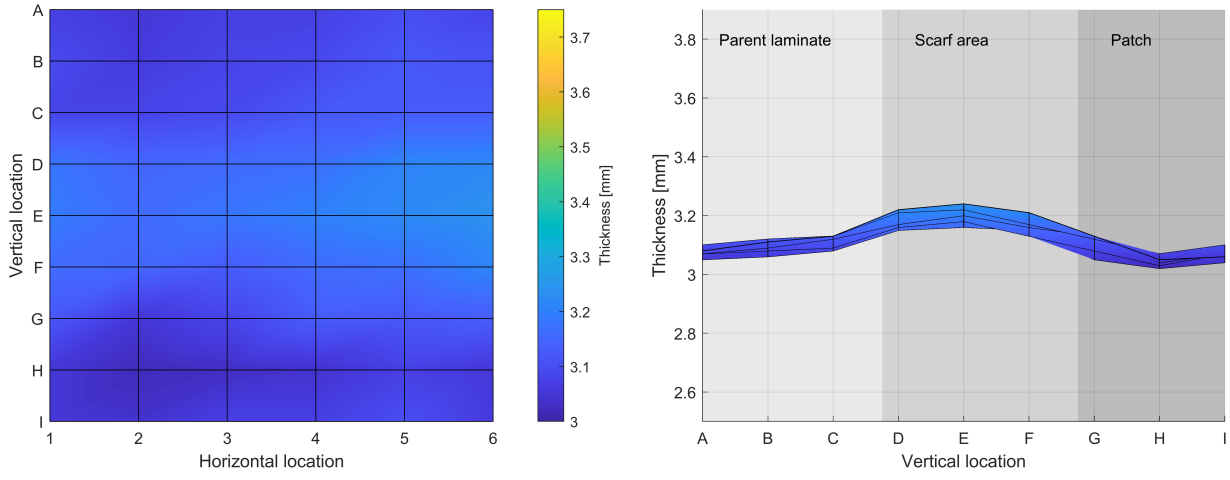

(a) Top view of the plate

(b) Side view of the plate

Figure 8.14: Surface flushness of the plate repaired with the re-milled patch, after re-milling

Whereas, Figure 8.14 plots the thickness measurements for the plate after the re-milling procedure was completed. In this way, it is possible to directly show the improvement achievable with such process. Also in this case, an interpolation of the measurement points is depicted, Figure 8.13a and 8.14a show a top view of the plate, while Figure 8.13b and 8.14b a side view.

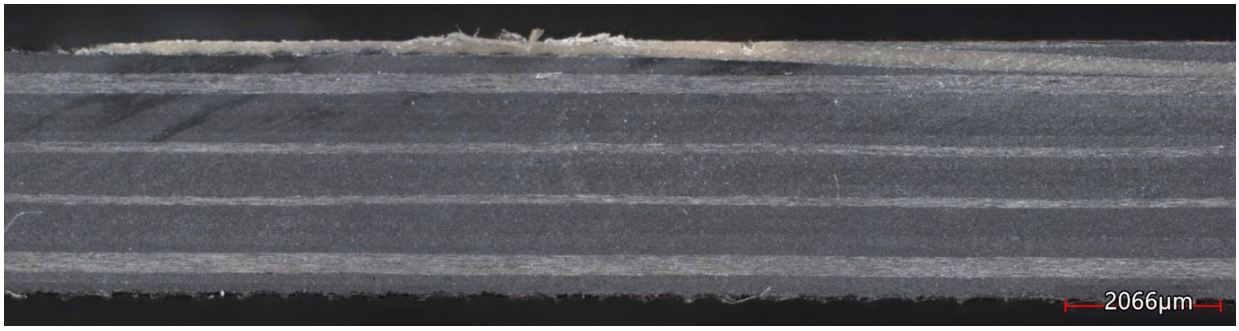

(a) Photomicrograph depicting a section view in the transition area between parent laminate and repair patch

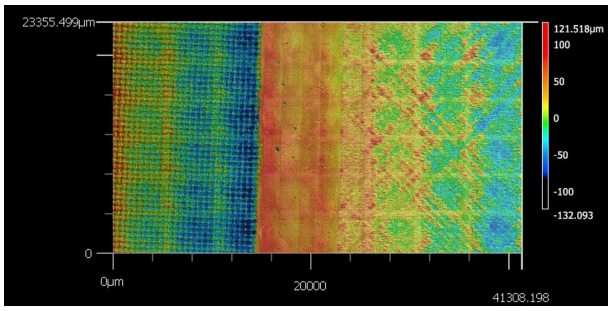

(b) 3D scan of a portion of the top surface in the transition area between parent laminate and repair patch

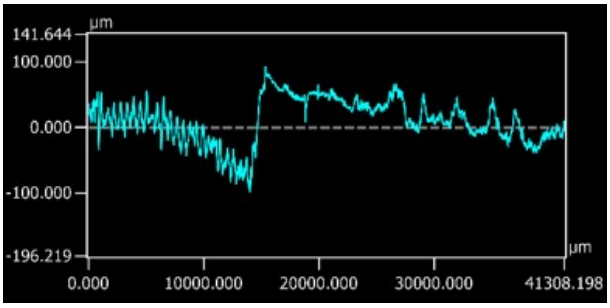

(c) Thickness of a portion of the top surface in the transition area between parent laminate and repair patch

Figure 8.15: Side view and top surface analysis of a re-milled patch specimen, obtained with a laser microscope

8.3.3. Re-designed patch specimens

Figure 8.16 plots the thickness measurement for the plate repaired with the modified patch. Figure 8.16a shows a top view of the plate, while Figure 8.16b a side view.

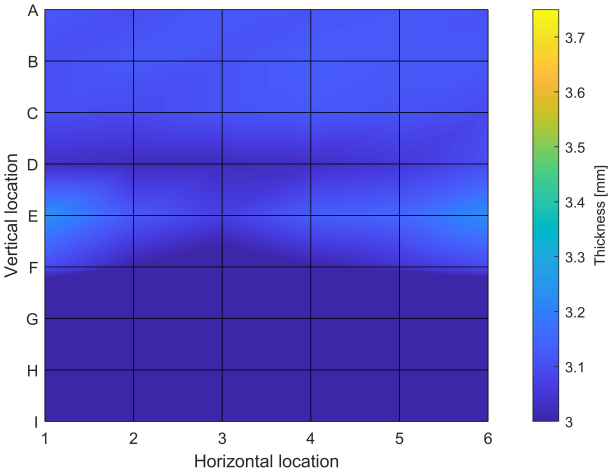

(a) Top view of the plate

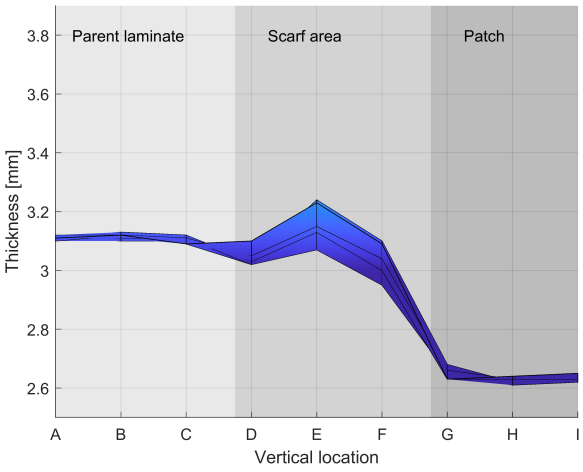

(b) Side view of the plate

Figure 8.16: Surface flushness of the plate repaired with the modified, thinner patch

Figure 8.16b seems to clearly suggest that the plate is not flat — in other words that the parent laminate and the patch are not flush — since the thickness after the scarf area (from F to I, considering Figure 8.16b) is lower than that before the scarf (from A to D, considering Figure 8.16b). This is due the aforementioned limitation of assessing the surface flushness based on the thickness of plates rather than analysing the surface directly. In reality, a thin empty gap (visible in Figure 8.10) remains on the bottom side of the repaired plate, while the top surface is completely levelled (exemption made for the concavity between measurement points C and E, due to the transition between the parent laminate and the patch).
As aforementioned, having this kind of irregularity is detrimental from a stealth standpoint and therefore manual re-work would be most-likely needed to even it out. As for the previous two cases, Figure 8.17a shows a side view of the beginning of the scarf area, while Figure 8.17b and 8.17c depict the results of the 3D scan performed on an area of roughly 2x4 cm (if comparing Figure 8.17c with 8.15c and Figure 8.12c, please notice the difference in scale on the vertical axis).

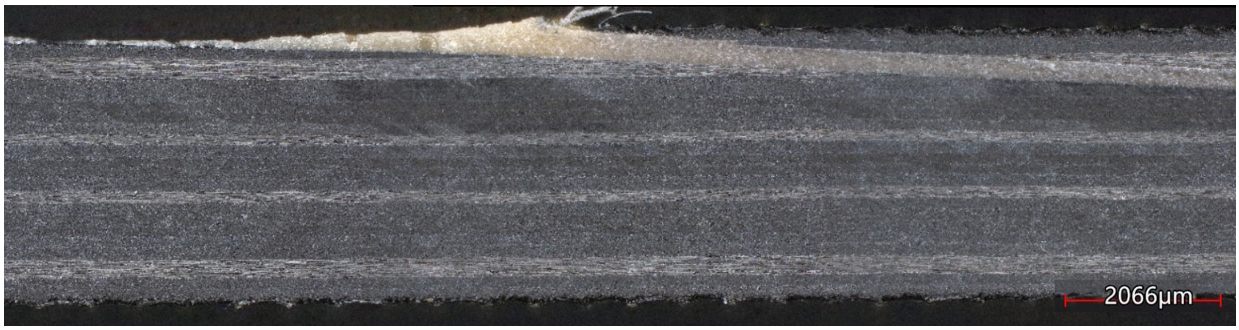

(a) Photomicrograph depicting a section view in the transition area between parent laminate and repair patch

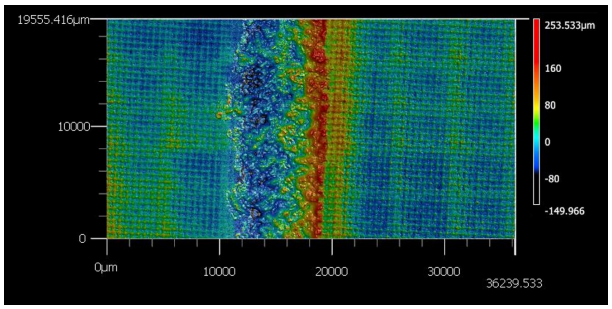

(b) 3D scan of a portion of the top surface in the transition area between parent laminate and repair patch

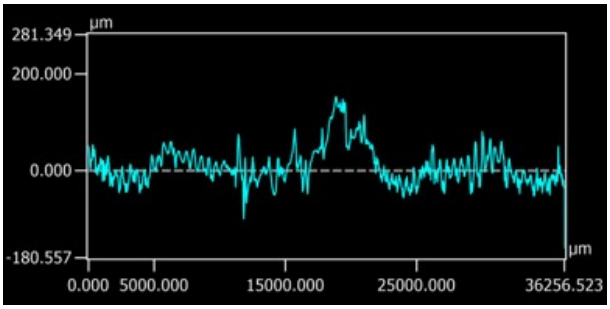

(c) Thickness of a portion of the top surface in the transition area between parent laminate and repair patch

Figure 8.17: Side view and top surface analysis of a modified patch specimen, obtained with a laser microscope

9

Testing and results

In order to assess the mechanical performance of the different repair patches, the EN6066 specimens were tested both quasi-statically and dynamically. This chapter deals with the details and results of this testing phase: first, the quasi-static tests are presented, then the fatigue tests are addressed. The outcomes shown here are then discussed in the next chapter.
For the sake of clarity, it is important to mention that the results of the tests performed in this thesis are presented together with data generated in previous investigations throughout this entire chapter, for comparison purposes. It is also worth remarking that the current work only considered secondary bonded hard patches, and included three repair/patch configurations, namely: the conventional scarf repair (labelled as ”Reference”), the re-milled scarf repair (labelled as ”Re-milled”) and the one using a thinner patch with a different layup (labelled as ”Modified patch”). On the other hand, previous investigations only considered co-bonded soft patches. Nonetheless, all the specimens adopted the same layup and the same scarf ratio. In more detail, Scholz [5] tested both conventional repairs and re-milled repairs in 2021, Keil [48] only considered conventional repairs in 2019, while D’Arduini [4] only tested re-milled specimens in 2022. The source of such test data is clearly labelled in all the plots presented throughout this chapter.

9.1. Quasi-static tests

The quasi-static tests were carried out using a ZwickRoell Z250 (Zwick GmbH & Co. KG, Ulm, Germany) able to reach loads up to 250 kN, equipped with hydraulic clamping jaws and a DIC system. The strain fields over the specimens’ surface were obtained locally by creating virtual extensometers via DIC (over a length of 1 cm, in the vicinity of the scarf region). The machine was set to tension the specimens at a constant rate of 2 mm/min until failure.
This section presents all the relevant results: failure loads, failure stresses, elongation at break and E-modulus are shown, right before presenting the failure modes and paths. The results are presented in the form of boxplots, each box is determined using at least five data-points — in other words, at least five specimens were tested (either in this thesis or as part of previous ones) for each configuration.

9.1.1. Results

Figure 9.1 shows the ultimate failure load achieved by the various specimens under static, tensile testing conditions. The data are grouped by repair type (i.e. reference, re-milled and modified patch), and further separated based on the type of patch (secondary bonded hard patch or

co-bonded soft path). The year when the various specimens were tested is also provided in the legend.
Generally, the reference specimens failed later than the re-milled specimens, which in turn proved superior to the modified patch specimens. This is most likely due to the different cross-sectional areas in the bond region of the various configurations.

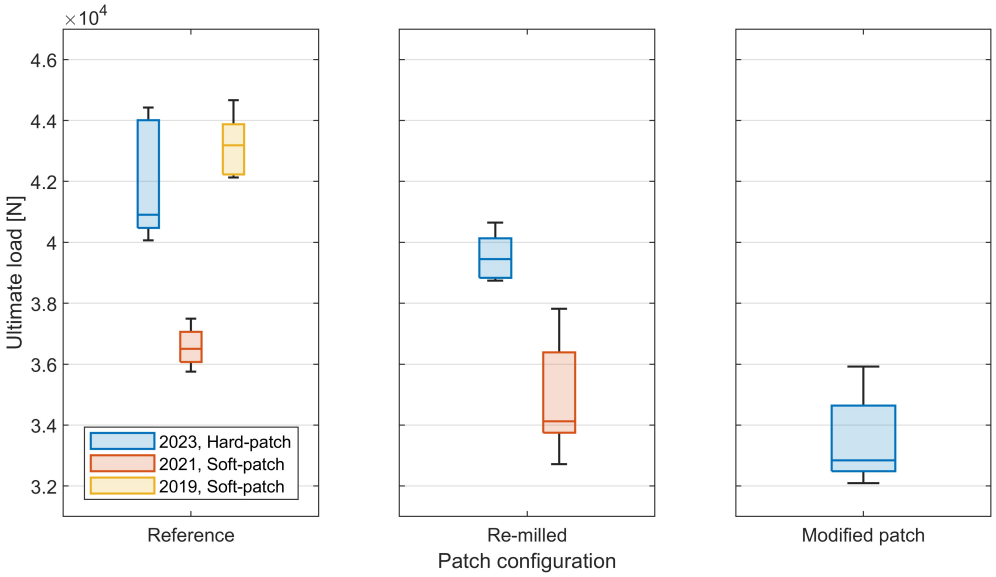

Figure 9.1: Ultimate tensile load reached by the different patch configurations during static testing

Figure 9.2 shows the ultimate tensile strength achieved by the various specimens under static, tensile testing conditions. These were calculated dividing the ultimate load by the cross-sectional area in the region of the overlap. Also in this case, the data are grouped based on both the repair and the patch type, as well as the test date.
Plotting the strength allows to reduce the effect of the cross-sectional area mentioned above. Indeed, the reference specimens appear now more closely matched to the re-milled ones and stronger than the modified patch specimens by a larger margin — but smaller than in Figure 9.1.

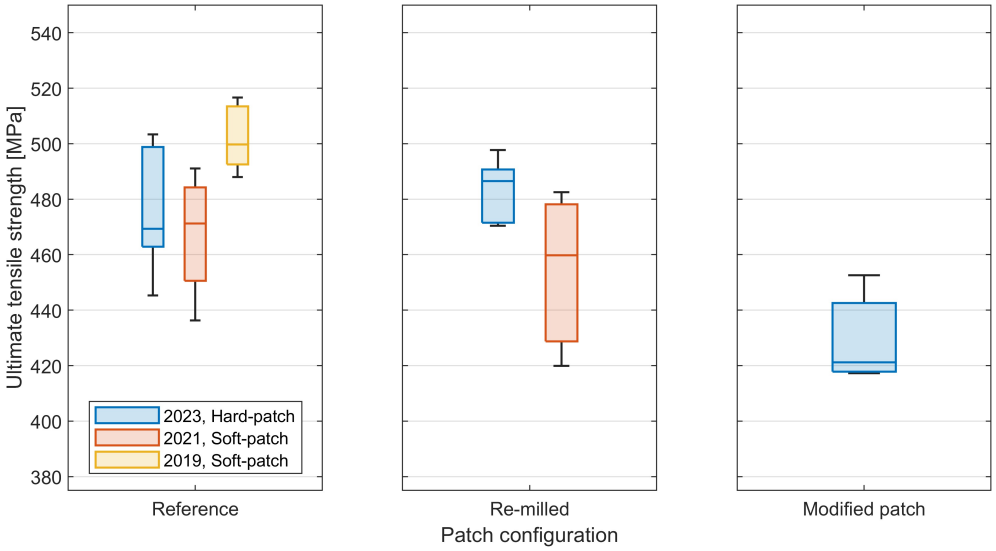

Figure 9.2: Ultimate tensile strength reached by the different patch configurations during static testing

Figure 9.3 shows the elongation at break reached by the various specimens under static, tensile testing conditions. Once again, the data are grouped based on both the repair and the patch type, as well as the test date. It must be noted that different measuring systems were adopted over the years: the tests performed in 2023 relied on DIC, the tests conducted in 2021 used mechanical extensometers, while strain gauges were adopted in 2019.
Generally, all the specimens — regardless of the type of patch and the repair configuration — showcased comparable levels of failure strain. The only exception is represented by the batch of reference specimens tested in 2019: this discrepancy might be explained by the positioning of the strain gauges, which possibly were glued in the vicinity of regions experiencing stress concentrations.

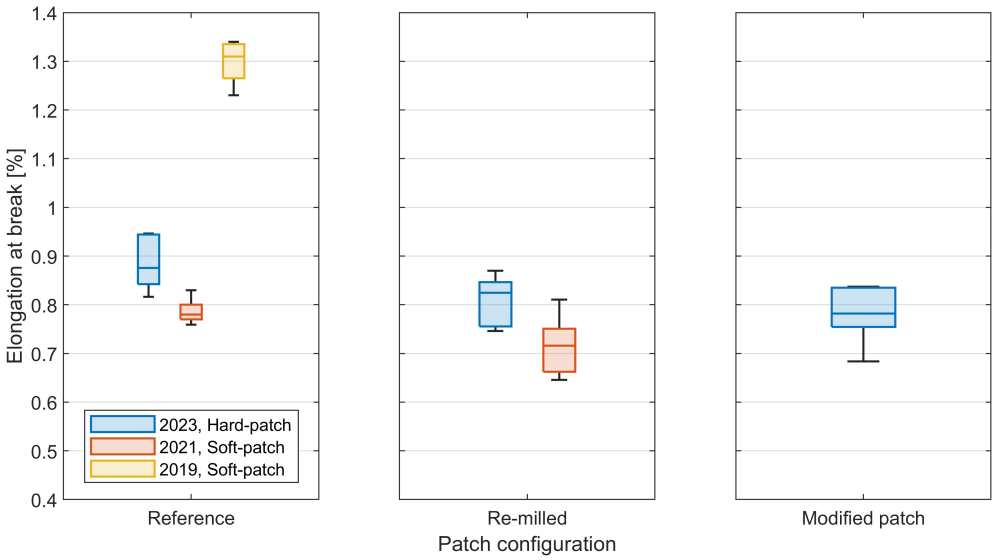

Figure 9.3: Elongation at break reached by the different patch configurations during static testing

Figure 9.4 shows the tensile modulus for the various specimens. Also in this case, the data are grouped based on both the repair and the patch type, as well as the test date. The E-modulus values for each specimen were obtained from their stress-strain curves, according to the applicable standard [89] (which describes how to determine tensile properties from mechanical testing). Therefore, stress-strain values between 1000 με and 3000 με were generally considered, exemption made for the modified patch specimens, whose early deviations from linearity required to take into account a shorter range (between 1000 με and 2000 με).
In this case, the re-milled and modified patch specimens generally show higher values compared to the reference, most likely due to the higher proportion of plies in the load direction (more on that in the upcoming chapter). As noticeable in Figure 9.4, the largest data point for the modified patch specimens is considered an outlier. The following commonly adopted rule was followed: a data point is identified as outlier if it is greater than $Q_3 + 1.5 \cdot IQR$ or less than $Q_1 - 1.5 \cdot IQR$ [90], where Q_3 and Q_1 are respectively the third and first quartile, IQR is the interquartile range (i.e. the range between the first and third quartile) and 1.5 is approximately equal to $\pm 2.7\sigma$ (i.e. a 99.3% coverage) assuming a normal distribution.

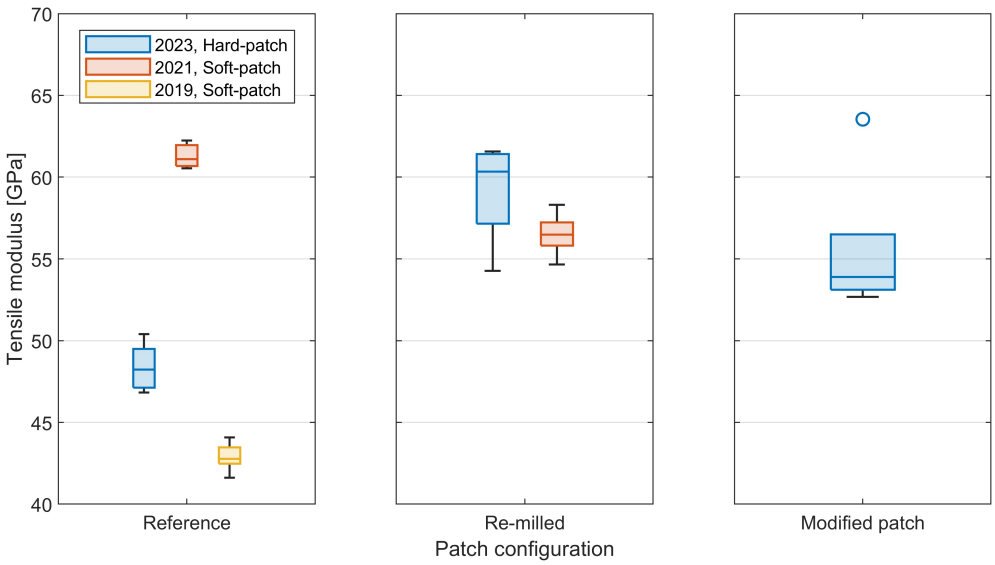

Figure 9.4: Tensile modulus of the different patch configurations, obtained from static testing data

Table 9.1 provides an overview of the static test results presented above. In more detail, the median values for the considered variables are listed for the various specimen configurations. It was chosen to display the median rather than the mean because the test data tend to be skewed, and thus this should provide a more truthful representation. The values for each single specimen are provided in Appendix A.

Table 9.1: Overview of the EN6066 tensile static tests, median values for various relevant parameters

Repair patch			F_{max} [kN]	**UTS** [MPa]	ε_{max} [%]	$\mathbf{E_x}$ [GPa]
Type	Configuration	Year				
Hard	Reference	2023	40.90	469.3	0.87	48.22
Soft	Reference	2021	36.50	471.2	0.78	61.10
Soft	Reference	2019	43.18	499.7	1.31	42.78
Hard	Re-milled	2023	39.45	486.5	0.83	60.33
Soft	Re-milled	2022	34.12	459.8	0.72	56.48
Hard	Modified	2023	32.84	421.2	0.78	53.89

At last, it is important to mention that all the specimens failed well above the required load and stress levels, defined for this specific conditions according to the relevant design guidelines [91]. The critical load and stress — which turn out to be, respectively, 24.31 kN and 319 MPa — are calculated as follows, starting from the Hooke's law:

$$\sigma_{critical} = E \cdot \varepsilon_{critical} \quad \rightarrow \quad F_{critical} = E \cdot \varepsilon_{critical} \cdot A \qquad \text{where} \qquad A = b \cdot t$$

where E is the Young's modulus of the CFRP (HexPly® 8552/IM7), which is estimated to be 58 GPa, according to experimental data provided in Airbus documentation [91]; $\varepsilon_{critical}$ the maximum allowable strain in pure tension (set at 5500 µm/m in [91]), b and t the dimensions

of the specimens' cross-sectional area (namely, 25.4 and 3 mm respectively, as already depicted in Figure 6.3).

9.1.2. Failure mode and path

All the specimens showed a similar failure behaviour, despite presenting some differences especially in terms of fracture path. A combination of cohesive and adherend failure was observed; in addition, delaminations in one — or both — of the adherends were visible in certain specimens. Since all the fracture surfaces look alike, only a representative picture for each specimen configuration is provided here in Figure 9.5, while the pictures for every specimen are given in Appendix A. In addition, Figure 9.6 proposes schematic representations of the different fracture paths observed in the specimens.

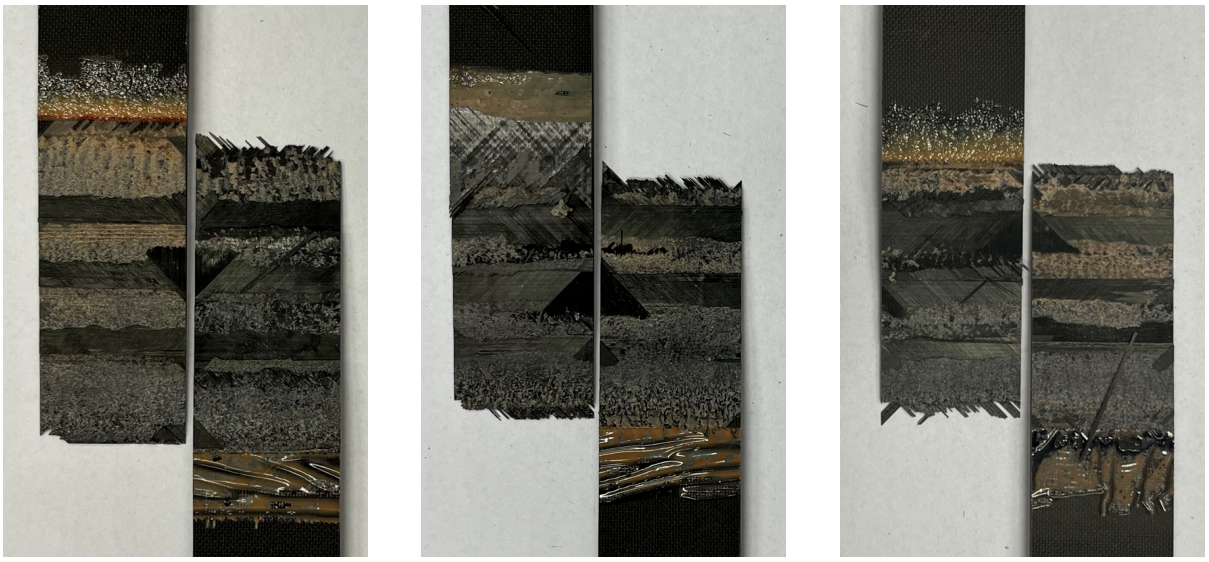

(a) Reference **(b)** Re-milled **(c)** Modified patch

Figure 9.5: Fracture surfaces of the EN6066 specimens, static tests (in every picture: parent laminate on the LHS, repair patch on the RHS)

Considering the fracture along the scarf surface, as already observed in the MCLS specimens, cohesive failure is visible in the plies aligned with the load direction (i.e. the 0° plies) while interlaminar failure in the others (i.e. the 45°/90°/135° plies). This seems to suggest that the adhesive is weaker than the 0° plies, but stronger than all the ones aligned in all the other directions.
Regarding the fracture path, the reference and the modified patch specimens showed the exact same behaviour, with the fracture taking place along the entire scarf line. On the other hand, in the re-milled specimens, the fracture generally initiates in the patch and then propagates to the bondline. This is most likely because the re-milling procedure effectively eliminates the free edge, meaning that the peel stresses in this region are lower than in the other two specimen configurations and thus failure initiates elsewhere.
It is also worth mentioning that delaminations consistently occurred in the modified patch specimens, always in the parent laminate — most likely due to the higher stiffness of the repair patch. Delaminations were also sporadically visible in a few of the other specimens, however they were less extensive and did not always take place in the same adherend.

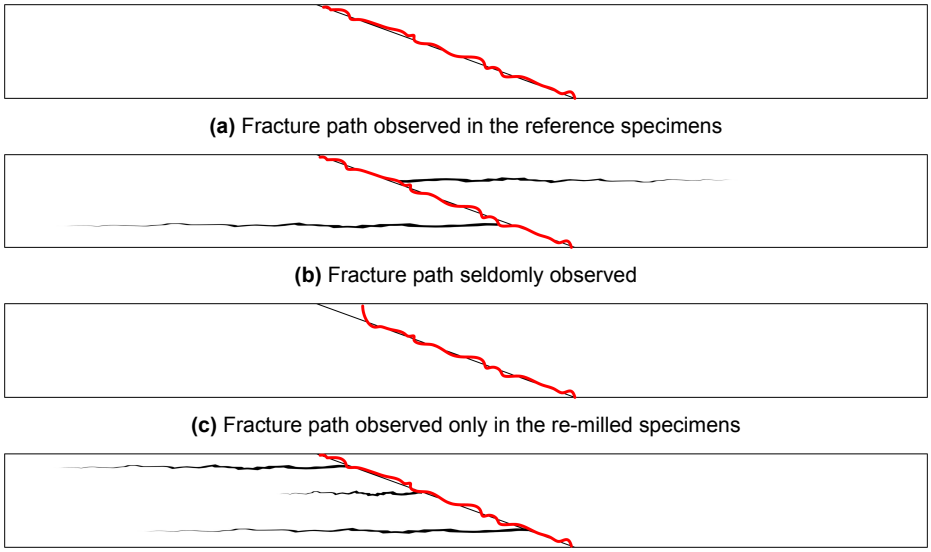

(a) Fracture path observed in the reference specimens

(b) Fracture path seldomly observed

(c) Fracture path observed only in the re-milled specimens

(d) Fracture path observed only in the modified patch specimens

Figure 9.6: Schematic, cross-sectional illustrations of the fracture paths of the EN6066 specimens, static tests (in all the figures: parent laminate on the LHS, repair patch on the RHS)

9.2. Fatigue tests

The fatigue tests were performed with a servo-hydraulic testing rig from MTS Systems Corporation (Eden Prairie, Minnesota, United States) able to reach loads up to 100 kN. The upper load for the fatigue tests was straightforwardly calculated applying Hooke's law, as shown in section 9.2

$$\sigma = E \cdot \varepsilon \quad \rightarrow \quad F_{upper} = E \cdot \varepsilon_{max} \cdot A \qquad \text{where} \qquad A = b \cdot t$$

where E is the Young's modulus of the CFRP (HexPly® 8552/IM7), which is estimated to be 58 GPa, according to experimental data provided in Airbus documentation [91]; ε_{max} the maximum allowable strain (set at 4000 µm/m according to the applicable design guidelines), b and t the dimensions of the specimens' cross-sectional area (namely, 25.4 and 3 mm respectively, as already depicted in Figure 6.3). Therefore, F_{upper} is equal to 17.68 kN and then, since the R value is set at 0.1, the lower load limit F_{lower} results to be 1.77 kN.
It is important to point out that the Young's modulus and the strain value are valid for undamaged specimens, and it is therefore assumed that the repaired ones are capable of withstanding the same loads (i.e. that the repairs completely restore the original load-bearing capability). The specimens were tested up to 54000 cycles, in accordance with requirements defined at Airbus for this kind of application. If failure did not occur within this threshold, the specimens were then statically tested for residual strength.

Table 9.2 provides an overview of the key testing parameters adopted for these fatigue tests. It is worth pointing out that the exact same values were also used in previous investigations with soft patch scarf repairs [4], [5], [48]: a comparison between hard and soft patches will therefore be proposed in the coming sections.

Table 9.2: Parameters used for the fatigue tests of the EN6066 specimens

Parameter	Value	Unit
Upper load, F_{upper}	17.68	[kN]
Lower load, F_{lower}	1.77	[kN]
R value	0.1	[-]
Frequency	6	[Hz]
Max elongation	4000	[µm/m]

9.2.1. Fatigue life

Figure 9.7 provides an overview of the fatigue tests, and it also includes the results of the exact same type of test previously performed at Airbus with soft patch repair specimens. In more detail, the soft patch reference specimens were manufactured and tested by Keil [48] and Scholz [5], while the soft patch re-milled specimens were included in the work of D'Arduini [4]. As one can see, the specimens are grouped according to the type of repair patch (hard or soft patch) and the type of repair concept, i.e. conventional (reference), re-milled or modified patch.

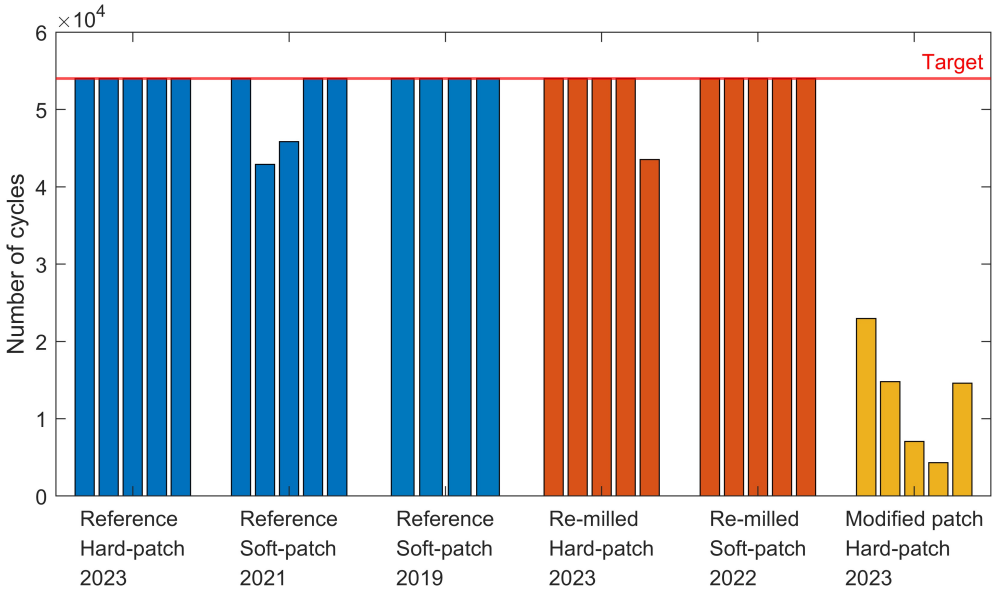

Figure 9.7: Fatigue life of the different patch configurations

As evidently shown in Figure 9.7 most of the specimens reached the required threshold of 54000 cycles, exception made for the ones with the modified patch that consistently failed well below the target. It is also worth mentioning that Scholz [5] traced back the overall inconsistent performance of the soft patch, reference specimens tested in 2021 to manufacturing defects. Whereas, it is debatable how to interpret the only re-milled, hard patch specimen that failed below the target number of cycles. It cannot be safely deemed an outlier, considering that the specimens were only tested up to 54000 cycles, and so applying an outlier detection rule (like the one mentioned above) would be misleading. This approach could be appropriate if all the specimens were tested until failure.

9.2.2. Failure mode and path

The fracture surfaces of the specimens that did not meet the target and thus failed during the fatigue test are mentioned here. First, the fracture surface of the only re-milled specimen that did not reach the threshold (Figure 9.8a) shows a combination of cohesive and adherend failure, in accordance to what was also observed in the static tests. However, the fracture path is now different, since it is fully along the bondline (while before it started in the parent laminate, as evident when comparing Figure 9.8a with Figure 9.5b) and no delamination is visible in any of the adherends. Second, the fracture surfaces of the modified patch specimens — which all failed well below the threshold — also show a combination of cohesive and adherend failure (a sample fracture surface is depicted in Figure 9.8b, the remaining ones can be found in Appendix B). Also in this case, the fracture path differs from what was noticeable in the static tests: adherend delamination is predominantly absent, only a minor one is visible in the parent laminate of a single specimen.

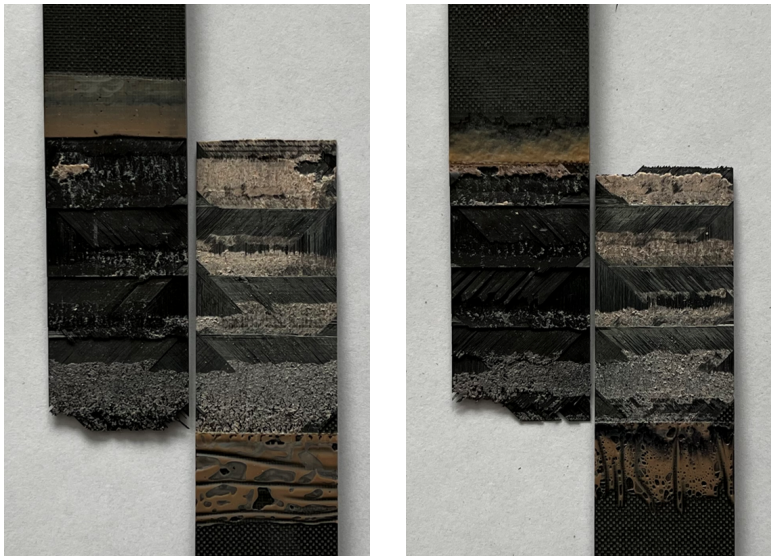

(a) Re-milled **(b)** Modified patch

Figure 9.8: Fracture surfaces of the EN6066 specimens that failed below the threshold during the dynamic tests (in both pictures: parent laminate on the LHS, repair patch on the RHS)

9.2.3. Residual strength

All the specimens that reached the target number of cycles during the fatigue tests were then statically tested, in order to obtain their residual strength. The testing conditions described for the previously discussed static, tensile tests apply also in this case (see section 9.1). For these tests aimed at assessing the residual strength after a certain fatigue life, less data are available from previous investigations: only a batch of soft patch, re-milled specimens (tested in 2022) is directly comparable — and thus plotted as well hereafter.

Figure 9.9 shows the ultimate tensile load achieved during the residual strength tests. As for the static tests presented above, the reference specimens proved superior, most likely due to the larger cross-sectional area.

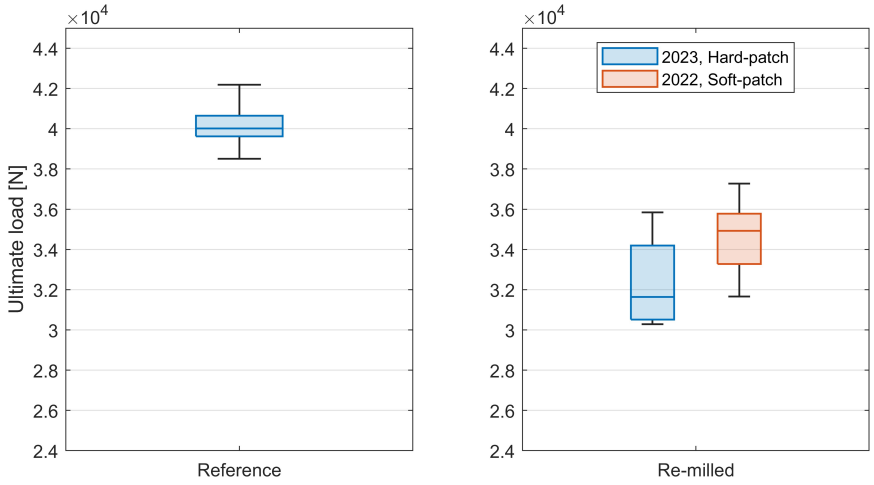

Figure 9.9: Ultimate tensile load reached by the different patch configurations during the residual strength static tests

Figure 9.10 shows the residual strength for the tested specimens. Once again, as previously explained for the static tests, removing the cross-sectional area from the equation diminishes the difference without however changing the overall outcome.

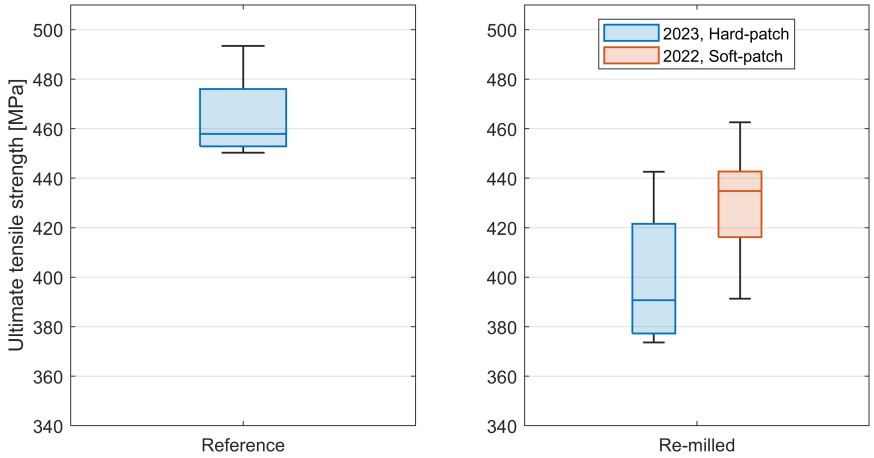

Figure 9.10: Ultimate tensile residual strength reached by the different patch configurations during the residual strength static tests

Figure 9.11 shows the elongation at break reached by the various specimens. In this case, the re-milled specimens deform significantly less than the reference ones (around 20% less). This might be due to the more prominent presence of plies aligned in the load directions, as already explained above in subsection 9.1.1. In addition, no large discrepancy is noticeable when comparing hard and soft patches. The small differences might be due to many aspects, or the combinations thereof, and so cannot be confidently justified by the patch type.

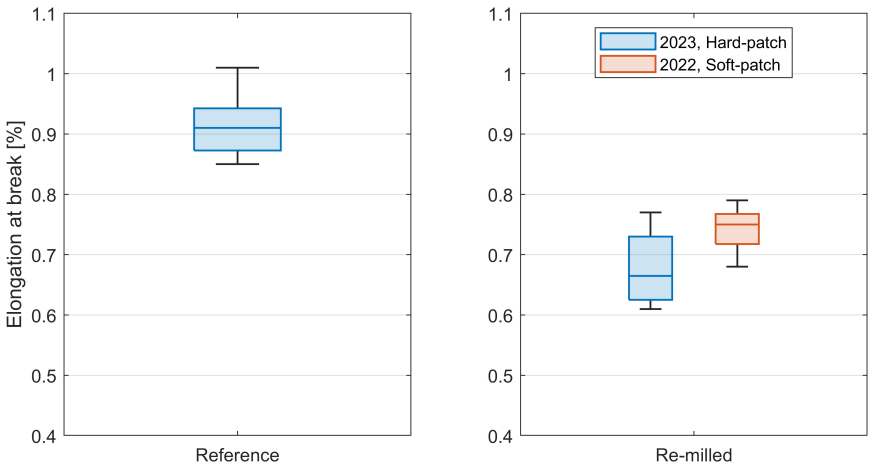

Figure 9.11: Elongation at break reached by the different patch configurations during the residual strength static tests

Figure 9.12 shows the tensile stiffness of the tested specimens. The E-modulus values were obtained from the specimens' stress-strain curves, according to the applicable standard [94] — therefore, stress-strain values between 1000 με and 3000 με were considered. The higher modulus achieved by the re-milled specimens seem to support the explanation proposed above for the static tests, i.e. that the re-milled specimens are stiffer due to a higher relative content of 0° plies.

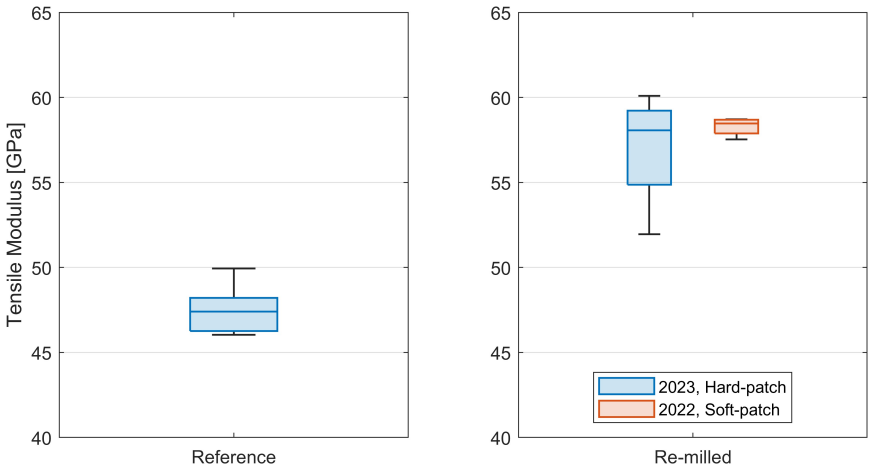

Figure 9.12: Tensile modulus of the different patch configurations, obtained from the residual strength static testing data

Table 9.3 provides an overview of the residual strength test results presented in this section. In more detail, the median values for the variables plotted above are listed for the various specimen configurations, while the values for each single specimen can be found in Appendix C. Do note how the specimens still comply with the mechanical requirements previously mentioned in subsection 9.1.1 (i.e. ultimate load of 24.31 kN and UTS of 319 MPa), even after the 54000 fatigue cycles.

Table 9.3: Overview of the EN6066 residual strength tensile static tests, median values for various relevant parameters

Repair patch			F_{max} [kN]	**UTS** [MPa]	ε_{max} [%]	$\mathbf{E_x}$ [GPa]
Type	Configuration	Year				
Hard	Reference	2023	40.01	457.9	0.91	47.41
Hard	Re-milled	2023	31.64	390.7	0.67	58.07
Soft	Re-milled	2022	34.93	434.8	0.75	58.46

Since the specimens tested statically and dynamically in this thesis were manufactured altogether in a single batch, it is also interesting to compare the values obtained in these residual strength static tests — performed after the dynamic tests — with the ones achieved in the static tests with pristine specimens presented in subsection 9.1.1. This allows to assess the impact of a 54000 cycles fatigue life on the mechanical properties of the different repair options.

Table 9.4: Comparison between the specimens statically tested after fatigue and the ones statically tested in pristine conditions (delta values calculated using the median values listed in Table 9.1 and Table 9.3)

Repair patch			ΔF_{max}	**ΔUTS**	$\Delta\varepsilon_{max}$	$\mathbf{\Delta E_x}$
Type	Configuration	Year				
Hard	Reference	2023	-2%	-2%	+4%	-2%
Hard	Re-milled	2023	-20%	-20%	-19%	-4%

It is evident that the reference specimens are less severely affected by the considered fatigue life, since their static mechanical properties are closer to their corresponding pristine ones, compared to the re-milled specimens. Indeed, while the delta in stiffness is rather close for the two configurations, the same can not be said for all the other quantities, where the reference specimens registered a significantly lower decrease.

9.2.3.1. Fracture surfaces

All the specimens showed once again a similar failure behaviour, with more noticeable difference in terms of fracture path. Since all the fracture surfaces look similar, only a representative example for each specimen configurations is provided in Figure 9.13 (the pictures for each single specimen can be found in Appendix C).

As in the previous tests, cohesive failure is visible in the plies aligned in the load direction, while adherend failure is dominant in the others. In this case, cohesive failure seems less evident in certain areas, and could be therefore described as thin-layer cohesive failure (according to Figure 2.7.
In terms of fracture path, all the reference specimens present limited delaminations in both adherends, but more evidently in the repair patch. Also the re-milled specimens showcase some small delaminations, always in the parent laminate. It is interesting to notice some differences compared to the static tests performed on pristine specimens. In the reference configuration, the fracture seems to initiate a few millimeters into the repair patch, before propagating completely

within the bondline (Figure 9.13a). In the re-milled configuration, the fracture develops completely along the bondline in the re-milled configuration. This different behaviour — which will be further discussed in the next chapter — is most likely a consequence of the cyclic loading that the specimens experienced during dynamic testing.

(a) Reference **(b)** Re-milled **(c)** Modified patch

Figure 9.13: Fracture surfaces of the EN6066 specimens, static tests (in every picture: parent laminate on the LHS, repair patch on the RHS)

10

Discussion and conclusions

This chapter presents the discussion and the conclusions associated with all the work described in this part of the thesis, dedicated to repairs in the structural material. First, the different repair patch configurations tested in this thesis are compared and the associated conclusions are derived. Second, the differences between the secondary bonded, hard repair patches adopted in this thesis and the co-bonded, soft patches tested in previous investigations are discussed. The conclusions presented here will then be re-called — and partially reiterated — in chapter 16, to underpin the answers to the research questions.

10.1. Repair configuration

The analysis and the tests presented in the previous chapters allowed to obtain a comprehensive comparison of the different repair configurations tested in this thesis, namely: reference, re-milled and modified patch. The aforementioned results are discussed right before drawing the associated conclusions.

10.1.1. Discussion

This section discusses the following: surface finish, static tests, dynamic tests and residual strength tests.

10.1.1.1. Surface finish

In terms of surface finish, as presented in section 8.3, both the re-milled and modified patch configurations allowed to significantly improve the overall flushness compared to the standard scarf repair procedure. However, the re-milled patch achieved a superior outcome: in fact, milling over the full surface allows to obtain a continuously smooth finish, free of any sharp change in thickness. The same can not be said for the modified patch, which — despite improving the overall thickness mismatch — still showcases a sort of concavity at the interface between the parent laminate and the patch, due to the different lengths of the scarf edges.

10.1.1.2. Static tests

The static tests showed that the reference configuration is slightly superior in terms of ultimate load compared to the re-milled one, while the modified patch falls behind by a larger margin (altough all the configurations surpassed the critical load defined by the applicable design guidelines). This trend might be explained considering that the reference specimens possess the largest cross-sectional area in the bond region, while the modified patch specimens have the lowest one. A larger cross-sectional area implies less severe stress concentrations, ultimately delaying failure. This also explains why the difference between the three repair configurations is reduced when looking at UTS: calculating the strength from the load removes the cross-sectional area from the equation.
All the configurations are similar in terms of elongation at break, with the reference specimens tending to stretch slightly more due to their inferior tensile modulus. This stiffness difference might be explained considering that the re-milled and modified patch specimens have a proportion of plies in the load direction: in the first case, the most superficial 45°/135° plies are partially milled out, while the modified patch contains a lower number of such plies compared to the parent laminate. Therefore, in these two cases, the patches' stiffness in the load direction is higher, and this may ultimately affect the overall stiffness of the specimen.
No difference between the three configurations could be identified in terms of failure mode: all the specimens consistently failed with a combination of cohesive and adherend failure. In terms of failure path, the reference and modified patch showed the same behaviour with the crack propagating completely within the bondline. On the other hand, the crack initiates in the repair patch in the re-milled specimens: this may be explained considering that the milling process evens out the surface, thus minimizing the peel stresses at the free edge of the repair patch (in fact, re-milling effectively eliminates this edge). In addition, the delaminations consistently observed in the modified patch specimens — always in the parent laminate — could be explained considering the higher stiffness of the repair patch.
Overall, these tests proved that the reference and re-milled configurations are rather closely matched, while the modified patch one performed significantly worse — albeit all could meet the target loads.

10.1.1.3. Dynamic tests

The dynamic tests proved that the reference and re-milled configurations are generally capable of meeting the target fatigue life, while the modified patch specimens failed consistently well below the set threshold.
Only one re-milled hard patch specimen did not meet the target, the reason behind this is not easily identifiable. It cannot be safely deemed as an outlier, since all the other specimens were not tested until failure: applying any outlier detection rule based on their distribution would be therefore inappropriate. It might be due to the absence of excess adhesive around the free edge — which is removed while re-milling — that normally helps reducing peel stresses around in the area. This may not be relevant in static conditions, but may become influential in dynamic testing where the joint tends to progressively open up cycle by cycle. In any case, more investigations into the dynamic behaviour of this repair configuration should be performed. It is important to understand whether the single premature failure observed in this work represents a rare occurrence, or can be motivated by certain features of this configuration.
For the modified patch specimens, the difference in stiffness between the parent laminate and the repair patch most likely causes the bond to experience higher stresses, and thus fail prematurely. Nonetheless, it is not trivial to justify why this affects much more severely the fatigue performance

compared to the static one. Overall, this behaviour can not be fully explained with the available data, more investigation and modelling would be beneficial to provide a better understanding of the phenomenon. Nonetheless, this would create little value form an industrial standpoint, given that the inability to meet the target fatigue life (and eventually the inferior static performance) are already sufficient to rule out the modified patch configuration with this specific layup from further investigations. It may also be that the layup defined here is not ideal, and that a different one would allow for better mechanical results. Thus, FE modelling would once again come in handy to iteratively find the optimal layup. Nonetheless, also this is not highly recommended: while it may improve mechanical performance, it would not change the surface finish. In fact, the latter — which is the main driver of this entire investigation, and ultimately the aspect to prioritize — would still remain worse than in the re-milled configuration, as it is independent of the layup and only determined by the patch alignment.
It is also worth mentioning a few things regarding the fracture path of the specimens that did not meet the threshold. For the single re-milled specimen that failed, the fracture fully developed along the bondline, contrary to what was observed in the static tests. This may be explained considering that — during dynamic testing, as a consequence of cyclic loading — the joint tends to progressively open up, starting from the top edge, and so the fracture naturally initiates there. For the modified path specimens, contrary to the static tests, no delaminations are visible in the parent laminate. This may be explained considering that the maximum load level reached in the fatigue tests is significantly lower than that of the static ones (less than half). This means that the difference in stiffness between the parent laminate and the patch —– which had been previously identified as the most likely reason behind these delaminations in the parent laminate —– is now less influential.

10.1.1.4. Residual strength tests

In terms of residual strength after the dynamic tests, both the reference and re-milled configurations met the critical thresholds, but the former proved superior by over 20% in terms of ultimate load and strength — and so by a larger margin compared to the initial static tests. This might be explained considering that the smaller cross-sectional area of the re-milled specimens causes higher stresses, which on the long-term are detrimental for the integrity of the specimens — and thus reduces their strength after cyclic loading.
Looking at the fracture path, in the reference specimens, the fracture initiates a few millimeters into the repair patch, before propagating completely within the bondline (in contrast to the initial static tests, where it was fully within the bondline). This may be because the excess adhesive around the free edge reduces the effect of peel stresses during the dynamic tests, thus preventing the joint from starting to open. This condition perhaps causes the initiation of damage at the beginning of the repair patch, possibly explaining why the fracture then begins right there in the residual strength tests. This effect of the excess adhesive is most likely more influential in the dynamic tests (and for the residual strength ones as well) rather than in the initial static ones due to the very different load levels reached. For the re-milled specimens, the consideration previously made for the only one that failed during the dynamic tests applies here as well.

10.1.2. Conclusion

In conclusion, the re-milled configuration can be deemed a truly valid option to the reference one: it proved able to significantly enhance the surface finish — eliminating any sharp kink and improving the overall smoothness — while performing only marginally worse from a mechanical

standpoint. Therefore, it seems reasonable to further develop and eventually certify this procedure, so that it can be applied in all those applications where low observability is key, and eventually in future concepts requiring extremely smooth surfaces for aerodynamic reasons. As mentioned above, the fatigue behaviour should be closely observed, to confidently explain the single premature failure observed in this work. Of course, it is reasonable to implement this option only for those applications where surface smoothness and flushness are an absolute priority. It is indeed unnecessary to extend this procedure to all scarf repairs in general, since it requires more work, resources, downtime and — despite meeting all the loads requirements in this case — is still slightly inferior to the reference one from a mechanical standpoint.
On the other hand, the modified patch consistently failed to meet the fatigue life requirement by a large margin, and also proved inferior in terms of ultimate load and UTS. Therefore, it is not worth further developing this alternative. It is also not recommended to define and test alternative layups: while this may improve the mechanical performance, would not be able to change the surface finish, which is still worse than the one of the re-milled configuration.

10.2. Patch type

The tests presented in the previous chapter also allowed to compare the secondary bonded hard patch specimens produced in this thesis with the co-bonded soft patch ones manufactured and tested in previous investigations. As already mentioned, the comparison is limited to the reference and the re-milled configurations. The aforementioned results are discussed right before drawing the associated conclusions.

10.2.1. Discussion

In terms of surface finish, hard and soft patches allow to achieve very similar results. The thickness mismatch of both the reference and re-milled specimens manufactured in this thesis is comparable to the one of the samples previously produced by Scholz [5] and D'Arduini [4].
Since the surface finish was assessed in slightly different ways in the various investigations — i.e. with slightly different measurement systems and/or procedures — it is not possible to compare hard and soft patches in absolute terms (i.e. precisely looking at the absolute value of the quantity). Nonetheless, the fact that the values are in the same range suggests that both patch type can in principle achieve very similar results.

Also looking at the static tests, hard and soft patch specimens performed comparably, there are of course small differences, but it can not be surely concluded that one is superior to the other. The fact that the hard patches match more precisely the parent laminate (exact same resin system and curing cycle, and so very similar properties) does not seem to significantly benefit the mechanical performance as one would expect. Indeed, looking at the test results, while the re-milled hard patches perform generally better than the soft patches counterpart, this does not hold true for the reference configuration: the two patch types perform either equally or in certain cases the soft patches seem slightly superior. The discrepancies may well also be explained with manufacturing imperfections and/or slightly different testing conditions.
The same considerations can be extended to the dynamic tests: hard and soft patches proved very closely matched, with no remarkable difference and/or evident trend.

10.2.2. Conclusion

In conclusion, neither of the two options emerged as the superior one in this comparison. The theoretical advantage of the hard patches — which are a closer match to the parent laminate in terms of fibre volume and void content, since they are manufactured in the exact same way — did not translate into a better performance. The same can be said regarding the surface finish, since both alternatives proved capable of achieving very similar outcomes.
It would be surely useful to manufacture and test both options at the same time, rather than resorting to old data for some of them like in this case. This would allow to have a better control over the manufacturing and testing conditions of all the specimens, and thus being able to eventually justify some discrepancies (on top of having a more consistent assessment of the final surface finish).
In any case, for the time being, it is possible to conclude that — since they are closely matched in terms of mechanical properties and surface finish — the choice between the two options shall be driven by the other aspect mentioned in subsection 3.2.5, i.e. primarily cost and accessibility of the damaged area.

10.3. Additional remark

As mentioned in the literature review (section 3.2 and subsection 3.3.5), scarf repair procedures (such as [88]) often require the use of overplies, although these clearly contribute to generating an uneven surface. This is because having a small step is not influential in most applications. This aspect has been so far disregarded in previous Airbus work focused on improving surface flushness, nonetheless it is worth addressing.
First, as already mentioned, overplies are beneficial to seal off the repaired area, thus preventing — or at least slowing down — the bondline from absorbing moisture, which is clearly detrimental for the adhesive properties. While this is undoubtedly true, theoretical studies often disregard that repaired areas are generally painted over, in such a way that the paint itself can serve as a protection barrier against moisture absorption. This theoretical advantage of overplies is therefore of secondary importance on actual repairs.
Second, it is known that overplies reduce peak stresses near the free edges, thus increasing the overall repair strength. The static tests presented above showed how the re-milled configuration showcases a distinctive failure path, where failure initiates somewhere in the repair patch rather than at the beginning of the bondline — as in the other configurations. As aforementioned, this suggests that the re-milling procedure reduces the peel stresses around the edge of the patch, since it smoothens the surface eliminating any free edge prone to generate stress concentrations. Therefore, one may suggest that the re-milling procedure brings the same advantage of the overply, while actually improving the surface finish rather than worsening it. It is however important to mention that this effect seems to fade throughout the life of the repair: indeed, in the static tests performed after the dynamic ones, the failure path is the same as for the other configurations.
In conclusion, while these considerations sound reasonable and backed by the results presented above, more work on real-conditions repairs is needed in order to further investigate this aspect and draw stronger evidence-based conclusions.

III

Functional Material Repairs

11

Problem statement

This part of the thesis deals with repairs localised in the functional part of the considered reference component, i.e. the demonstrator structure already introduced and depicted in Figure 1.3. This chapter serves as a sort of introduction for the work performed in this phase of the thesis. At first, the background and the previous work performed at Airbus are presented, together with the connection with the research questions that were answered in this phase. Then, the adopted approach and all the steps performed in this phase are summarised, and a graphical workflow is presented.

11.1. Background

As previously mentioned, limited studies are available on repairs for the functional material and type of structures considered in this thesis. This lack of resources can be explained with the relative novelty of the technology, but also — and mainly — due to its field of application limited to the defence industry, and thus the associated shortage of publications.
Therefore, the work performed in this domain as part of this thesis builds up exclusively on the research carried out at Airbus in recent years. In more detail, the aspect treated in this second part of the thesis has been previously investigated in the work of D'Arduini [4], where several repair procedures were defined at conceptual level. These are briefly summarised hereafter.

First, a repair process based on the use of pre-cured hard patches (*Procedure 1*, depicted in Figure 11.1) was proposed. Repair patches with standardised dimensions are intended to be produced via Resin Transfer Moulding (RTM) and kept in stock. In case of damages, the affected area of the functional profile is removed via CNC milling (Figure 11.1a). Then, the standardized repair patch needs to be trimmed to match the exact shape of the removed damaged area (Figure 11.1b), before being slotted in and secondary bonded to the structure with a paste adhesive (Figure 11.1c).

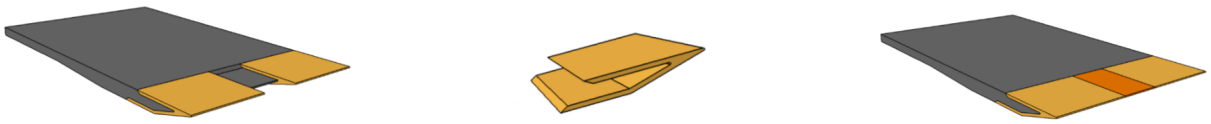

(a) Removal of the damaged section via CNC milling

(b) Trimming of the standardized repair patch to correct size

(c) Application of the repair patch via secondary bonding

Figure 11.1: Repair procedure for damages in the functional material, based on the use of hard patches [4]

Second, another similar procedure was proposed (*Procedure 2*), with a different repair patch. In this case, the patch includes both the core structural material and the functional one, as shown in Figure 11.2. The repair procedure itself is similar to the previous one, the only difference being that now also the core material is removed in the damaged area. The only advantage of this option compared to the previous one is that it requires a less precise removal of the damaged region, since not only the function material layer needs to be removed but an entire section.

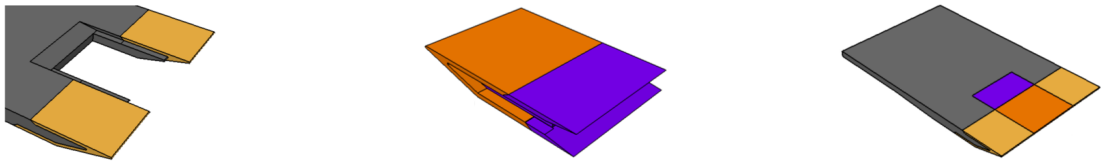

(a) Removal of the damaged section via machining

(b) Trimming of the sacrificial patch to correct size

(c) Application of the sacrificial patch via secondary bonding

Figure 11.2: Repair procedure for damages in the functional material, based on the use of a ”sacrificial” patch [4]

Third, a repair process based on the use pre-preg was also introduced (*Procedure 3*, Figure 11.3). In this case, as in *Procedure 1*, the damaged area of the functional profile is removed via CNC milling (Figure 11.3a). Then, a soft patch is created layer by layer using pre-preg material and then co-bonded to the structure (Figure 11.3b and 11.3c). Compression plates are required during curing to ensure a smooth surface finish, and eventual post-processing might also be necessary to re-fine the edge profile.

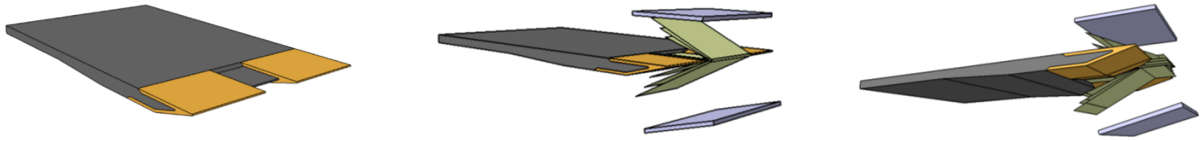

(a) Removal of the damaged section via CNC milling

(b) Application and co-bonding of the pre-preg layers

(c) Application and co-bonding of the pre-preg layers

Figure 11.3: Repair procedure for damages in the functional material, based on the use of pre-preg soft patches [4]

In any case, it is evident that all these proposed methods are not convenient — albeit applicable — to repair small damages (such as dents, or small impact damages up to a few centimeters in size), especially if the repair needs to be carried out on-site with minimal downtime. This is because such procedures require a significant time to be completed, on top of specific equipment (e.g. CNC milling systems) and a stock of bespoke repair patches. Therefore, it is necessary to also define alternative procedures using paste-like substances (similar to body-fillers), which are quicker to perform and more suited to tackle small damages.

11.2. Approach and limitations

This part of thesis aims at addressing this specific gap, investigating possible ways to repair such small damages, thus providing an answer to research question SQ2.1 and SQ2.2. (Table 5.1). In order to do that, the composition of a suitable repair filler compound was defined at first, possible procedures to carry out the repair using such compound were then considered. Eventually, stemming from the previous work performed by D’Arduini [4], improvements for the proposed hard patch approach were defined.

In order to determine in detail the scope of this part of the thesis, the requirements of repairs in the functional material were first defined. Such basic requirements are listed in Table 11.1.

Table 11.1: Requirements for the repairs in the functional material

ID	Requirement
FR-RQ1	The material's functionality shall be re-instated
FR-RQ2	A good adhesion between the repair area and the parent material shall be ensured
FR-RQ3	The repair shall restore the component's contour with a smooth and seamless surface finish

It was not possible to directly verify the first and second requirements within the framework of this thesis due to the following reasons. In order to verify the first one, it would have been necessary to test the low observability properties of the repaired region via electromagnetic testing. This was not possible due to formal reasons related to the topic sensitivity. In order to verify the second one, it would have been necessary to perform mechanical tests aimed at assessing the adhesion between the parent laminate and the repair compound. This was not possible due to the lack of the functional material required to manufacture the needed specimens. Nonetheless, qualitative considerations and analyses were made in order to at least indirectly address these two requirements. On the other hand, it was possible to directly verify the last requirement in this thesis: a few sample repairs were implemented and qualitatively assessed.

11.3. Workflow

Figure 11.4 provides an overview of all the steps that will be performed in this phase of the thesis, with the aim of investigating repairs localised in the functional material and thus answering the related research questions.

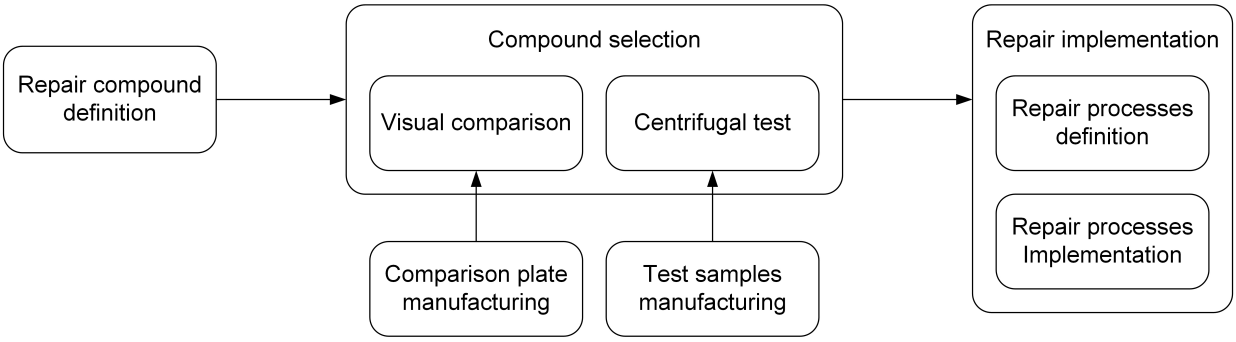

Figure 11.4: Flowchart depicting the steps performed to tackle the research questions related to the repairs localised in the functional part of the considered composite component

To summarise and clarify the aim and the content of this first part of the thesis, its goal and its scopes are stated in Table 6.2.

Table 11.2: Goal and scope of the second part of the thesis, aimed at investigating functional repairs

Goal	
	Investigate how to repair damages located in the functional edges on the demonstrator panel
Scope	
1	Develop repair procedures based on the use of a filler compound
	1.1 Define the optimal composition of the repair filler compound
	1.2 Consider and evaluate different repair procedures
2	Improve the repair procedure based on the use of hard patches

12

Repair compound design

This chapter describes the procedure followed to define the composition of the repair compound intended to address small damages. To begin with, some general characteristics of the functional material are provided and several possible repair compounds with different composition are defined. The mixing, comparison and testing of such compounds are then described, in order to select the ones suitable to be used for actual repairs.
It is important to point out that details about the exact composition of the functional material are omitted throughout this chapter, due to the sensitivity of the topic. For this reason, no exact figures are given, certain details are either described in a purposely vague manner or completely omitted, and some charts are displayed without revealing any sensitive value and their associated unit.

12.1. Repair compound definition

This section deals with the definition of different possible repair compounds. Before delving into details, it is important to specify some basic characteristics of the functional material considered in this thesis. As already mentioned, the functionality of such material is to absorb radar waves, with the aim of enhancing the low observability feature of a given structure. Such radar absorbent material is a composite, which therefore comprises a resin component and a fibre component, plus a microparticle additive that adds stealth functionality. The material is currently only available in the form of a dry fabric — which already embeds the additive — that is later infused with resin, although more options might become available in the future as its development advances.

The definition of the various repair compounds options was driven by the following high-level guidelines. First, the repair compound needs to closely match the properties of the functional material, since the primary goal is to re-instate the material's functionality. The exact final volume fractions of the cured material are not precisely known. Nonetheless, boundaries were defined for the minimum and maximum content of each constituent, starting from the estimated composition of the actual material. Second, it needs to possess a paste-like viscosity, in such a way that it can be applied like a body filler — or eventually be injected as well — during repairs.
It was established to consider various compound options, each including variable proportions of the functional material's constituting elements (i.e. the resin, the fibres and the additive). Due to its high curing temperature, unsuitable to the repair conditions, the resin actually used in the functional material was replaced with an epoxy-based adhesive in the repair compounds. The continuous fibres were replaced with short fibres (3 mm), given the paste-like consistency desired

for the repair compounds. On the other hand, the exact same additive used in the actual functional material was adopted for the repair compounds.
It was initially also considered to shred the functional material fabric — which, as aforementioned, already embeds the additive — into short fibres and mix it directly with the adhesive, as this would be convenient from a practical standpoint. However, this option had to be discarded due to the low availability of the functional material, even though it might still be worth considering in the future. Figure 12.1 provides a graphical representation of all the possible constituents' combinations — and thus possible repair compounds — considering the defined boundaries.

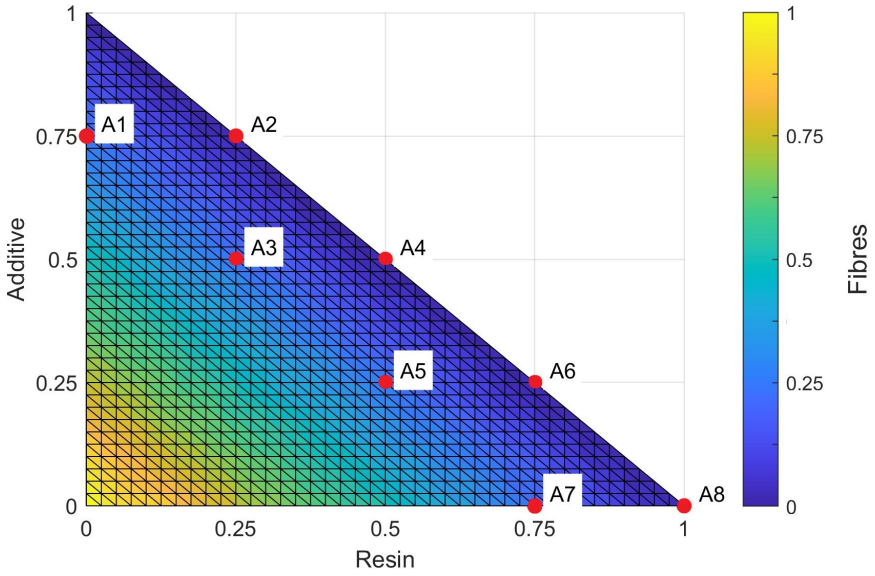

Figure 12.1: Range of all the possible repair compounds for the functional material

Among all these possible options, eight combinations — depicted in Figure 12.1 — were selected and mixed. No compounds located in the lower-left corner of the chart were selected, given that preliminary trials highlighted their unfeasibility. These repair compounds are listed in Table 12.1, which qualitatively shows the content of their constituents ("0" represents no content, while an increasing number of "+" represents an increasingly higher content). Additionally, the feasibility of achieving a uniformly homogeneous compound is also mentioned. All the doable compounds were then compared, as detailed in the next section.

From a practical standpoint, the compounds were obtained in the following way. First, the two adhesive parts were mixed, then the additive and fibre were progressively added while keep on mixing the resulting compound. The mixing itself was performed with a drill-mounted mixing screw, in order to facilitate the procedure and minimize the risk of trapping air in the compound. Once a homogeneous consistency was reached (i.e. no agglomerations were noticeable, the color was uniform and so the viscosity) the compounds were further mixed with a centrifugal mixer, also in order to minimize the air content.

Alternatives were also considered: it was initially intended to embed the additive in one of the two parts of the adhesive, so that the repair compounds could be kept in stock like normal two-components adhesives. Indeed — considering the long-term field application of this repair procedure — it would be more convenient to have shelf-ready compounds, whose usage procedure would be no different from that of conventional two-components paste adhesives, rather than mixing them from scratch on the spot. However, this approach turned out to be

unfeasible — due to the impossibility of achieving a uniformly homogeneous compound, as a consequence of the insufficient volume of the adhesive part compared to the two other solid constituents — and was therefore discarded.

Table 12.1: Adhesive, additive and fibre content for all the tested compounds intended to repair damages in the functional material

Compound	**Adhesive content**	**Additive content**	**Fibre content**	**Feasibility** [Y/N]
Compound A1	+	++++	+	N
Compound A2	++	++++	0	Y
Compound A3	++	+++	+	N
Compound A4	++	+++	0	Y
Compound A5	+++	++	+	Y
Compound A6	++++	++	0	Y
Compound A7	++++	+	+	Y
Compound A8	+++++	+	0	Y

12.2. Compounds comparison

The different compounds were compared via microscopy, plus other aspects — such ease of handling and application — were also considered. This chapter discusses such analysis in detail, after providing a brief description on the manufacturing of the functional material plate used for such comparison.

12.2.1. Comparison plate manufacturing

The plate depicted in Figure 12.2 was designed in order to assess how the different possible repair compounds compare with the parent functional material. A base laminate was first produced with the functional material fabric via a vacuum infusion procedure, a hole pattern was later drilled. The holes' conical shape was selected in order to maximise the contact surface between the parent material and the repair compound. The top diameter of such conical cavities was selected based on the size of the impact damages generated on the demonstrator structure. In this way, it was possible to assess the suitability of the different repair compounds to damages of various sizes.

12.2.2. Visual comparison

Once mixed, the various repair compounds — whose compositions are listed in Table 12.1 — were poured in the comparison plate and then cured according to the adhesive's curing cycling. Figure 12.3a shows the cured compounds, while Figure 12.3b depicts the plate after the compounds in excess were removed and the surface grinded flush.
Considering Figure 12.3a — and recalling Table 12.1 — it is evident that an increasing amount of additive and/or fibres progressively increase the compound's viscosity, thus hindering its ability to easily flow. All three compounds comprising only the adhesive and the additive (i.e. A2, A4, A6 and A8), despite having different consistencies and viscosities due to the varying additive's

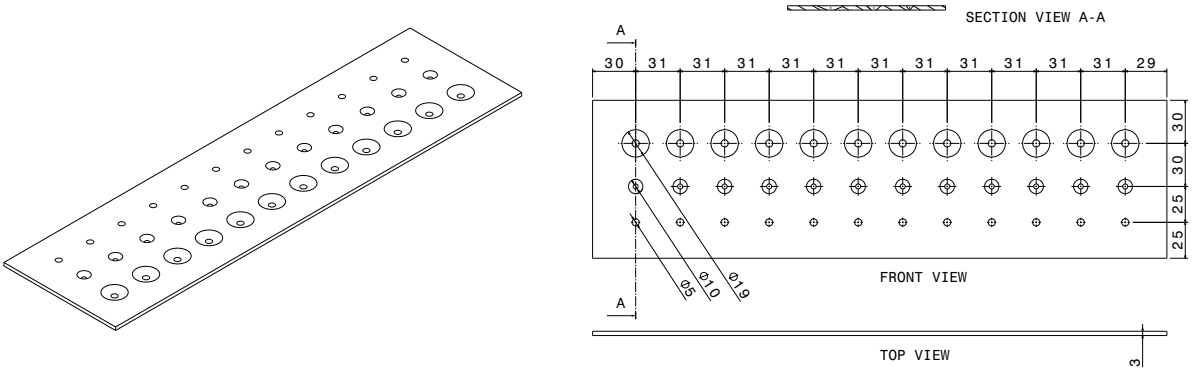

(a) Isometric view of the comparison plate

(b) Front, top and section views of the comparison plate

Figure 12.2: Drawings of the comparison plate manufactured with the functional material (dimensions in mm)

content, demonstrated ease of application and also the capability of properly fill in a uniform manner all the three differently sized cavities (as visible in Figure 12.3b). On the other hand, the compounds also containing the fibres (i.e. A5 and A7) were extremely dry and unable to flow, despite appearing rather homogeneous. Furthermore, as clearly visible in Figure 12.3b and 12.5e, they are unsuited to fill up the smaller holes (which represent the damages of smallest size), plus they could not ensure a uniform coverage and interface with the laminate in the two larger holes either. These considerations were deemed sufficient to disregard A5 and A7 from further steps, being clearly unsuited to the intended purpose.
It was eventually considered to replace the 3 mm fibres with shorter ones (in the order of 0.1-0.5 mm), however this alternative was also dismissed for the following two reasons. First, considering that the material has no structural function, the fibres would not serve any purpose but only increase the viscosity, ultimately worsening the ease of handling. Additionally, no suitable shorter fibres were available at the time of this investigation, and causing delays in acquiring some stock was considered unworthy.

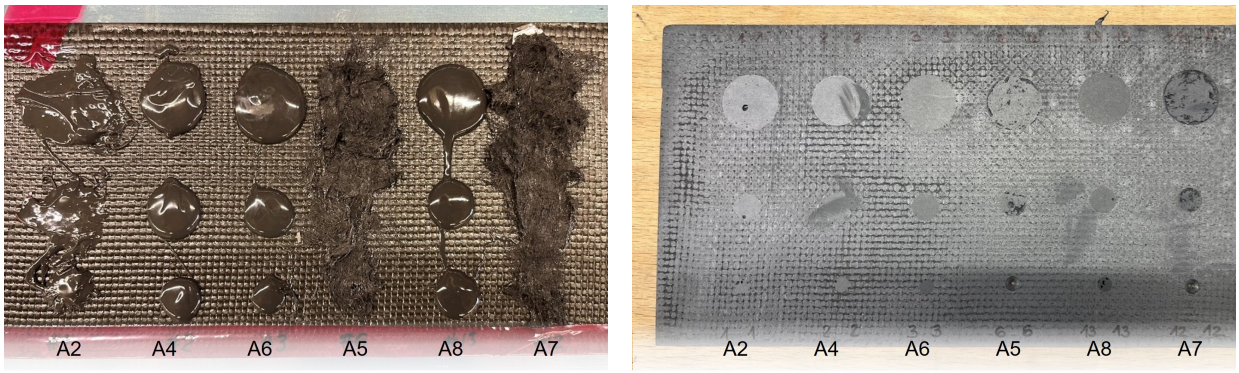

(a) After curing

(b) After grinding

Figure 12.3: Comparison tool filled with different repair compounds

Figure 12.4 shows, for each compound, a photomicrograph of the plate's section, in the area of the largest conical cavity. Figure 12.4c and 12.4e confirm what has already been stated above about the compounds that include fibres (A5 and A7), i.e. that they are unable to ensure uniform coverage and present several voids and imperfections. Regarding the other compounds

(Figure 12.4a, 12.4b, 12.4d and 12.4f), they seem to ensure and smooth interface with the parent laminate. Overall, it is worth noticing that from these pictures — and from others taken with different levels of magnification but not displayed here — it is not possible to clearly distinguish the different compounds. Furthermore, it is also worth pointing that, as visible in Figure 12.4c, 12.4d and 12.4, the laminate presents widespread manufacturing defects in the form of voids, most likely due to an insufficient amount of resin. This has, however, no impact on the comparison made here.

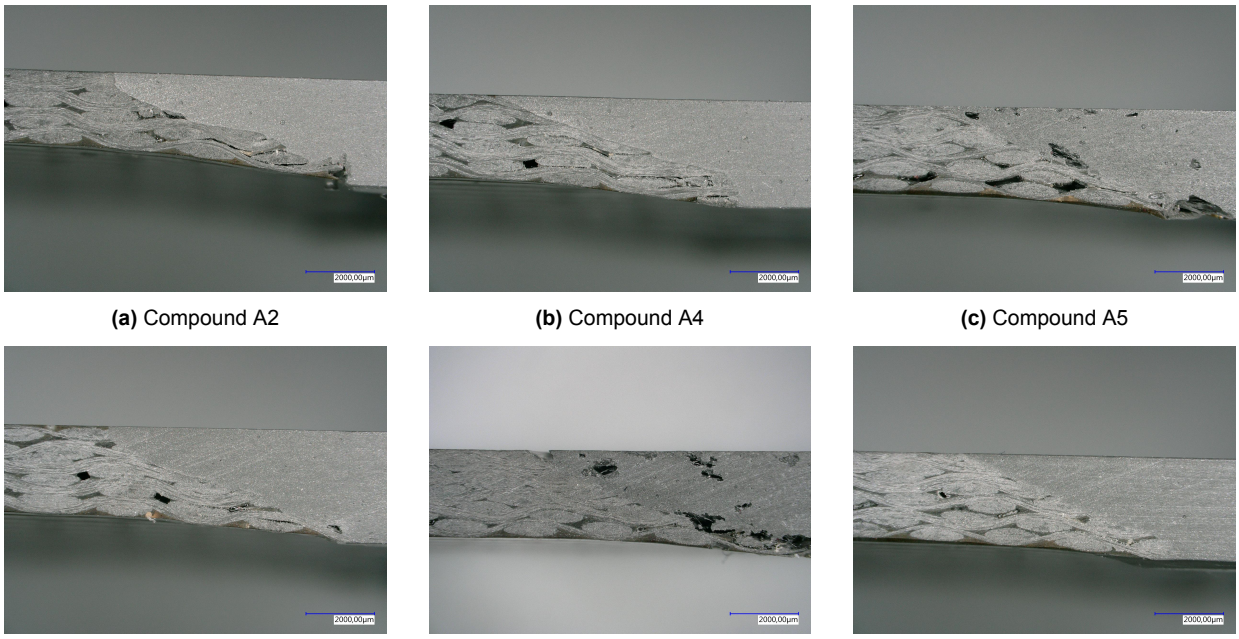

(a) Compound A2 **(b)** Compound A4 **(c)** Compound A5

(d) Compound A6 **(e)** Compound A7 **(f)** Compound A8

Figure 12.4: Photomicrographs depicting the cross section of the larger hole for the different repair compounds

Figure 12.5 shows, for each compound, a photomicrograph of the plate's section, depicting the smallest conical cavity. The considerations made above are further confirmed by such pictures (do note that Figure 12.5e depicts an empty cavity, given the inability of compound A7 to fill it due its consistency). Additionally, as noticeable in Figure 12.5d and 12.5f, air bubbles can be found in some compounds in certain cases. Ways to address such issue should be investigated in order to eliminate the risk of having such imperfections in final repairs. It is also interesting to mention that Figure 12.5a and 12.5b depict the exact same region, with the lighting conditions being the only difference. This clearly shows how well the repair compounds match — at least from a visual standpoint — the original functional material.

Overall, this visual comparison confirmed the ruling out of the repair compounds that also contain fibres. Regarding the others, it did not allow to draw any relevant conclusion, since these compounds appear hardly distinguishable, and no evident difference is observable. For this reason, it was decided to proceed in the following way: the compound with the highest amount of adhesive was also discarded, since this is expected to have worse LO properties compared to the ones with a higher additive content. Therefore, the mechanical tests described in the following section only considered three compounds, namely A2, A4 and A6.

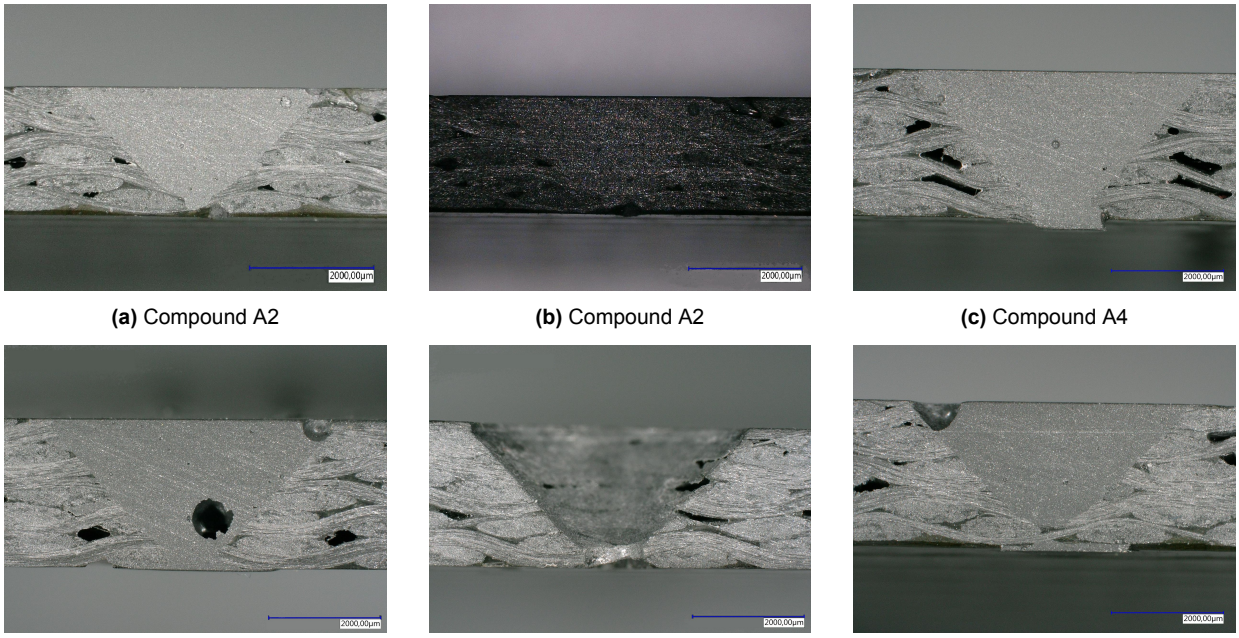

(a) Compound A2 **(b)** Compound A2 **(c)** Compound A4

(d) Compound A6 **(e)** Compound A7 **(f)** Compound A8

Figure 12.5: Photomicrographs depicting the cross section of the smaller hole for the different repair compounds

12.3. Compounds mechanical testing

The goal of these tests was to assess the impact of the additive on the mechanical properties of the pure adhesive. This allowed to quantify the adhesion capability of the various considered repair compounds, thus indirectly addressing the requirement FR-RQ2. In order to do that, the tensile strength of adhesive bond implemented with the various compounds was obtained via the mechanical tests discussed in this chapter. Three different compounds — with a varying concentration of additive, namely: A2, A4 and A6 — were compared to the pure adhesive.

12.3.1. Centrifugal tests

The mechanical tests were performed with a testing machine — commercially known as LUMiFrac® — from LUM GmbH (Berlin, Germany). This testing method employs centrifugal force to measure the tensile strength of adhesive bonds. The test specimens comprise four items: the adherend, the test sample, a copper cylinder and a metallic sleeve.

First, the metallic sleeve is positioned on top of the adherend, the adhesive is applied on the stamp (which is screwed to the copper cylinder) and then slid into the sleeve (Figure 12.6a). The adhesive then cures under the weight of the cylinder.
The specimens are then loaded in the machine's rotor (Figure 12.6b), which spins at a progressively higher speed (up to 13000 rpm), thus increasing the test load. Once the bond fails, the stamp separates from the adherend and then — together with the copper cylinder — slides into the metallic sleeve, ultimately triggering the recording of time and rotational speed. Then, the failure strength is straightforwardly calculated as follows:

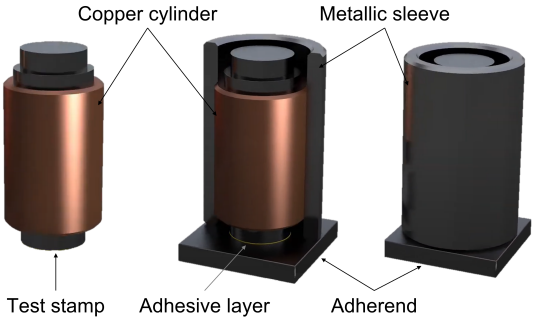

(a) Centrifugal tensile test specimen

(b) LUMiFrac® rotor loaded with a specimen

Figure 12.6: Test equipment used to measure the tensile strength of different repair compounds
Edited figures from LUMiFrac® webpage: `https://www.lum-gmbh.com/lumifrac_en.html`, visited on November 6, 2023

$$\sigma = \frac{F_c}{A} \qquad \text{where} \qquad F_c = m \cdot \omega^2 \cdot r$$

where σ is the tensile strength, F_c is the centrifugal force, A the bonding area (i.e. the area of the metallic stamp), m the mass of the sample, ω the angular velocity and r the distance to the rotational axis. The tensile failure strength is therefore obtained plugging in the above equation the maximum centrifugal force, i.e. the one corresponding to the rotational speed when the failure occurred.

12.3.2. Specimen & test details

The specimen and the test details were defined based on previous Airbus' studies that relied on the same testing procedure [92], [93]. The relevant parameters and details are listed in Table 12.2.

Table 12.2: Parameters used for the centrifugal tensile tests

Parameter	Value	Unit
Adherend material	HexPly® 8552/IM7	[-]
Adherend dimensions	25x25x6	[mm]
Stamp material	AlMgSi1	[-]
Bonding area, A	78.54	[mm^2]
Specimen mass, m	50.70	[g]
Distance to the rotational axis, r	62.80	[mm]
Adhesive quantity	10	[µl]

The composite samples were obtained from the same quasi-isotropic, 3mm-thick laminates previously used for the MCLS and EN6066 specimens (see section 8.1). Therefore, in order to ensure the desired 6 mm thickness, two plates were bonded together with a structural adhesive (Scotch-Weld™ EC-9323 B/A from 3M Company, Maplewood, Minnesota, U.S.).
In order to reduce the likelihood of observing pure adhesive failure, the CFRP adherends' surface was plasma-treated, with the same process parameters previously adopted and already listed in

Table 7.3. In addition, the test stamps underwent a laser surface treatment, the procedure was carried out with a 25 W laser unit with a frequency of 10 kHz, moving at 800 mm/s while keeping a distance of 200 mm from the surface. Different surface treatments were tested in previous investigations, these two ensured the best results, hence why they were selected in this instance. The specimens were then assembled using a bespoke tool, in order to enable the test stamp to remain perpendicular to the adherend throughout the curing phase, and in general to ensure consistency among all the samples. It is worth mentioning that the adhesive was manually dosed using a syringe. Twenty specimens were produced in total: five with the pure adhesive, and five for each of the three considered repair compounds.

12.3.3. Results & discussion

The results of the centrifugal tensile tests are presented and discussed in this section. Table 12.3 provides an overview of all the tested specimens, highlighting the achieved tensile failure strength and the failure mode.

Table 12.3: Summary of the tensile centrifugal tests, listing all the tested specimens

Compound	Specimen	Additive content	σ [MPa]	Failure mode
Adhesive	AE_1	0	43.12	Cohesive/Adherend, primarily adherend
	AE_2		44.77	Cohesive/Adherend, primarily adherend
	AE_3		43.48	Cohesive/Adherend, primarily adherend
	AE_4		40.55	Cohesive/Adherend, primarily adherend
	AE_5		39.94	Cohesive/Adherend, primarily adherend
Compound A6	CP1_1	Low	27.93	Cohesive/Adherend, primarily adherend
	CP1_2		31.40	Cohesive/Adherend
	CP1_3		20.73	Cohesive/Adherend
	CP1_4		27.19	Cohesive
	CP1_5		28.64	Cohesive/Adherend, primarily adherend
Compound A4	CP2_1	Medium	24.52	Cohesive/Adherend, primarily adherend
	CP2_2		24.71	Cohesive/Adherend
	CP2_3		22.63	Cohesive/Adherend
	CP2_4		25.85	Cohesive/Adherend
	CP2_5		26.52	Cohesive/Adherend
Compound A2	CP1_1	High	2.63	Adhesive
	CP3_2		6.92	Cohesive
	CP3_3		-	-
	CP3_4		8.10	Cohesive/Adherend, primarily cohesive
	CP3_5		6.62	Cohesive

In addition, Figure 12.7a graphically shows the ultimate tensile strength for all the performed tests, depicting the median, minima, maxima, 1st and 3rd quartiles for each of the tested components. Figure 12.7b individually plots the ultimate tensile strength of all the tested specimens, grouped

by compound and failure mode. Figure 12.8 shows the correlation between the additive content and the ultimate tensile strength. At last, Figure 12.9 gives an overview of the specimens' failure modes, including a picture for each of the encountered mode.

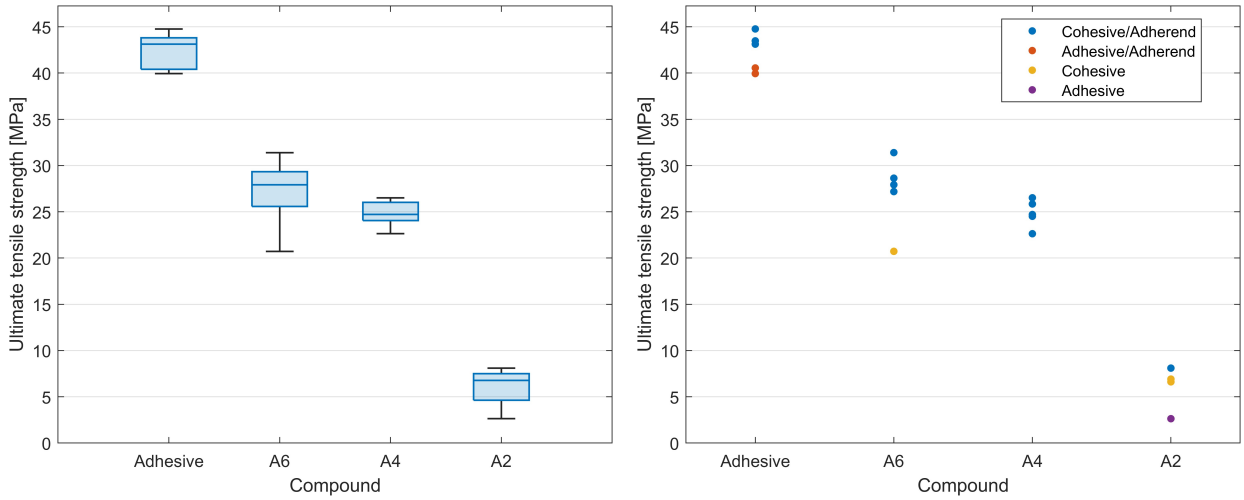

(a) Ultimate load

(b) Ultimate load and failure mode

Figure 12.7: Overview of the ultimate tensile strength and failure modes recorded during the centrifugal tests for all the tested compounds

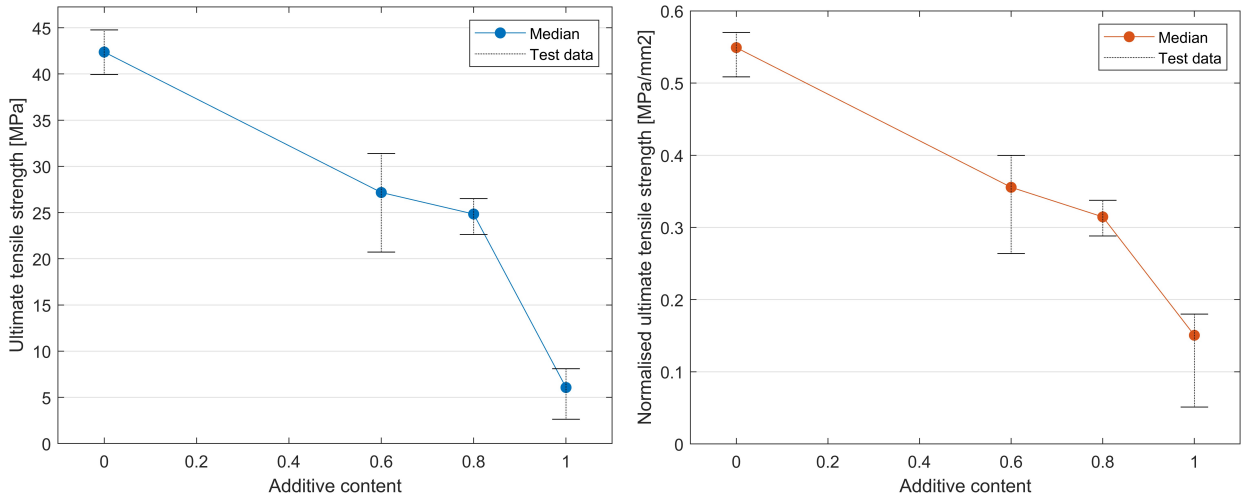

(a) Absolute values

(b) Values normalised per unit area

Figure 12.8: Correlation between ultimate tensile strength and additive content, based on the median values for each tested compound

The tests confirmed that increasing the amount of additive degrades the overall strength of the compound. However, with these results only, it is not possible to safely identify a function able to correlate the two variables.
This is partly because dosing the adhesive in a precise and consistent way on the specimens proved not to be straightforward, thus introducing scatter in the test results. Furthermore, and more importantly, the different compounds obviously have different densities and viscosities, which also affect their ability to uniformly cover the bond area. This issue is clearly depicted in Figure 12.9f, 12.9g and 12.9h: the compound with the highest additive content was significantly

more viscous than the others, this means that — under the weight of the copper cylinder — it was not able to flow well enough to spread and uniformly cover the full stamp's surface. This ultimately reduced the bond area (while increasing the bondline thickness), thus leading to higher stresses. In order to remedy such issue, the stresses were normalised per unit area (the effective bond areas for the high additive content specimens were directly estimated from the fracture surface pictures 12.9f, 12.9g and 12.9h), as shown in Figure 12.8b. This chart evidently shows a lower drop in strength between an additive content value of 0.8 and a value of 1, when directly compared to Figure 12.8a. Nonetheless, it is questionable whether applying such linear scaling yields realistic values, also considering that the higher bondline thickness remains unaddressed.

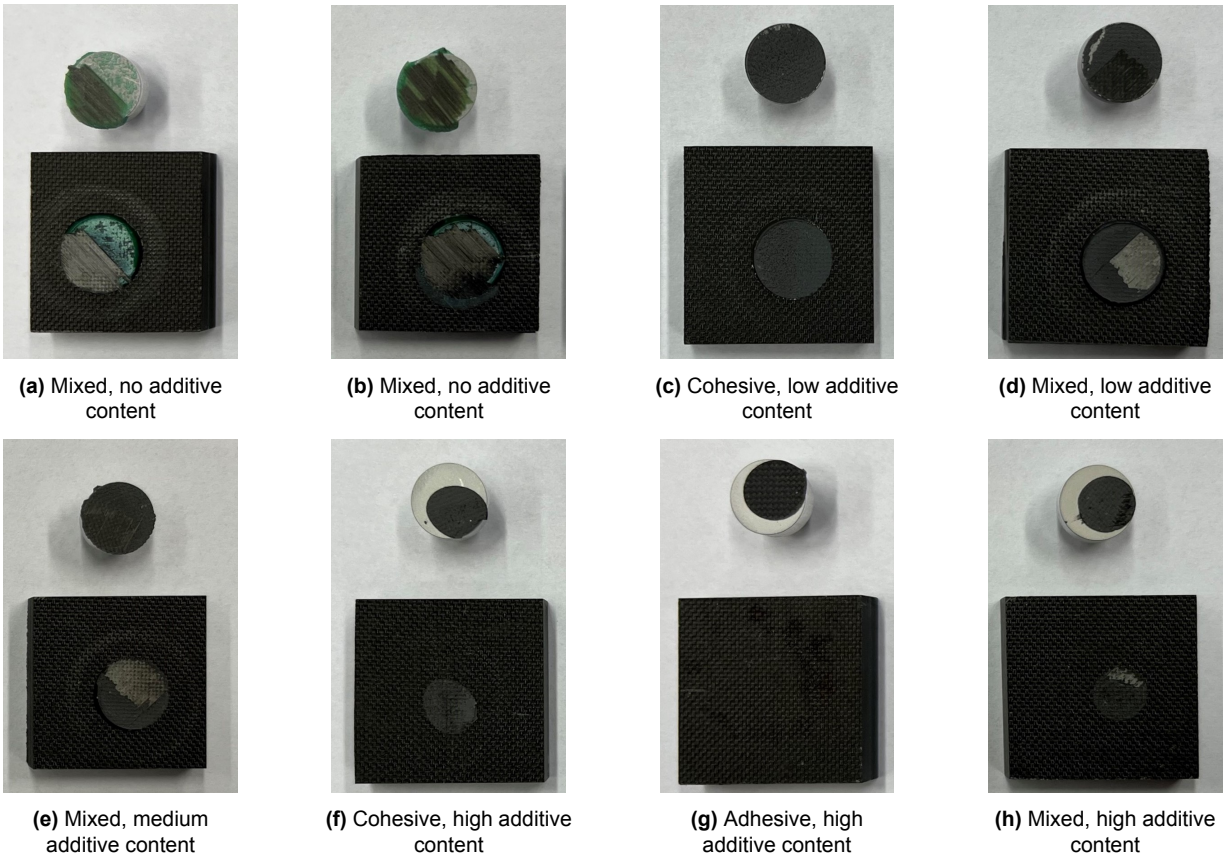

(a) Mixed, no additive content

(b) Mixed, no additive content

(c) Cohesive, low additive content

(d) Mixed, low additive content

(e) Mixed, medium additive content

(f) Cohesive, high additive content

(g) Adhesive, high additive content

(h) Mixed, high additive content

Figure 12.9: Fracture surfaces of some tensile centrifugal test specimens, depicting at least an example of all the encountered failure modes

Overall, these tests can be deemed inconclusive for defining a clear correlation between the additive content and the strength of the compound. In order to achieve that, it is necessary to dose the compound more precisely and possibly test more options with various additive contents. At the same time, the tests proved useful to verify that the compounds rarely showcase a pure adhesive failure behaviour. This is a positive fact, considering that such failure mode is not desirable nor allowed by regulations — as already mentioned.

12.4. Selection

The analysis conducted and presented here does not allow to safely identify a repair compound, since this choice needs to be primarily based on the electromagnetic properties — which could

not be assessed in this thesis, as already aforementioned. This is because restoring the LO properties of the structure is the most important requirement, and thus needs to lead to the selection. Nonetheless, a few aspects that emerged during this analysis constitute some useful insights, which will be able to support the final selection later on.

First, by mixing various compounds with different volume fractions for each component, certain thresholds establishing the practical feasibility could be defined. In other words, it was empirically established that, for instance, exceeding a certain additive content prevents from achieving a homogeneous consistency — or in certain cases from being physically able to blend the components in a uniform compound.
In addition, it was found out that 3 mm short fibres are unsuited to this purpose. It might be worthwhile trying even shorter fibres (i.e. in the range of 0.1-0.5 mm), or eventually chopping the functional material fabric in short fibres (so that they already include the additive particles, instead of adding it separately).

Second, despite no clear correlation between additive content and UTS could be established from the centrifugal tests, it was noted that at a certain additive content, the strength starts to decrease much more abruptly. Therefore — although mechanical strength is not the priority in this sort of repair — it is recommended to avoid very high additive contents, as this severely affects the mechanical properties of the compound.

In any case, taking into account these considerations, the repairs described in the upcoming chapter adopted the compound A4. This option represents a good compromise between additive content and mechanical strength, and has a viscosity that makes it convenient to work with.

13

Repair procedures

As already mentioned, no definitive repair procedures have been currently defined to address small damages localised in the functional material considered in this thesis. This chapter aims at defining and eventually implementing some feasible methods based on the use of the repair compound described in the previous chapter. Such methods were defined considering the requirements listed in Table 11.1, the functional material characteristics and the type of damage to be addressed. In more detail, this chapter defines two possible procedures, the first one is thought-out in detail, implemented and its outcome is assessed. Whereas, the second one is only conceptually outlined.

13.1. Manual repair procedure

The repair process defined and implemented here is based on the filling repair procedure already described in subsection 4.4.1. Since this work aims at laying down the foundation for a repair procedure to be eventually used in real cases, all the steps performed — including the more trivial ones — are reported here.
Such process was implemented on several portions (the figures below always depict the same one, but few others were repaired as well) of a panel like the one shown in Figure 1.3b, which had many impact damages on the functional material edge. The damages are shown in Figure 13.1, where the white marker lines delimit the regions affected by the impact. It is worth pointing out that, despite being generated in a similar fashion, not all the damages are identical: in some cases, large dents are visible (e.g. in Figure 13.1), while in others the edge is simply slightly pushed in and deformed vertically. This is due to the different position and orientation of the fibres in the vicinity of the edge, which was not consistent among the various panels. Nonetheless, this aspect does not affect the repair procedure, which remains the same in all the cases.

The first step consists in removing the material within the damaged region. This has a twofold purpose: on one hand the area affected by delaminations originated by the impacts are removed (thus preventing them from propagating). Additionally, the surface is prepared in order to achieve optimal bonding conditions. Given the size of the damages, this step was performed with a precision grinder equipped with a thin, cylindrical head. The damaged material was removed, as shown in Figure 13.2.

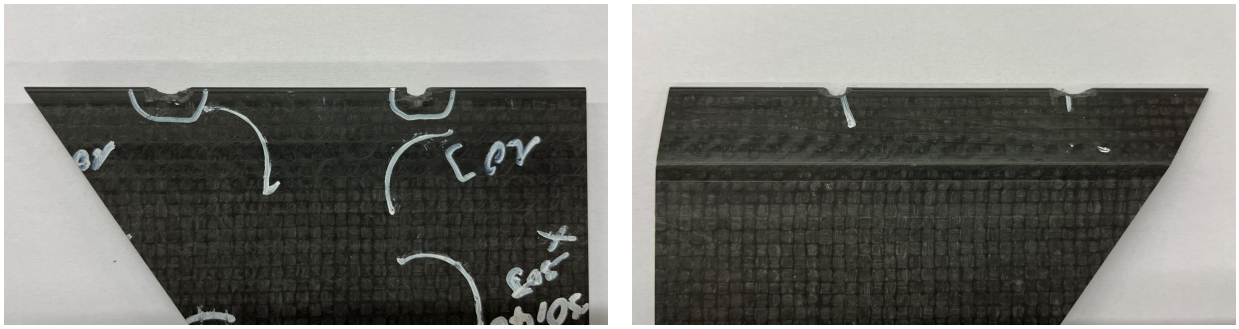

(a) Front side **(b)** Back side

Figure 13.1: Impact damages on the edge of the demonstrator component addressed with this repair procedure

The second step consists of cleaning the surface in order to remove any residual material left by the grinding: the grinded areas are therefore wiped with clothes moisted with acetone.
Third, the bond surfaces are activated using an abrasive material (Scotch-Brite™ pads, 3M Company, Saint Paul, Minnesota, United States) in order to promote adhesion, and then wiped once again with acetone first and de-ionized water after. These surface preparation steps are performed in several other qualified procedures for composite repairs, such as [73]. Nonetheless, their effect on the functional material considered here should be further studied, due to its novelty.

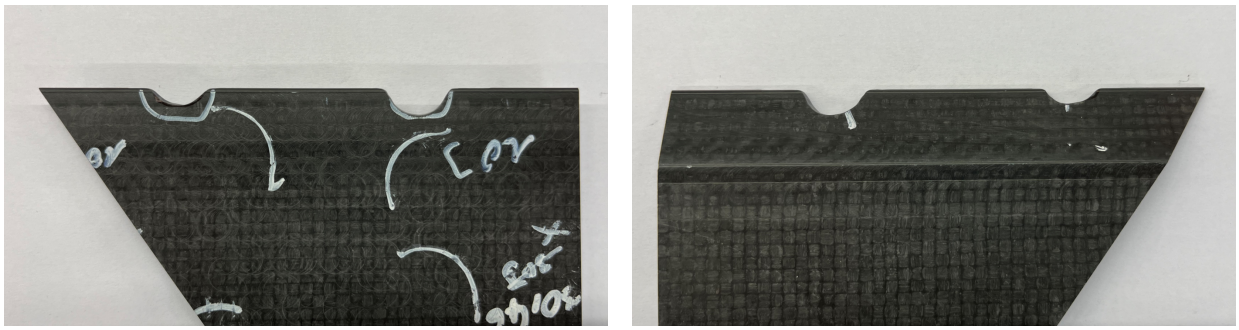

(a) Front side **(b)** Back side

Figure 13.2: Component repaired after removing the entire damaged areas via grinding

The next step consists of applying the repair compound (whose composition was discussed in the previous chapter) to fill up the prepared gaps. As visible in Figure 13.3, the components are strapped on aluminum plates with their damaged edge flush with a metallic block — intended to prevent the repair compound from flowing away. The compound is then applied: this can be done manually with either a spatula-like tool, or with a syringe (like in this case). It is important to make sure that the gaps are fully filled, excess material can be easily removed later once refining the edge profile. At this point, the curing cycle can be initiated, Figure 13.4 shows the cured repaired components prior to any post-processing.

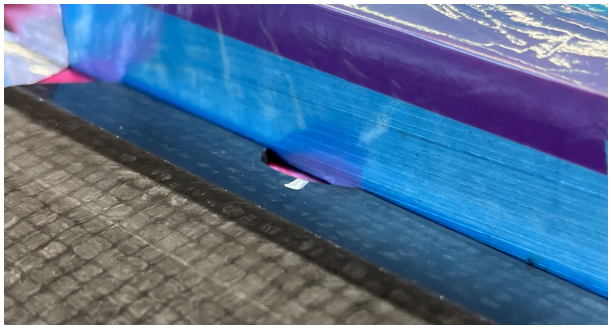

(a) Before pouring the compound

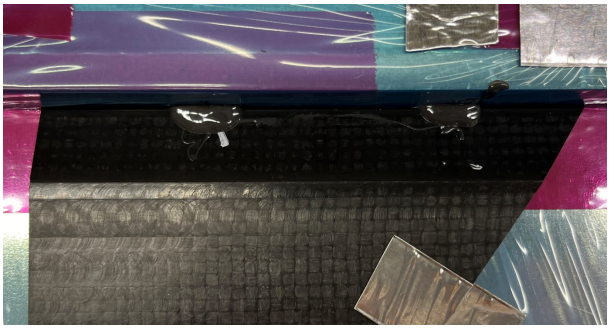

(b) After pouring the compound

Figure 13.3: Positioning of the component in a jig intended to keep the repair compound in place while curing

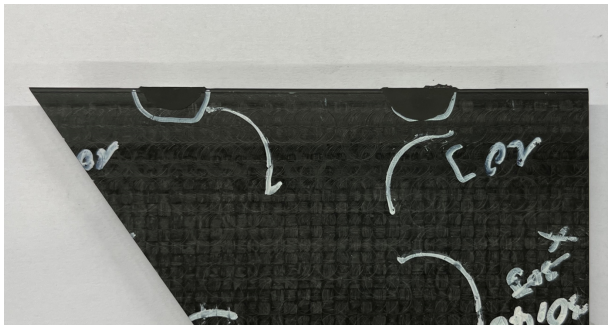

(a) Front side

(b) Back side

Figure 13.4: Repaired component at the end of the curing cycle, prior to the final surface post-processing

The final step consists of removing the excess repair compound and refining the surface in order to match as best as possible the original edge profile. The excess material is first removed with a precision grinder equipped with a thin, cylindrical head: a coarser grit size insert (P60) is used at first to remove most of the excess, before switching to a finer grit size (P120 or P150) to refine the surface. Then, the procedure is completed using fine sandpaper (grit size P320) to re-fine the entire edge profile, thus fully blending in the repaired areas with the unaffected ones. The very final step consists of wiping the surface with solvent (using cloth moisted with acetone) and de-ionized water. The final results is depicted in Figure 13.5.

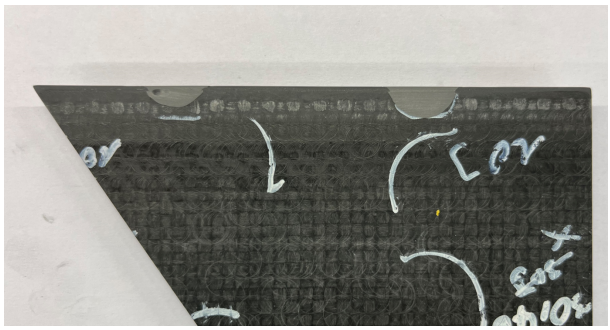

(a) Front side

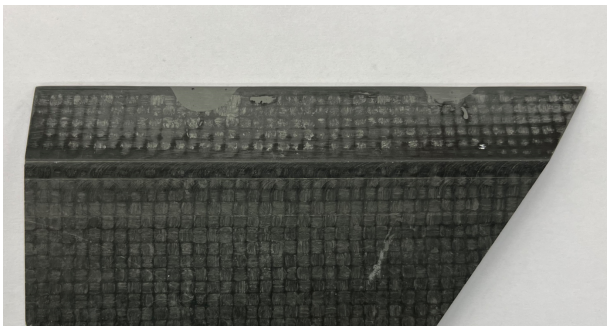

(b) Back side

Figure 13.5: Repaired component at the end of the procedure, after the final post-processing intended to re-fine the edge contour

As visible in Figure 13.5 this repair procedure allowed to achieve more than satisfactory results: the repaired areas blend in well with the surroundings, the edge contour is precisely restored, and the surface feels rather smooth and seamless. Even superior results could be achieved once the repair procedure is performed by trained, qualified personnel.
Figure 13.6 includes some micrographs of a repaired component: Figure 13.6a simply depicts a section view where the two different materials are visible (i.e. the structural composite in the core, and the functional one on the edges); whereas, Figure 13.6b and 13.6c show two different views of a repaired area. As visible in these two pictures, a few small air bubbles are noticeable. The impact of such minor imperfections should be quantified, and ways to further reduce this issue should be eventually investigated.

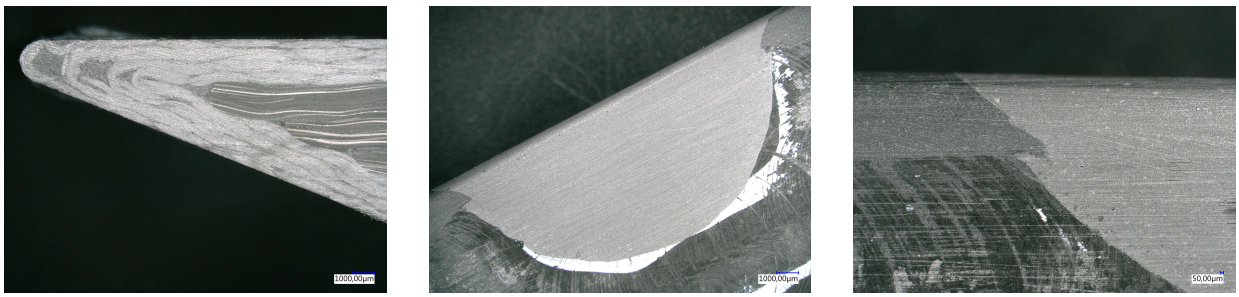

(a) Section view of the edge **(b)** Detail of a repaired area **(c)** Detail of a repaired area

Figure 13.6: Micrographs depicting the considered demonstrator component and some repaired areas

Do note that the ”swirl”, circular marks visible on the surface of the component in all the pictures shown above are created during the components’ manufacturing. They were therefore not generated during the repair procedure, which on the other hand left some straight marks on the edge due to sanding (well visible in Figure 13.6b and 13.6c).
At last, Figure 13.7 schematically summarises the procedure described above, mentioning all the steps necessary to carry out the repair.

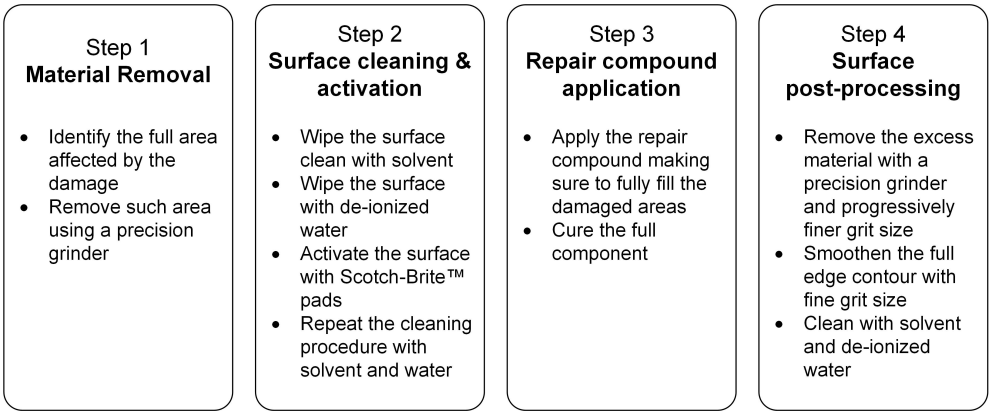

Figure 13.7: Step-by-step repair procedures to address small damages in the functional material using a paste-like repair compound

13.2. Injection repair procedure

A second alternative is inspired by the existing repair procedures based on resin injection, which were briefly described in subsection 4.4.2. While these repairs are generally adopted to address

minor damages located deep into the structure, the procedure conceptually presented here is intended to repair surface and/or edge damages. In order to do that, a bespoke tool matching the component edge contour needs to be designed. The repair procedure is then envisioned to be carried out via the following steps: first, the damaged area needs to be prepared by eliminating irregular edges to ensure a uniform substrate (in the same way adopted and presented for the previous procedure). Second, the injection tool — coated with release agent — is positioned and clamped in place. Third, the repair compound is injected and then cured by supplying localised heating. At last, the tool is removed, and eventual manual post-processing is performed to refine the edge contour.

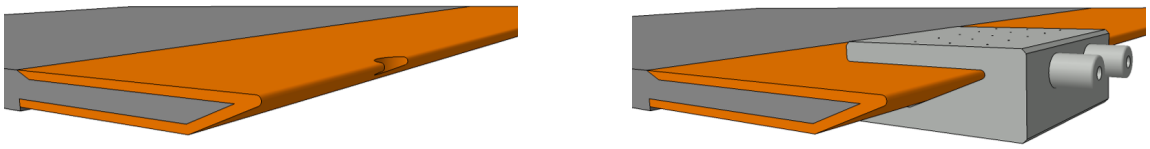

(a) Initial damage **(b)** Injection tool

Figure 13.8: Injection repair procedure to address small damages on the functional edge

The detailed design of the injection tool is outside the scope of this thesis, nonetheless a preliminary concept of how it may look like is provided in Figure 13.9.

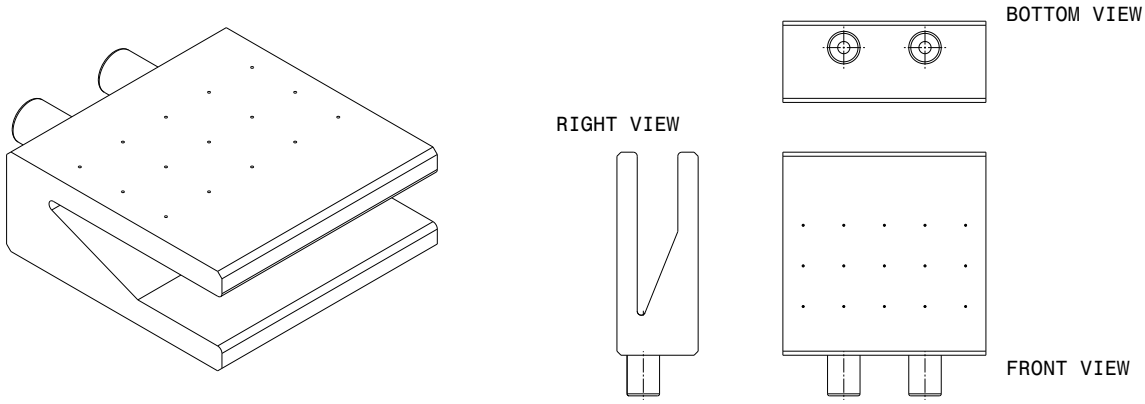

(a) Isometric view **(b)** Right, front and bottom views

Figure 13.9: Drawings of the concept tool defined for injection repairs (dimensions in mm)

The proposed injection repair process is feasible on paper, nonetheless its applicability should also be practically demonstrated. Additionally, it is also relevant to mention that this procedure might be convenient only if many components shared the exact same profile, so that a universal tool could be used. Otherwise, developing, producing and keeping available in multiple locations a high number of repair tools would be clearly illogical.

14

Discussion and conclusions

This chapter further discusses the work described in this part of the thesis dedicated to repairs in the functional material, and presents the associated conclusions. The key points mentioned here will then be re-called — and partially reiterated — in chapter 16, to underpin the answers to the research questions.

14.1. Repair compound

The work performed here did not allow to define a final composition for an optimal repair compound, given that the main requirement — i.e. its electromagnetic properties — could not be directly tested. Nonetheless, based on what is known about the considered functional material, different repair compounds were mixed and empirically deemed suitable to be used for repair purposes. Micrographs proved a close similarity between these compounds and the original material from a qualitative, visual standpoint; however, no quantity could be precisely measured. It was however possible to quantify the effect of the additive on the mechanical strength of the compound, thanks to centrifugal tensile test. Despite no clear correlation could be found, it was shown that additive content and strength are not linearly related. Such data may come in handy in the eventuality that the composition of the compound will be iterated. Additionally, it was also proven that all the tested compounds very rarely lead to adhesive failure, which is a positive aspect considering the stance of regulations regarding this failure mode.

In conclusion, the next step now consists in assessing the compounds' interaction with electromagnetic waves, and thus verifying which — if any — can closely match the behaviour of the original material. Based on this analysis, either one of the proposed compounds can be selected, or a new composition — based on insights from testing — can be defined.

14.2. Repair procedures

Two feasible repair procedures were outlined: a first one based on the already existing filling repair method, and a second one inspired by injections repairs. The former was also implemented on several components and proved to achieve the desired outcomes. Indeed, this procedure proved capable of restoring the edge profile of the component and smoothly blending in with the surrounding areas (therefore, requirement FR-RQ3 from Table 11.1 can be considered verified). On the other hand, it was not possible to verify the other two requirements. The functionality

(FR-RQ1) of the repaired region could not be assessed due to the aforementioned impossibility of performing electromagnetic tests. In future work, this aspect should be addressed, and in particular the behaviour of the transition region should be analysed in order to ensure that the component absorption behaviour is as uniform as possible. The adhesion between the parent laminate and the repaired areas (FR-RQ2) could not be directly quantified either, despite visually appearing and feeling sturdy. Nonetheless, the effects of the additive on the strength of the resin were quantified as mentioned above, in such a way that an indirect measure could be provided.
Another relevant aspect to mention is that the effect of various mainstream surface treatments on the functional material should be further investigated. The repair procedure implemented here relies on widely adopted treatments for other conventional materials, yet their suitability and effects on this material specifically should be investigated in detail.
It must be also noted that further investigations should be postponed, as long as more details about the components that will employ this functional material will be available. It is indeed not worth further developing any repair options in the absence of detailed information about the characteristics and the intended use cases of the components. As already mentioned, design choices significantly determine the requirements that a repair needs to fulfil, it is thus crucial to know more about the actual components before progressing further.

In conclusion, the work performed here provided very preliminary yet useful data that may come in handy during later design phases of components using this type of material. Rather than generating definitive conclusions, this work laid down the foundations for future detailed investigations in various directions.

15

Outlook

This chapter addresses some aspects that could not be thoroughly investigated throughout this project, with the aim of paving the way for future work. First, few aspects that may improve the procedure to address functional damages using hard patches are presented (procedure proposed by D'Arduini [4], and recalled in section 11.1). Then, some repair procedures to tackle damages affecting both the structural and functional parts are conceptually outlined.

First, in order to improve the results of the procedure implemented by D'Arduini [4], the following aspects should be considered.
To begin with, it is necessary to ensure that the patches precisely match the dimensions of the repair area, on top of the properties of the original functional material.
Furthermore, it would be most likely convenient to tapered, round the edges of the pocket generated when removing the damaged edge section. In this way, it would be easier to align the patch, stress concentrations would also be avoided, and less manual post-processing would be required. Fine tuning the parameters of the CNC milling systems used for these steps should allow to obtained the desirable results.
At last, it is beneficial to ensure that the patch remains precisely in place while the adhesive cures: relying on a tool able to constraint and apply uniform pressure would be better than using clamps.

Second, as mentioned in chapter 1 damages might also impact both the structural and functional part of the component, and so bespoke repair processes may be required. As for the rest of this work, only the removable hatch of the demonstrator structure depicted in Figure 1.3 is considered. Also in this instance, the damage size is very influential in determining the most suited repair method.
In case of large damages, it would most likely be convenient to use a procedure similar to the one recalled in section 11.1: a large section comprising the damaged region and the surroundings is removed, then a trimmed-to-size patch obtained from a sacrificial component is secondary-bonded in place.
However, damages more limited in size — such as the ones depicted in Figure 15.1a and 15.2a — may be addressed differently, in a more cost-effective way. The envisioned repair procedure is depicted step-by-step in Figure 15.1 and 15.2 (where the only difference is the damage location along the edge). The first step consists of removing the damaged area via milling, either manually or with a CNC system (Figure 15.1b and 15.2b). In the second step, a paste-like repair compound intended to match the properties of the structural material is applied and cured (Figure 15.1c and 15.2c). The third step consists of milling away the excess compound, in order to match the original layer, as visible in Figure 15.1d and 15.2d. At this point, the functional repair compound is applied and cured (Figure 15.1e and 15.2f). The final step consists of removing the excess compound

and smoothening the surface, in order to blend in the repaired are and achieve a seamless finish (Figure 15.1f and 15.2f). The feasibility of this procedure obviously needs to be assessed, and it is particularly important to prove that repair is capable of restoring both the structural integrity and the functionality of the component.

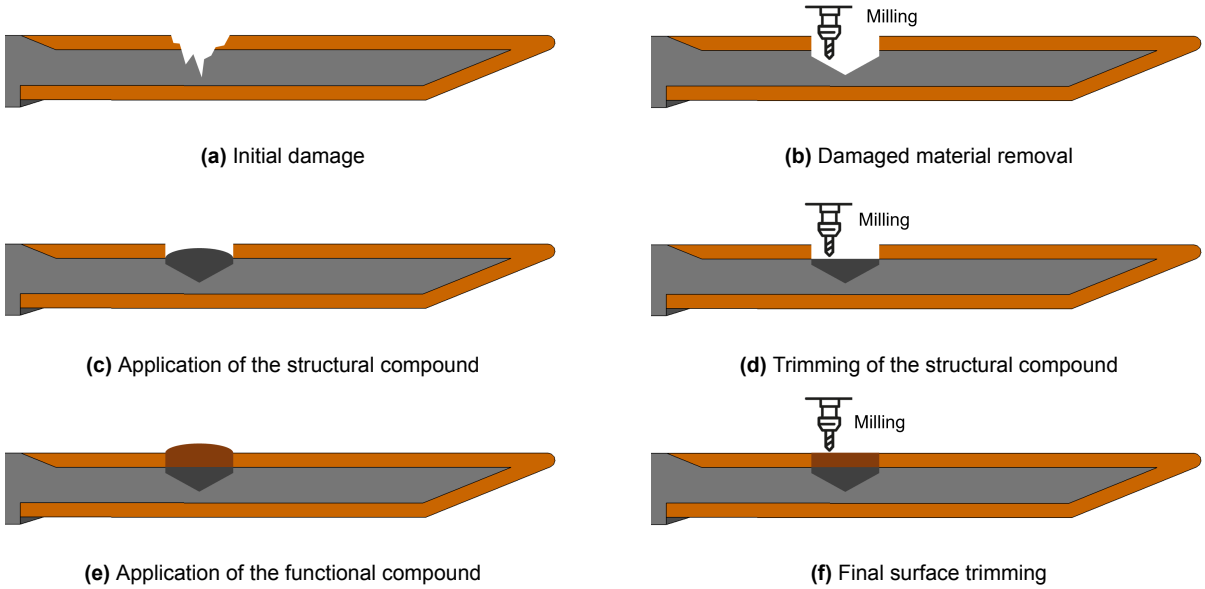

(a) Initial damage

(b) Damaged material removal

(c) Application of the structural compound

(d) Trimming of the structural compound

(e) Application of the functional compound

(f) Final surface trimming

Figure 15.1: Conceptual repair procedure to address damages impacting both the structural and the functional parts of the demonstrator component

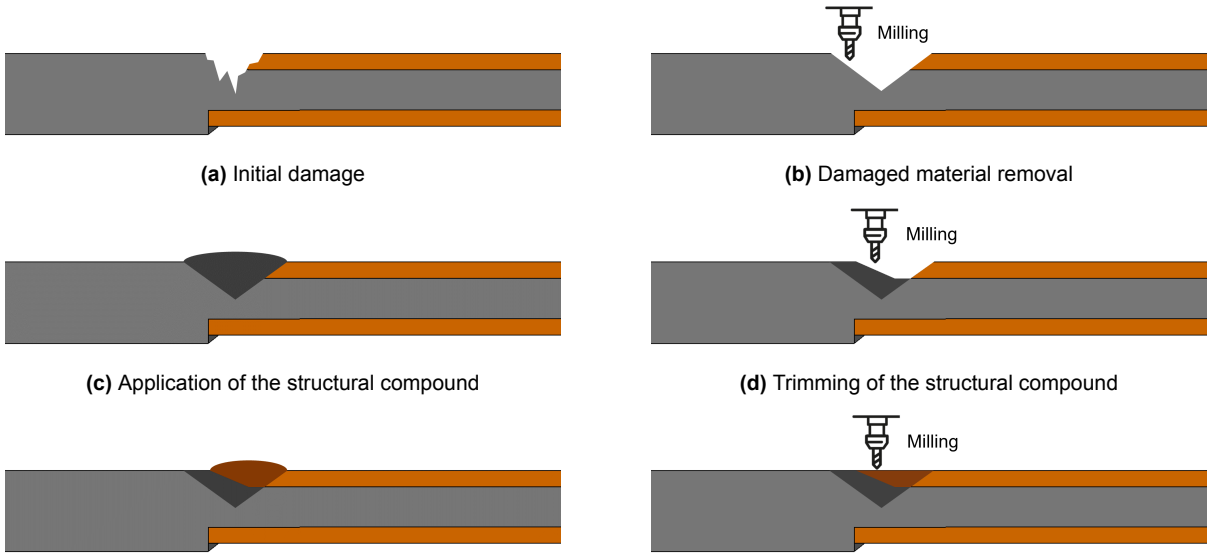

(a) Initial damage

(b) Damaged material removal

(c) Application of the structural compound

(d) Trimming of the structural compound

(e) Application of the functional compound

(f) Final surface trimming

Figure 15.2: Conceptual repair procedure to address damages impacting both the structural and the functional parts of the demonstrator component, damage located in the transition area between the two materials

An additional damage scenario is represented by delaminations that may originate in the vicinity of fastener holes. It is known that this kind of damage is quite frequent, and it is also rather common to have such holes on removable panels like this demonstrator structure. Therefore, it

is worth briefly mentioning this aspect as well.
Depending on the severity of the delaminations, different approaches may be considered. In case of defects limited in size, pure resin could be injected. In the presence of larger delaminations, it may be necessary to remove the entire affected area and replace it with a secondary-bonded patch — or even applying the procedure described above, based on the use of filler compounds. Overall, too little is known for the time being in order to define — even if only on paper — a suitable repair procedure for such scenario. Should it become necessary to address this aspect in the future, the considerations mentioned above can be taken as a starting point.

IV

Conclusive Remarks

16

Conclusions

This chapter aims at bridging the conclusions for the two parts of the thesis already presented in chapter 10 and 14 with the research questions defined in chapter 5. The goal is to provide the overall conclusions of the thesis and expand them to a generic level. First, the content of the thesis is concisely summarised, highlighting the main takeaways. Then, the answers to the research questions are provided.

16.1. Summary

This project investigated ways to address different damages scenarios in specific CFRP aircraft components, which are made out of a core structural material and a stealth functional one wrapped around some their edges. The thesis was divided into two macro-parts: the first one addressed the damages fully located in the structural section of the components, while the second one focused on the damages localised in the functional parts.

The first part focused on optimizing the conventional scarf repair procedure, which was identified as the most suited one to tackle structural damages. The main goal was to improve the surface finish of repaired parts, in order eliminate sudden changes in thickness that are detrimental for stealth and aerodynamic reasons.
Two innovative options were implemented, tested and compared with the conventional one, namely: the re-milled configuration — which smooths the repaired surface via a milling post-processing — and the modified patch configuration — which exploits a carefully aligned, thinner repair path to avoid major unevenness. The former proved capable of significantly improving the surface finish (≈80% improvement), while fulfilling the mechanical requirements with just a slightly inferior (roughly -4% in terms of failure load) performance compared to the conventional configuration. On the other hand, the latter did not prove capable of meeting most of such mechanical prerequisites, despite partially improving the surface finish.
Overall, this work highlighted that the re-milled configuration allows for a superior surface finish and is thus worth further developing. Nonetheless, its applicability is only convenient in those scenarios where having an extremely flush surface is of primary importance, given that it requires significantly more work compared to the conventional procedure. In addition, it showed a slightly lower ultimate load (roughly -4% compared to the conventional configuration) — despite all the load requirements could be met with ample margins in this study.

The second part focused on researching ways to repair small impact damages located on the functional material edge of the considered CFRP components.

First, a procedure to define the composition of a paste-like repair compound suitable to address such damages was outlined. A single optimal compound could not be unequivocally determined, given the impossibility of directly measuring the functionality of the material via electromagnetic tests. Restoring the stealth functionality is the key priority, and therefore the major driver in determining the composition of a repair compound and ultimately the effectiveness of a repair. Nonetheless, different options that are theoretically close in terms of composition to the original functional material were defined, and some of their properties were assessed.
Second, two different repair processes based on the use of such compound were thought out and one of them was practically implemented. The first one — which was also applied on several components — is similar to conventional filling repair procedures, while the second one relies on a bespoke tool to inject the repair compound. Also in this case, it was not possible to assess the repair's electromagnetic behaviour, the procedure proved capable of precisely restoring the edge profile of the component, ensuring a seamless repair finish.
Overall, this work produced some useful preliminary data. Nonetheless, any future investigation shall first of all evaluate the electromagnetic properties of the repair compounds and of the repaired components, since restoring the material's functionality is the key requirement.

16.2. Answers to the research questions

The research questions defined in chapter 5 are answered in the following section.

SQ1.1 How to manufacture a fully flush, bonded scarf repair by re-milling the repaired area?

A flush bonded scarf repair can be manufactured according to the following two main steps, as demonstrated in this thesis.

1. First, a conventional scarf repair needs to be implemented, this work relied on secondary-bonded repair patches, but the procedure is also applicable with co-bonded patches without any change needed.
2. Second, once the adhesive (and eventually the patch too) is cured, the milling post-processing step can be initiated. Due to the required degree of precision, a CNC milling system needs to be used. This work relied on a 6-axis robot, equipped with a high-frequency milling head. The repaired panels need to be firmly clamped in place (e.g. using a suction table, like in this case). Then, the origin of the robot vertical axis needs to be set to coincide with the top surface of the parent laminate, far away from the repaired region. The surface is then milled over keeping this z-coordinate fixed (in this work, a feed rate of 2 m/min with a carbide milling tool spinning at 12000 rpm was selected). This enables smoothening the surface, eliminating any sharp mismatch between the parent laminate and the repair patch. Re-milling the surface multiple times — first only the repaired area and then the full surface — might also be beneficial. No further processing is required.

In this thesis, the described re-milling procedure allowed for an improvement of over 80%, reducing the unevenness from over 1/2 of a millimeter to less than a 1/10, while ensuring a continuously smooth surface finish.

SQ1.2 How to optimize the repair patch layup in order to achieve a fully flush, bonded scarf repair while minimizing further surface post-processing?

This thesis proposed a procedure to optimize the layup of the repair patch, with the goal of obtaining a slightly thinner repair patch that — once properly aligned — can ensure a flush surface finish.
The patch's layup is defined starting from the original one, and then removing certain plies. The number of layers to be removed is determined in such a way that their total thickness corresponds to the mismatch between the parent laminate and the repaired area, which is usually generated by conventional scarf repairs. Then, the process to select what plies need to be removed is driven by the aim of obtaining the highest possible level of similarity with the parent laminate in terms of mechanical properties (which can be estimated relying on CLT).
In this specific case, it was found that conventional scarf repairs usually originate a mismatch of 0.5 mm. Hence, the thickness of the modified repair patch was reduced by such amount. Taking the original layup as a starting point, all the possible combinations of plies that once removed allowed to achieve the desired thickness were found. The selected layup was thinner than the original one by 1/6, stiffer in both the longitudinal and transverse direction by roughly 10% and with a shear modulus lower by roughly 15%. This was achieved by removing some of the inner 45°/135° plies, which was also reasonable considering the loading case of the specimens (pure tension, in the 0° direction).
This approach was found partially successful in improving the surface finish, although the desired result can not be achieved without some post-processing: while the parent laminate and the patch are well levelled away from the scarf region, a concavity remains at the interface between them (due to the shorter scarf length of the patch, given its decreased thickness yet equal scarf ratio). This unevenness is detrimental for stealth purposes and would thus need to be manually re-worked. In addition, this option proved incapable of meeting the mechanical requirements during testing in terms of fatigue life. While the second issue may be addressed selecting the new layup in a different way, the first one cannot be resolved. Therefore, it does not seem advisable to further develop this repair concept.

SQ2.1 What are the suitable procedures to repair localized, small, cosmetic damages using a filler compound?

This thesis proposed two possible procedures to address minor, cosmetic damage using a filler compound.
The first procedure consists of removing the damaged material and preparing the surface to promote bonding. Then, the repair compound is applied — either manually or with the help of a syringe — in the area of interest. Once cured, the excess compound is removed, and the overall edge is reworked in order to blend in the repaired areas and achieve a seamless surface finish. This repair process was implemented on several components in this study, and proved capable of restoring the edge profile.
The second procedure was not implemented but simply defined from a conceptual standpoint. It consists of first of all removing the damaged areas and preparing the substrate, like in the previous case. Then, the filled compound is applied using a bespoke injection tool, which precisely matches the profile of the component to be repaired. In this way, much less post-processing should be needed: there should be no need to extensively rework the edge to smoothen it like in the previous case. While this process is theoretically doable and similar to already existing ones, its feasibility and results should be practically assessed. Nonetheless, further developments should only be undertaken if many components had the exact same profile, and therefore if the exact same tool could be used in many instances. Otherwise, it would be clearly inconvenient to

have a high number of bespoke tools.

SQ2.2 How to define the optimal functional material filler compound to repair localized, small, cosmetic damages?

This thesis proposed a procedure to define a functional material filler compound to repair such damages, although an optimal composition could not be determined due to the impossibility of performing certain key tests.
The following were identified as the main guidelines to consider while establishing the compound's composition. First, the compound needs to match as closely as possible the functionality of the original material. Second, the compound needs to possess a paste-like viscosity, such that it can be applied as a conventional body filler — or eventually injected.
This thesis proposed various compounds able to achieve the desired consistency and viscosity, and also quantified their mechanical strength. However, tests to assess their functionality could not be performed. Therefore, the main guideline could not be assessed. A single compound was selected to implement some sample repairs, based on the fact that its composition is the closest to the original one. However, this does not guarantee that that the functionality is also exactly the same, since the compounds use the same additive but different resin (and eventually fibres) with respect to the original material — due to some processing parameters constraints.
Overall, this thesis put forward some guidelines to define filler compounds, as well as a series of options with suitable consistency and viscosity. Nonetheless, this work needs to be complemented with tests aimed at accessing the material functionality, whose results will ultimately allow to the select the optimal compound.

SQ2.3 How to improve the repair process using hard patches to tackle larger damages?

Due to resource constraints, no such repair could be implemented in this work. Therefore, only guidelines derived from an analysis of previous repairs could be defined. The following aspects were identified as practical to improve the overall repair quality.
To begin with, it would be useful to enhance the precision of the repair patch, as well as of the pocket generated by removing the damaged material, so that their dimensions precisely match (this should be achievable by fine tuning the CNC milling processing parameters).
In addition, the pocket should have tapered, round edges rather than sharp edges: this should facilitate the precise patch alignment, reduce stress concentrations and minimize the required manual post-processing.
At last, ways to keep the patch precisely in place while the adhesive cures should be considered: this may be achieved using a bespoke tool matching the full profile able to apply uniform pressure rather than conventional clamps.

SQ3.1 What are the suitable procedures to repair damages affecting both the structural and functional parts?

Also in this case, due to resource constraints, no actual repair procedure could be practically implemented. Nonetheless, several options were defined and discussed from a conceptual level.
In case of larger damages, it would be most likely convenient to completely remove the damaged area and secondary bond a trimmed-to-size patch obtained from a sacrificial component.
In case of smaller damages on the other hand, it would be probably more convenient to remove

the damaged area via CNC milling and then use paste-like repair compounds to fill the gaps. Since both materials are affected in this damaged scenario, two repair compounds — one for the structural material and one for the functional one — and multiple steps would be required: first the structural compound is poured to fill the core; once cured, excess material is milled off to match the original material stratification; the same procedure is then repeated with the functional compound, before smoothing the surface.

17

Recommendations

This chapter lists some key recommendations emerged throughout this thesis, offering actionable insights for further researching the topic considered in this study. These concise guidelines represent the starting point for an eventual continuation of this work.

The first recommendation regards the comparison between the film adhesive (Loctite EA9695 AERO) and the paste adhesive (Solvay Aeropaste 1006) using MCLS specimens. As discussed in the dedicated chapter (chapter 7), the large difference in terms of fatigue life is most likely explainable by their different chemical composition. Nonetheless, since it was pointed out that some aspects — which could be better controlled — might have had a contribution, it is advised to perform additional tests to clear any doubt.
This additional investigation should ensure a better control of the bondline thickness (to ensure more consistency in terms of thickness and voids content), and avoid approaching the paste adhesive's glass transition while bonding the specimen tabs. At last, it is advised to use a fresh, recent batch of paste adhesive, since the one used here had reached the end of its shelf-life. In addition, being the adhesive still under-development, it may be that newer batches come with an improved formulation able to achieve a superior performance. Moreover, should it be desired to precisely track the crack growth propagation within the bondline, it is recommended to tailor the DIC analysis script to the feature of this specimen.
Should the results obtained in this work be confirmed by further tests, it would then be recommended to carefully evaluate the applicability of such paste adhesive for assembly and/or repair scenarios — also recalling that it predominantly showed adhesive failure.

The second recommendation regards the re-milled scarf repair configuration. This alternative proved extremely valid, since it eliminates sharp mismatches while only slightly compromising mechanical strength. It is therefore advised to continue the development, moving up in the test pyramid and eventually defining a certifiable repair procedure.
It is specifically recommended to assess how this configuration performs with respect to a conventional, certified repair that also includes an overply. It is clear that it is far better from a surface finish standpoint, nonetheless the environmental durability and the ability to reduce peel stresses in the interface region — which are proven for conventional repairs — needs to be further assessed. For this, it would be necessary to test full repairs up to component or system level.
Overall, it is reasonable to say that the choice of repair configuration is a sort of trade-off between surface flushness and repair strength. This work showed that the re-milled option was able to meet the load requirement with ample margin, however this should be further confirmed — especially with respect to fatigue life — before considering the application of this procedure in

real-life cases.

Regarding the modified patch, it is recommended not to proceed further and archive this concept, given the unsatisfactory performance. Generally speaking, it would be surely interesting to explain why the fatigue life is much shorter than the other options — and modelling would surely provide valuable insights in this direction. Nonetheless, this would be of little usefulness at industrial level, since the configuration already proved largely incapable of meeting the requirements, and is therefore not recommended.
Even trying to define a different layup based on an iterative modelling approach is not highly recommended: while another layup may be superior in terms of mechanical performance, it would not change the surface finish. The latter — which is the main behind this study, and ultimately the aspect to prioritize — would still remain inferior to the other repair configuration (the re-milled option). The surface finish is indeed independent of the layup and only determined by the patch alignment.

In addition, it would be surely useful to manufacture and test both soft co-bonded patch repairs and hard secondary-bonded patch repairs at the same time. This would allow to perform a more precise comparison between the two alternatives, rather than resorting to old data like in this thesis. In fact, it would be possible to have better control over the manufacturing and testing conditions of all the specimens, and thus being able to eventually justify some discrepancies.

The next recommendation regards the surface finish requirement, and how this is measured. In this project, as well as in the previous ones, the goal was to reduce the mismatches generated by repairs as much as possible. Nonetheless, it would be useful to have a specific number to aim for, and formulate requirements such as: "*The repaired surface shall not present any mismatch larger than x.xx [mm]*". It might indeed be that unevenness below a certain level is non influential, and it clearly does not make sense to go below a certain level if not needed. It is therefore recommended to define a clear requirement directly derived from stealth — and eventually aerodynamic — needs.
In addition, the way of measuring the repaired surface flushness also needs to be standardised: this work, as well as the previous ones, relied on ultrasonic techniques that allow to measure the components' thickness at discrete locations. The mismatch was then derived subtracting the average thickness of the undamaged section from the average thickness of the repaired section. On top of the mentioned shortcomings of ultrasonic measurement, the absence of a measuring procedure causes the results of the different works not to be fully comparable. It is therefore recommended to clearly define a protocol, and rely on more precise 3D scans of the full surface rather than on discrete ultrasonic measurements.

The next consideration is about the definition of a repair compound for the functional material. It is recommended to perform electromagnetic tests on the proposed compounds, and then select the suitable one(s) or eventually iterate their compositions based on the result. Further proceeding without such experimental data is not recommended, since the primary requirement is to restore the material functionality.
Should more centrifugal tensile tests be performed, it is recommended to implement the following actions: 1) rely on an automated dosing system to apply more precise quantities on the samples, 2) if the compounds are very liquid and thus difficult to dose, wait for them to start curing and become more viscous before dosing on the samples, 3) if the compounds are very viscous and can't autonomously cover the full bond area, apply a heavier weight to ensure a more uniform spread.

Regarding the manual repair procedure implemented in this work, it is recommended to perform tests to quantify the durability and strength of the repairs. This may be achieved by repeating the same impact tests, and assessing the different outcomes. In addition, it is also recommended to evaluate their durability over time. Furthermore, it is advised to investigate the effect of different surface treatment procedures on the functional material: the most conventional ones have been applied in this work, it is nonetheless necessary to deeply analyse this aspect in order to properly define — and eventually qualify — repair methods. At last, it is recommended to postpone the detailed development and eventual standardization of any procedure until more details of the components that will use the considered material are available.

References

[1] J. Zhang, G. Lin, U. Vaidya, and H. Wang, “Past, present and future prospective of global carbon fibre composite developments and applications,” *Composites Part B: Engineering*, vol. 250, p. 110 463, Feb. 2023, issn: 13598368. doi: 10.1016/j.compositesb.2022.110463.

[2] R. Dilger, H. Hickethier, and M. D. Greenhalgh, “Eurofighter a safe life aircraft in the age of damage tolerance,” *International Journal of Fatigue*, vol. 31, no. 6, pp. 1017–1023, Jun. 2009, issn: 01421123. doi: 10.1016/j.ijfatigue.2008.05.014.

[3] B. Esp, *Practical Analysis of Aircraft Composites*. United States: Grand Oak Publishing, Oct. 2017, isbn: 9780983245391.

[4] R. D’Arduini, *Reparaturkonzepte Komplexer CFK-Flugzeugstrukturen*, Master Thesis, Manching, Germany: Airbus Defence and Space GmbH, Oct. 2022.

[5] A. Scholz, *Reparatur von Komplexen CFK-Flugzeugstructuren*, Master Thesis, Manching, Germany: Airbus Defence and Space GmbH, Nov. 2021.

[6] M. Giobbio, *Repair Methods for CFRP Aircraft Structures with Functional Inserts*, Literature Study, Delft, Netherlands: Delft University of Technology, Aug. 2023.

[7] A. J. Jefferson, V. Arumugam, and H. N. Dhakal, “Overview of different damage and common repair methods in composite laminates,” *Repair of Polymer Composites*, pp. 45–95, Jan. 2018. doi: 10.1016/B978-0-08-102263-4.00002-8.

[8] E. Archer and A. McIlhagger, “Repair of damaged aerospace composite structures,” *Polymer Composites in the Aerospace Industry*, pp. 393–412, Jan. 2015. doi: 10.1016/B978-0-85709-523-7.00014-1.

[9] G. A. O. Davies and R. Olsson, “Impact on composite structures,” *The Aeronautical Journal*, vol. 108, no. 1089, pp. 541–563, 2004. doi: 10.1017/S0001924000000385.

[10] A. Birur, *Time-dependent damage evolution in multidirectional polymer composite laminates*, Master Thesis, Winnipeg, Canada: University of Manitoba, 2008.

[11] EASA, *AMC 20-29. Composite Aircraft Structure. Annex II to ED Decision 2010/003/R*. Cologne, Germany: European Aviation Safety Agency, 2010.

[12] FAA, *AC 20-107B - Composite Aircraft Structure*. Washington, D.C., United States: U.S. Department of Transportation - Federal Aviation Administration, 2010.

[13] S. Omairey, N. Jayasree, and M. Kazilas, “Injection repair of advanced composites: a prospective method for delamination damage repair,” *Sustainable Biopolymer Composites: Biocompatibility, Self-Healing, Modeling, Repair and Recyclability: A Volume in Woodhead Publishing Series in Composites Science and Engineering*, pp. 183–211, Jan. 2022. doi: 10.1016/B978-0-12-822291-1.00002-6.

[14] A. J. Kinloch, *Adhesion and Adhesives*. Dordrecht: Springer Netherlands, 1987, isbn: 978-90-481-4003-9. doi: 10.1007/978-94-015-7764-9.

[15] ASTM, *D5573 Standard Practice for Classifying Failure Modes in Fiber-Reinforced-Plastic (FRP) Joints*. West Conshohocken, Pennsylvania: ASTM International, 2019.

[16] J. Kupski, S. T. De Freitas, D. Zarouchas, P. Camanho, and R. Benedictus, “Composite layup effect on the failure mechanism of single lap bonded joints,” *Composite Structures*, vol. 217, pp. 14–26, 2019. doi: 10.1016/j.compstruct.2019.02.093.

[17] J. Kupski, D. Zarouchas, and S. T. de Freitas, “Thin-plies in adhesively bonded carbon fiber reinforced polymers,” *Composites Part B: Engineering*, vol. 184, p. 107 627, 2020. doi: 10.1016/j.compositesb.2019.107627.

[18] B. Liu, F. Xu, W. Feng, R. Yan, and W. Xie, “Experiment and design methods of composite scarf repair for primary-load bearing structures,” *Composites Part A: Applied Science and Manufacturing*, vol. 88, pp. 27–38, Sep. 2016, issn: 1359-835X. doi: 10.1016/J.COMPOSITESA.2016.05.011.

[19] A. Karolak, J. Jasieńko, and K. Raszczuk, “Historical scarf and splice carpentry joints: state of the art,” *Heritage Science*, vol. 8, no. 1, p. 105, Dec. 2020, issn: 2050-7445. doi: 10.1186/s40494-020-00448-2.

[20] A. J. Jefferson, V. Arumugam, and H. N. Dhakal, “Key stages of adhesively bonded repairs,” *Repair of Polymer Composites*, pp. 97–224, Jan. 2018. doi: 10.1016/B978-0-08-102263-4.00003-X.

[21] J. Holtmannspötter, J. V. Czarnecki, F. Feucht, *et al.*, “On the Fabrication and Automation of Reliable Bonded Composite Repairs,” *The Journal of Adhesion*, vol. 91, no. 1-2, pp. 39–70, Jan. 2014, issn: 15455823. doi: 10.1080/00218464.2014.896211.

[22] K. B. Katnam, L. F. Da Silva, and T. M. Young, “Bonded repair of composite aircraft structures: A review of scientific challenges and opportunities,” *Progress in Aerospace Sciences*, vol. 61, pp. 26–42, Aug. 2013, issn: 0376-0421. doi: 10.1016/J.PAEROSCI.2013.03.003.

[23] M. C. Shaw, *Metal cutting principles*, 2nd ed. Oxford, United Kingdom: Oxford University Press, 2004, isbn: 9780195142068.

[24] S. Psarras, T. Loutas, G. Galanopoulos, G. Karamadoukis, G. Sotiriadis, and V. Kostopoulos, “Evaluating experimentally and numerically different scarf-repair methodologies of composite structures,” *International Journal of Adhesion and Adhesives*, vol. 97, p. 102 495, Mar. 2020, issn: 0143-7496. doi: 10.1016/J.IJADHADH.2019.102495.

[25] J. de Freese, J. Holtmannspötter, S. Raschendorfer, and T. Hofmann, “End milling of Carbon Fiber Reinforced Plastics as surface pretreatment for adhesive bonding – effect of intralaminar damages and particle residues,” *The Journal of Adhesion*, vol. 96, no. 12, pp. 1122–1140, Sep. 2018, issn: 15455823. doi: 10.1080/00218464.2018.1557054.

[26] J. ALYousef, A. Yudhanto, R. Tao, and G. Lubineau, “Laser ablation of CFRP surfaces for improving the strength of bonded scarf composite joints,” *Composite Structures*, vol. 296, p. 115 881, Sep. 2022, issn: 0263-8223. doi: 10.1016/J.COMPSTRUCT.2022.115881.

[27] B. Whittingham, A. A. Baker, A. Harman, and D. Bitton, “Micrographic studies on adhesively bonded scarf repairs to thick composite aircraft structure,” *Composites Part A: Applied Science and Manufacturing*, vol. 40, no. 9, pp. 1419–1432, Sep. 2009, issn: 1359-835X. doi: 10.1016/J.COMPOSITESA.2008.12.011.

[28] J. L. Lubkin, “A Theory of Adhesive Scarf Joints,” *Journal of Applied Mechanics*, vol. 24, no. 2, pp. 255–260, Jun. 1957, issn: 0021-8936. doi: 10.1115/1.4011506.

[29] H. Schürmann, *Konstruieren mit Faser-Kunststoff-Verbunden*, 2nd ed. Berlin: Springer-Verlag, 2007.

[30] J. S. Yoo, V. H. Truong, M. Y. Park, J. H. Choi, and J. H. Kweon, “Parametric study on static and fatigue strength recovery of scarf-patch-repaired composite laminates,” *Composite Structures*, vol. 140, pp. 417–432, Apr. 2016, issn: 0263-8223. doi: 10.1016/J.COMPSTRUCT.2015.12.041.

[31] A. J. Gunnion and I. Herszberg, “Parametric study of scarf joints in composite structures,” *Composite Structures*, vol. 75, no. 1-4, pp. 364–376, Sep. 2006, issn: 0263-8223. doi: 10.1016/J.COMPSTRUCT.2006.04.053.

[32] E. Sonat and S. Özerinç, “Failure behavior of scarf-bonded woven fabric CFRP laminates,” *Composite Structures*, vol. 258, p. 113 205, Feb. 2021, issn: 0263-8223. doi: 10.1016/J.COMPSTRUCT.2020.113205.

[33] J. Li, Y. Yan, Z. Liang, and T. Zhang, “Experimental and Numerical Study of Adhesively Bonded CFRP Scarf-Lap Joints Subjected to Tensile Loads,” *The Journal of Adhesion*, vol. 92, no. 1, pp. 1–17, Jan. 2015, issn: 15455823. doi: 10.1080/00218464.2014.987343.

[34] U. A. Khashaba and I. M. Najjar, “Adhesive layer analysis for scarf bonded joint in CFRE composites modified with MWCNTs under tensile and fatigue loads,” *Composite Structures*, vol. 184, pp. 411–427, Jan. 2018, issn: 0263-8223. doi: 10.1016/J.COMPSTRUCT.2017.09.095.

[35] C. H. Wang, V. Venugopal, and L. Peng, “Stepped Flush Repairs for Primary Composite Structures,” *The Journal of Adhesion*, vol. 91, no. 1-2, pp. 95–112, 2015. doi: 10.1080/00218464.2014.896212.

[36] H. Bendemra, P. Compston, and P. J. Crothers, “Optimisation study of tapered scarf and stepped-lap joints in composite repair patches,” *Composite Structures*, vol. 130, pp. 1–8, Oct. 2015, issn: 02638223. doi: 10.1016/j.compstruct.2015.04.016.

[37] J. Tomblin, C. Yang, and P. Harter, “Investigation of Thick Bondline Adhesive Joints,” Wichita State University, Wichita, KS, Tech. Rep., Jun. 2001.

[38] C. H. Wang and A. J. Gunnion, “On the design methodology of scarf repairs to composite laminates,” *Composites Science and Technology*, vol. 68, no. 1, pp. 35–46, Jan. 2008, issn: 0266-3538. doi: 10.1016/J.COMPSCITECH.2007.05.045.

[39] T. D. Breitzman, E. V. Iarve, B. M. Cook, G. A. Schoeppner, and R. P. Lipton, “Optimization of a composite scarf repair patch under tensile loading,” *Composites Part A: Applied Science and Manufacturing*, vol. 40, no. 12, pp. 1921–1930, 2009, issn: 1359-835X. doi: 10.1016/j.compositesa.2009.04.033.

[40] J. Zhang, X. Cheng, Y. Cheng, X. Guo, and L. Yang, “Effect of over-ply on moisture absorption behavior of scarf-repaired composite laminate,” *International Journal of Adhesion and Adhesives*, vol. 102, p. 102 683, 2020, issn: 0143-7496. doi: 10.1016/j.ijadhadh.2020.102683.

[41] J. B. Orsatelli, E. Paroissien, F. Lachaud, and S. Schwartz, “Bonded flush repairs for aerospace composite structures: A review on modelling strategies and application to repairs optimization, reliability and durability,” *Composite Structures*, vol. 304, Jan. 2023, issn: 02638223. doi: 10.1016/j.compstruct.2022.116338.

[42] H. Adin, “The investigation of the effect of angle on the failure load and strength of scarf lap joints,” *International Journal of mechanical sciences*, vol. 61, no. 1, pp. 24–31, 2012. doi: 10.1016/j.ijmecsci.2012.04.010.

[43] R. D. S. G. Campilho, M. De Moura, A. Pinto, J. Morais, and J. Domingues, “Modelling the tensile fracture behaviour of cfrp scarf repairs,” *Composites Part B: Engineering*, vol. 40, no. 2, pp. 149–157, 2009. doi: 10.1016/j.compositesb.2008.10.008.

[44] V.-H. Truong, J.-S. Yoo, C.-H. Kim, M.-Y. Park, J.-H. Choi, and J.-H. Kweon, “Failure load prediction of laminates repaired with a scarf-bonded patch using the damage zone method,” *Advanced Composite Materials*, vol. 26, no. 2, pp. 115–133, 2017. doi: 10.1080/09243046.2016.1232008.

[45] Y. Kwon and A. Marron, “Scarf joints of composite materials: Testing and analysis,” *Applied Composite Materials*, vol. 16, pp. 365–378, 2009. doi: 10.1007/s10443-009-9104-8.

[46] S. Kumar, S. Sivashanker, A. Bag, and I. Sridhar, “Failure of aerospace composite scarf-joints subjected to uniaxial compression,” *Materials Science and Engineering: A*, vol. 412, no. 1-2, pp. 117–122, 2005. doi: 10.1016/j.msea.2005.08.033.

[47] R. D. Campilho, M. De Moura, D. Ramantani, J. Morais, and J. Domingues, “Buckling behaviour of carbon–epoxy adhesively-bonded scarf repairs,” *Journal of Adhesion Science and Technology*, vol. 23, no. 10-11, pp. 1493–1513, 2009. doi: 10.1163/156856109X433045.

[48] T. Keil, *Untersuchung von Einflussparametern auf die strukturmechanischen Eigenschaften von geklebten CFK-Reparaturen*, Master Thesis, Manching, Germany: Airbus Defence and Space GmbH, 2019.

[49] B. Wang, S. Fan, J. Chen, W. Yang, W. Liu, and Y. Li, “A review on prediction and control of curing process-induced deformation of continuous fiber-reinforced thermosetting composite structures,” *Composites Part A: Applied Science and Manufacturing*, p. 107 321, 2022. doi: 10.1016/j.compositesa.2022.107321.

[50] N. Traiforos, T. Turner, P. Runeberg, *et al.*, “A simulation framework for predicting process-induced distortions for precise manufacturing of aerospace thermoset composites,” *Composite Structures*, vol. 275, p. 114 465, 2021. doi: 10.1016/j.compstruct.2021.114465.

[51] T. Breitzman, E. Iarve, B. Cook, G. Schoeppner, and R. Lipton, “Optimization of a composite scarf repair patch under tensile loading,” *Composites Part A: Applied Science and Manufacturing*, vol. 40, no. 12, pp. 1921–1930, 2009. doi: 10.1016/j.compositesa.2009.04.033.

[52] C. H. Wang and A. J. Gunnion, “Optimum shapes of scarf repairs,” *Composites Part A: Applied Science and Manufacturing*, vol. 40, no. 9, pp. 1407–1418, 2009, issn: 1359-835X. doi: 10.1016/j.compositesa.2009.02.009.

[53] M. Niedernhuber, J. Holtmannspötter, and I. Ehrlich, “Fiber-oriented repair geometries for composite materials,” *Composites Part B: Engineering*, vol. 94, pp. 327–337, 2016, issn: 1359-8368. doi: 10.1016/j.compositesb.2016.03.027.

[54] R. S. Pierce and B. G. Falzon, “Modelling the size and strength benefits of optimised step/scarf joints and repairs in composite structures,” *Composites Part B: Engineering*, vol. 173, p. 107 020, 2019, issn: 1359-8368. doi: 10.1016/j.compositesb.2019.107020.

[55] M. Damghani, S. Bolanos, A. Chahar, *et al.*, “Design, novel quality check and experimental test of an original variable length stepped scarf repair scheme,” *Composites Part B: Engineering*, vol. 230, p. 109 542, 2022, issn: 1359-8368. doi: 10.1016/j.compositesb.2021.109542.

[56] M. Y. Pitanga, M. O. H. Cioffi, H. J. C. Voorwald, and C. H. Wang, “Reducing repair dimension with variable scarf angles,” *International Journal of Adhesion and Adhesives*, vol. 104, p. 102 752, 2021, issn: 0143-7496. doi: 10.1016/j.ijadhadh.2020.102752.

[57] C. Sun, W. Zhao, J. Zhou, *et al.*, “Mechanical behaviour of composite laminates repaired with a stitched scarf patch,” *Composite Structures*, vol. 255, p. 112 928, Jan. 2021, issn: 0263-8223. doi: 10.1016/J.COMPSTRUCT.2020.112928.

[58] FAA, *PS-AIR100-14-130-001 - Bonded Repair Size Limits.* Washington, D.C., United States: U.S. Department of Transportation - Federal Aviation Administration, 2014.

[59] A. Baker, A. J. Gunnion, and J. Wang, “On the Certification of Bonded Repairs to Primary Composite Aircraft Components,” *The Journal of Adhesion*, vol. 91, no. 1-2, pp. 4–38, 2015. doi: 10.1080/00218464.2014.883315.

[60] T. A. Schmid Fuertes, T. Kruse, T. Körwien, and M. Geistbeck, “Bonding of CFRP primary aerospace structures – discussion of the certification boundary conditions and related technology fields addressing the needs for development,” *Composite Interfaces*, vol. 22, no. 8, pp. 795–808, Oct. 2015, issn: 0927-6440. doi: 10.1080/09276440.2015.1077048.

[61] P. Kumari, A. Alam, and Saahil, “Influence of the impact position on scarf repair composite under low velocity impact: FEA investigation,” *Materials Today: Proceedings*, vol. 38, pp. 3005–3013, 2021, issn: 2214-7853. doi: 10.1016/j.matpr.2020.09.323.

[62] X. Cheng, X. Du, J. Zhang, J. Zhang, X. Guo, and J. Bao, “Effects of stacking sequence and rotation angle of patch on low velocity impact performance of scarf repaired laminates,” *Composites Part B: Engineering*, vol. 133, pp. 78–85, Jan. 2018, issn: 1359-8368. doi: 10.1016/J.COMPOSITESB.2017.09.020.

[63] L. Sui, G. Zhidong, G. Xia, C. Jianhua, X. Guofen, and C. Jing, “Tensile Behavior of Hybrid Plain Woven Fabric Laminate Repaired by Scarfing Method,” *Polymers and Polymer Composites*, vol. 21, no. 9, pp. 599–606, Nov. 2013, issn: 0967-3911. doi: 10.1177/096739111302100908.

[64] S. Budhe, M. D. Banea, and S. de Barros, “Bonded repair of composite structures in aerospace application: a review on environmental issues,” *Applied Adhesion Science*, vol. 6, no. 1, p. 3, 2018, issn: 2196-4351. doi: 10.1186/s40563-018-0104-5.

[65] M. Parker, “Chapter 18 - Radar Basics,” in *Digital Signal Processing 101 (Second Edition)*, M. Parker, Ed., Second Edition, Newnes, 2017, pp. 231–240, isbn: 978-0-12-811453-7. doi: 10.1016/B978-0-12-811453-7.00018-4.

[66] H. Pang, Y. Duan, L. Huang, *et al.*, “Research advances in composition, structure and mechanisms of microwave absorbing materials,” *Composites Part B: Engineering*, vol. 224, p. 109 173, 2021, issn: 1359-8368. doi: 10.1016/j.compositesb.2021.109173.

[67] Y. Wu, S. Tan, Y. Zhao, L. Liang, M. Zhou, and G. Ji, “Broadband multispectral compatible absorbers for radar, infrared and visible stealth application,” *Progress in Materials Science*, vol. 135, p. 101 088, 2023, issn: 0079-6425. doi: 10.1016/j.pmatsci.2023.101088.

[68] M. R. M. Asyraf, A. Syamsir, N. M. Nurazzi, *et al.*, “Synthetic nanofillers in polymer composites for aerospace industry,” in *Synthetic and Natural Nanofillers in Polymer Composites*, Elsevier, 2023, pp. 291–311. doi: 10.1016/B978-0-443-19053-7.00018-4.

[69] B. Fiedler, F. H. Gojny, M. H. Wichmann, M. C. Nolte, and K. Schulte, “Fundamental aspects of nano-reinforced composites,” *Composites Science and Technology*, vol. 66, no. 16, pp. 3115–3125, Dec. 2006, issn: 02663538. doi: 10.1016/j.compscitech.2005.01.014.

[70] P.-C. Ma, N. A. Siddiqui, G. Marom, and J.-K. Kim, “Dispersion and functionalization of carbon nanotubes for polymer-based nanocomposites: A review,” *Composites Part A: Applied Science and Manufacturing*, vol. 41, no. 10, pp. 1345–1367, Oct. 2010, issn: 1359835X. doi: 10.1016/j.compositesa.2010.07.003.

[71] Y. Zare, “Study of nanoparticles aggregation/agglomeration in polymer particulate nanocomposites by mechanical properties,” *Composites Part A: Applied Science and Manufacturing*, vol. 84, pp. 158–164, May 2016, issn: 1359835X. doi: 10.1016/j.compositesa.2016.01.020.

[72] X. Ma, Y. Zare, and K. Y. Rhee, “A Two-Step Methodology to Study the Influence of Aggregation/Agglomeration of Nanoparticles on Young’s Modulus of Polymer Nanocomposites,” *Nanoscale Research Letters*, vol. 12, no. 1, p. 621, Dec. 2017, issn: 1931-7573. doi: 10.1186/s11671-017-2386-0.

[73] Airbus, BAE, Leonardo, and EuroFighter GmbH, *P-J-513-S-0156 Surface Smoothening / Filling Repairs Standard Procedures*, Manufacturing procedure, Hallbergmoos, Germany, 2004.

[74] X. Sheng, M. Akinc, and M. R. Kessler, “Cure kinetics of thermosetting bisphenol E cyanate ester,” *Journal of Thermal Analysis and Calorimetry*, vol. 93, no. 1, pp. 77–85, Jul. 2008, issn: 1388-6150. doi: 10.1007/s10973-007-8803-3.

[75] M. Thunga, A. Bauer, K. Obusek, R. Meilunas, M. Akinc, and M. R. Kessler, “Injection repair of carbon fiber/bismaleimide composite panels with bisphenol E cyanate ester resin,” *Composites Science and Technology*, vol. 100, pp. 174–181, Aug. 2014, issn: 02663538. doi: 10.1016/j.compscitech.2014.05.024.

[76] W. Lai, H. Saeedipour, and K. Goh, “Mechanical properties of low-velocity impact damaged carbon fibre reinforced polymer laminates: Effects of drilling holes for resin-injection repair,” *Composite Structures*, vol. 235, p. 111 806, Mar. 2020, issn: 02638223. doi: 10.1016/j.compstruct.2019.111806.

[77] M. A. A.-S. B. Rahman, W. L. Lai, H. Saeedipour, and K. L. Goh, “Cost-effective and efficient resin-injection device for repairing damaged composites,” *Reinforced Plastics*, vol. 63, no. 3, pp. 156–160, Jun. 2019, issn: 0034-3617. doi: 10.1016/j.repl.2018.11.001.

[78] G. Savage and M. Oxley, “Repair of composite structures on Formula 1 race cars,” *Engineering Failure Analysis*, vol. 17, no. 1, pp. 70–82, Jan. 2010, issn: 13506307. doi: 10.1016/j.engfailanal.2008.11.006.

[79] P. Slattery, C. McCarthy, and R. O’Higgins, “Assessment of residual strength of repaired solid laminate composite materials through mechanical testing,” *Composite Structures*, vol. 147, pp. 122–130, Jul. 2016, issn: 02638223. doi: 10.1016/j.compstruct.2016.03.036.

[80] P. Zelinski, “Composites Machining for the F-35,” *Modern Machine Shop*, Aug. 2010 [Online], Available: Database, www.mmsonline.com/articles/composites-machining-for-the-f-35/ [Accessed: November 27, 2023].

[81] Determination Of Tensile Strength Of Tapered And Stepped Joints, *DIN EN 6066*, 1996.

[82] T. Brussat, S. Chiu, and S. Mostovoy, “Fracture mechanics for structural adhesive bonds,” *DTIC Document*, 1977.

[83] M. Hamberger, *Entwicklung einer Probe zur Charakterisierung des Rissfortschritts in geklebten CFK-Reparaturen*, Master Thesis, Manching, Germany: Airbus Defence and Space GmbH, 2019.

[84] B. J. Preisz, *Untersuchung der Anwendbarkeit des BCS auf CFK-Reparaturen*, Master Thesis, Manching, Germany: Airbus Defence and Space GmbH, Jan. 2021.

[85] T. Thäsler, J. Holtmannspötter, and H.-J. Gudladt, "Monitoring the fatigue crack growth behavior of composite joints using in situ 2d-digital image correlation," *The Journal of Adhesion*, vol. 95, no. 5-7, pp. 595–613, 2019. doi: 10.1080/00218464.2018.1562923.

[86] Hexcel Corporation, *HexPly® 8552*, Product Data Sheet, Stamford, Connecticut, United States, 2016.

[87] Airbus Defence & Space GmbH, *Fertigungsanweisung Herstellen von Bauteilen aus vorimprägnierten Faserwerkstoffen, 80-M-31-2910*, Manufacturing procedure, Taufkirchen, Germany, 2015.

[88] Airbus Defence & Space GmbH, *P-J-513-M-0079 Bondline preparation for bonded Composite Repairs*, Manufacturing procedure, Taufkirchen, Germany, 2021.

[89] ASTM International, *ASTM standard D3039/D3039M, Standard Test Method for Tensile Properties of Polymer Matrix Composite Materials*, 2002.

[90] A. Smiti, "A critical overview of outlier detection methods," *Computer Science Review*, vol. 38, pp. 100–306, 2020. doi: 10.1016/j.cosrev.2020.100306.

[91] ALENIA, BAES, EADS-CASA, and EADS-MAS, *JST-D-104 EF2000 Series Production Aircraft, CFC Properties and Design Allowables*, Design document, Manching, Germany, 2007.

[92] D. Santl, *Untersuchung des Rissfortschritts in geklebten Faserverbundwerkstoff-Verbindungen unter Einfluss verschiedener Oberflächenmodifikationen*, Master Thesis, Manching, Germany: Airbus Defence and Space GmbH, 2022.

[93] C. Thümmler, *Einfluss der Klebschichtdicke auf die Festigkeit unter Berücksichtigung unterschiedli-cher Lastfälle und Umweltbedingungen*, Master Thesis, Manching, Germany: Airbus Defence and Space GmbH, Jul. 2023.

A

EN6066 Static tests

This appendix collects all the static test data. Table A.1 lists the relevant dimensions and test results for all the specimens, Figure A.1 provides their stress-strain curves, while the pictures of their fracture surfaces are collected in Figure A.2.

Table A.1: Parameters and test results for all the EN6066 specimens statically tested (a and b represent, respectively, the thickness and the width of the specimens measured along the scarf)

Specimen	Patch configuration	a [mm]	b [mm]	F_{max} [kN]	UTS [MPa]	ε_{max} [%]	E_x [GPa]	Failure mode
REF_QI_1	Reference	3.49	25.75	40.06	445.29	0.82	50.40	Cohesive/Adherend
REF_QI_2	Reference	3.42	26.09	44.42	497.28	0.95	49.19	Cohesive/Adherend
REF_QI_3	Reference	3.41	25.56	43.87	503.35	0.94	46.82	Cohesive/Adherend
REF_QI_4	Reference	3.41	25.56	40.90	468.75	0.85	48.22	Cohesive/Adherend
REF_QI_5	Reference	3.39	25.53	40.61	469.34	0.88	47.22	Cohesive/Adherend
MIL_QI_1	Re-milled	3.23	25.53	38.87	471.91	0.76	61.57	Cohesive/Adherend
MIL_QI_2	Re-milled	3.22	25.57	38.75	470.44	0.83	60.33	Cohesive/Adherend
MIL_QI_3	Re-milled	3.20	25.56	39.96	488.39	0.84	58.11	Cohesive/Adherend
MIL_QI_4	Re-milled	3.19	25.58	40.65	497.70	0.87	54.27	Cohesive/Adherend
MIL_QI_5	Re-milled	3.17	25.56	39.45	486.55	0.75	61.36	Cohesive/Adherend
NMP_QI_1	Modified	3.10	25.58	35.92	452.55	0.83	53.89	Cohesive/Adherend
NMP_QI_2	Modified	3.08	25.52	32.84	417.32	0.84	53.25	Cohesive/Adherend
NMP_QI_3	Modified	3.05	25.56	34.21	439.29	0.78	54.16	Cohesive/Adherend
NMP_QI_4	Modified	3.03	25.58	32.61	421.17	0.78	52.68	Cohesive/Adherend
NMP_QI_5	Modified	3.01	25.53	32.10	417.94	0.68	63.54	Cohesive/Adherend

Do note that the sudden offsets visible in Figure A.1 — particularly in Figure A.1b, MIL_QI_1 curve — are most likely measurement errors due to the DIC system used to determine the strains.

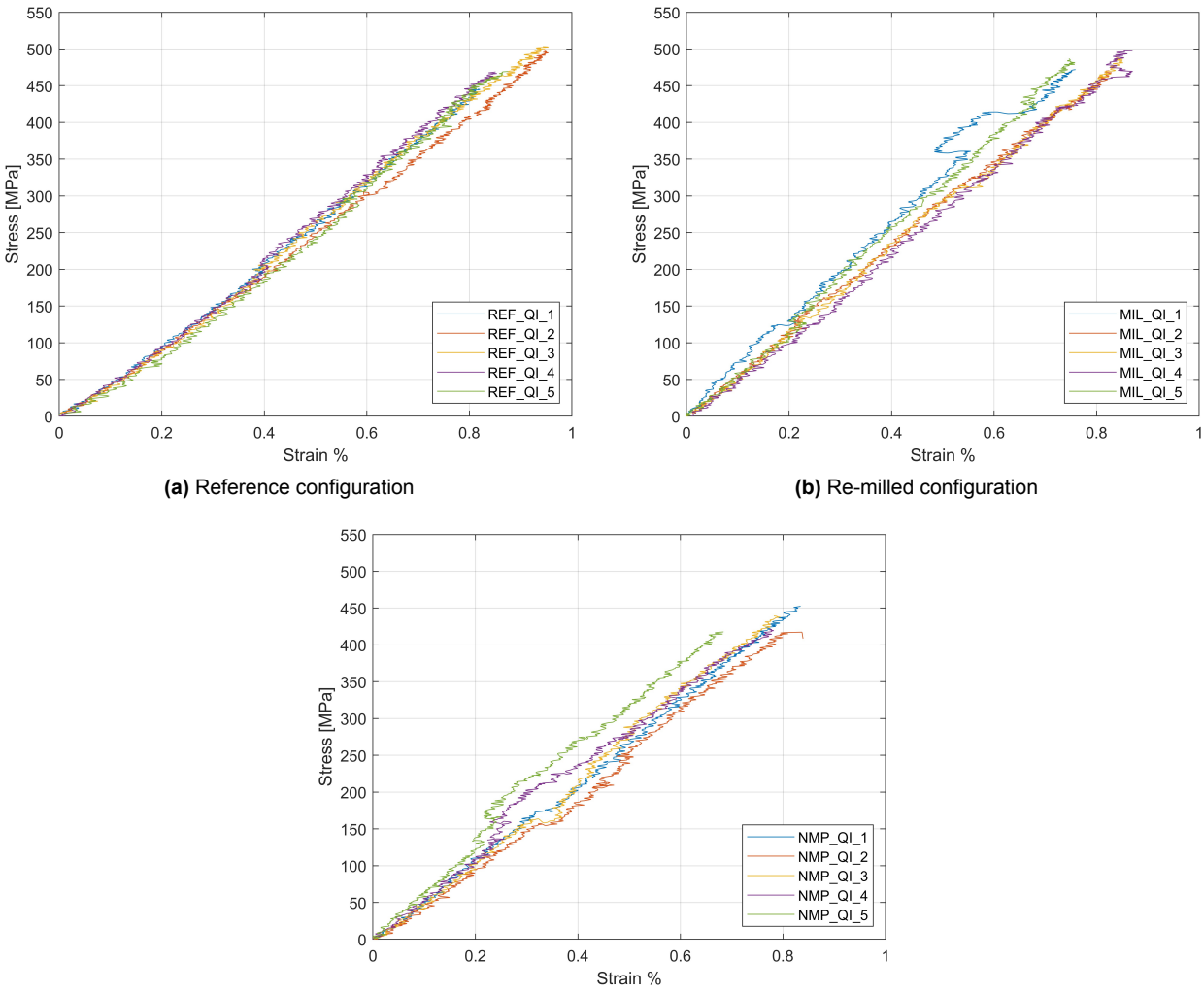

(a) Reference configuration

(b) Re-milled configuration

(c) Modified patch configuration

Figure A.1: Stress-strain curves for the EN6066 specimens, static tests

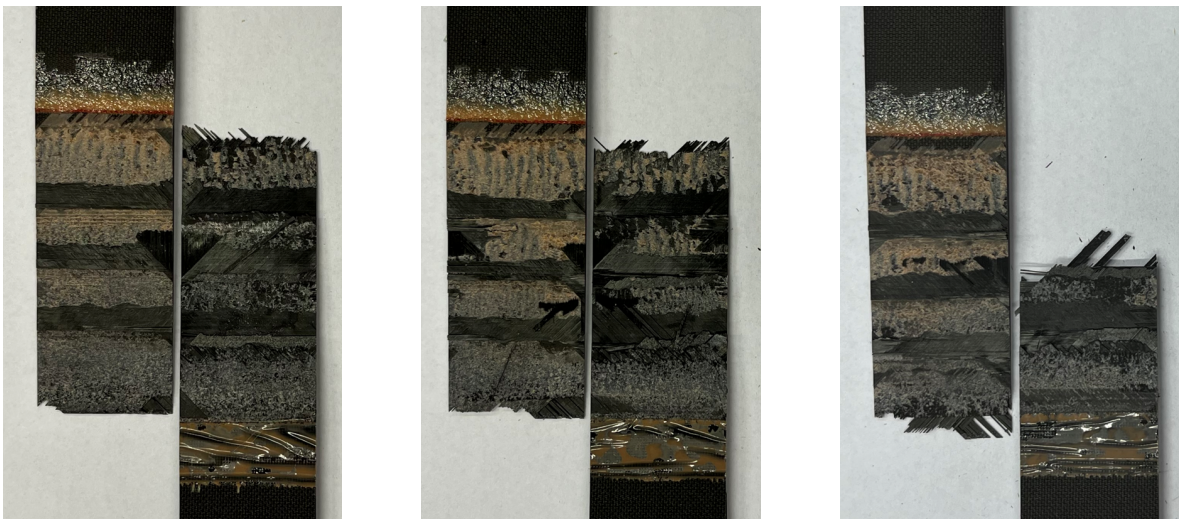

(a) REF_QI_1

(b) REF_QI_2

(c) REF_QI_3

(d) REF_QI_4

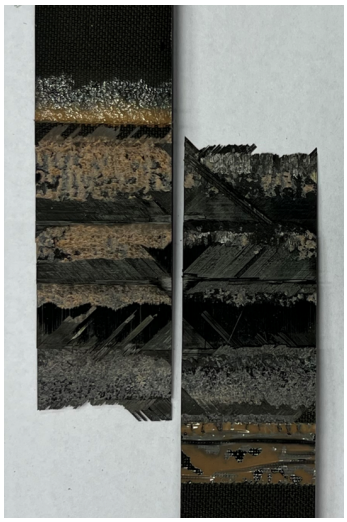

(e) REF_QI_5

(f) MIL_QI_1

(g) MIL_QI_2

(h) MIL_QI_3

(i) MIL_QI_4

(j) MIL_QI_5

(k) NMP_QI_1

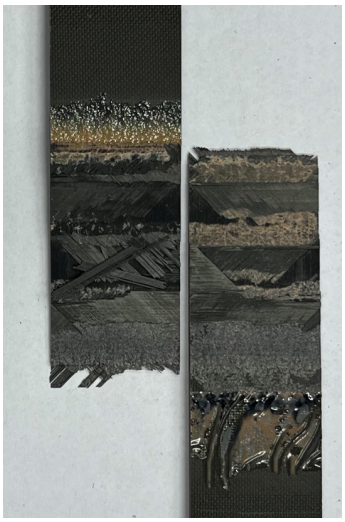

(l) NMP_QI_2

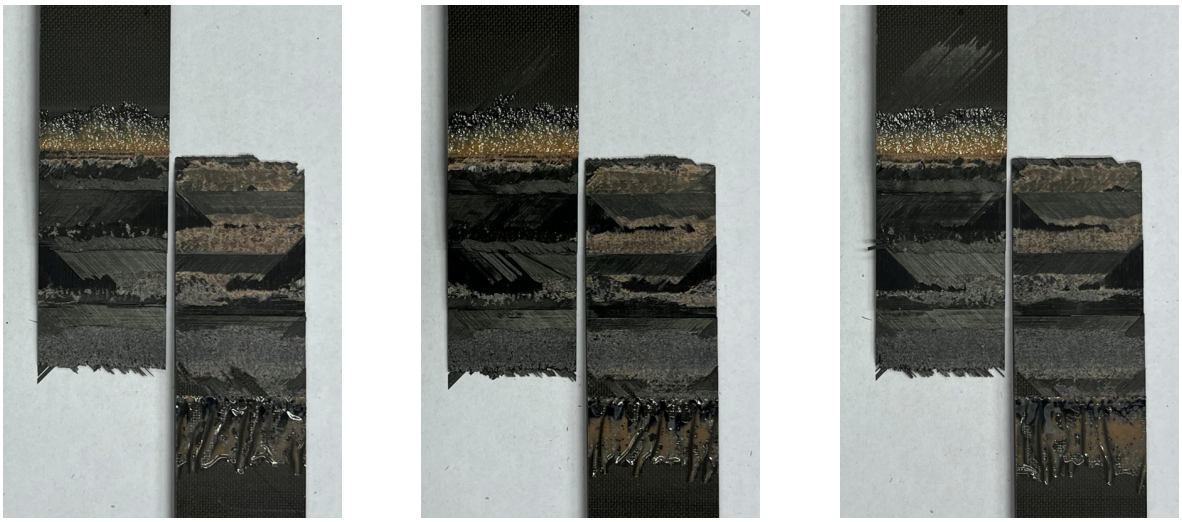

(m) NMP_QI_3 **(n)** NMP_QI_4 **(o)** NMP_QI_5

Figure A.2: Fracture surfaces of the EN6066 specimens, static tests (in every picture: parent laminate on the LHS, repair patch on the RHS)

B

EN6066 Fatigue tests

Figure B.1 provides the fracture surfaces of the specimens that failed before reaching the target threshold (54000 cycles) during the fatigue tests.

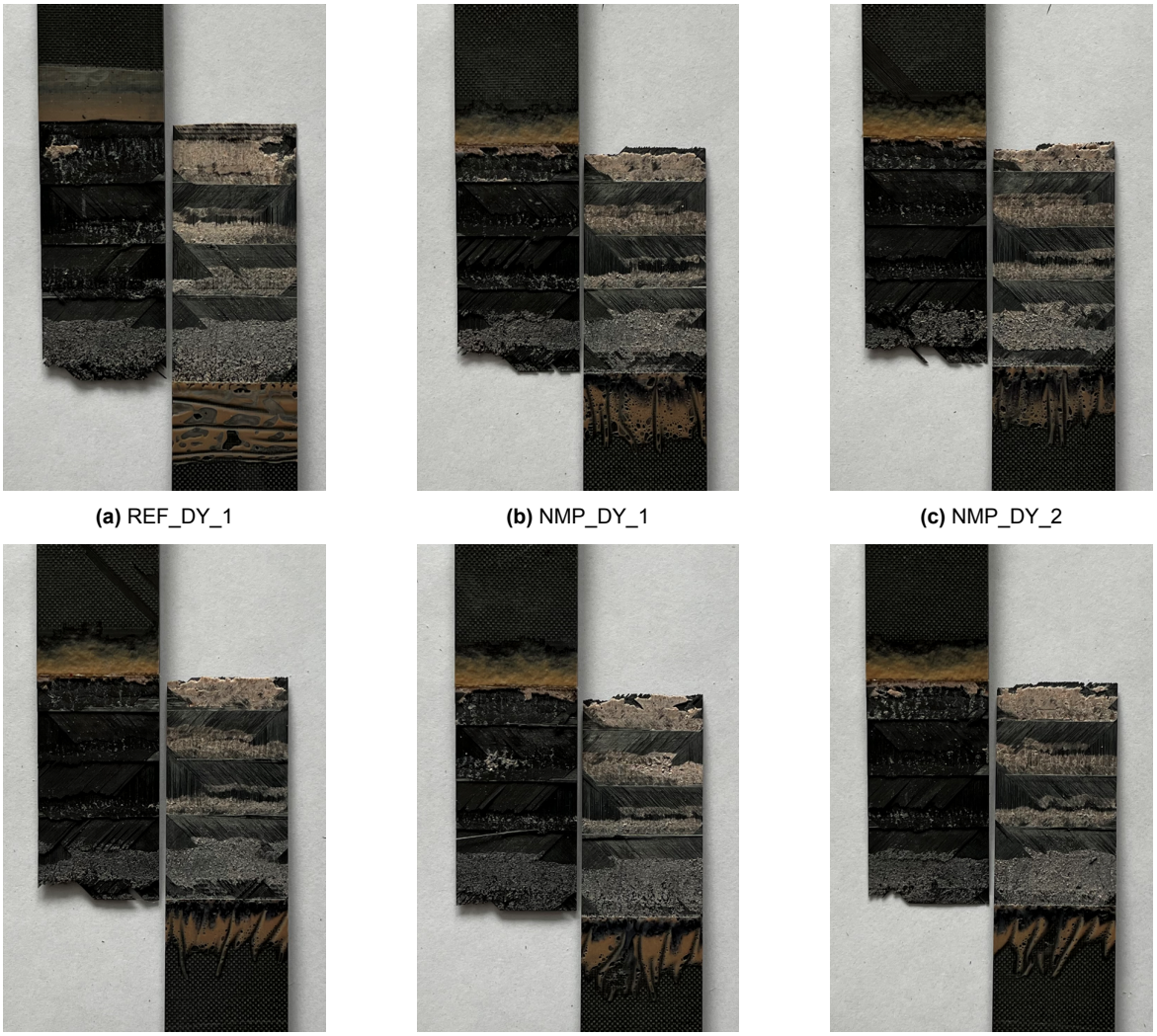

(a) REF_DY_1 **(b)** NMP_DY_1 **(c)** NMP_DY_2

(d) NMP_DY_3 **(e)** NMP_DY_4 **(f)** NMP_DY_5

Figure B.1: Fracture surfaces of the EN6066 specimens failed below 54000 cycles during the fatigue tests (in every picture: parent laminate on the LHS, repair patch on the RHS)

C

EN6066 Residual strength tests

This appendix collects all the residual strength test data. Table C.1 lists the relevant dimensions and test results for all the specimens, Table C.2 their residual properties compared to pristine specimens, Figure C.1 provides their stress-strain curves, while the pictures of their fracture surfaces are collected in Figure C.2.

Table C.1: Parameters and test results for all the EN6066 specimens residual strength tests (a and b represent, respectively, the thickness and the width of the specimens measured along the scarf)

Specimen	Patch configuration	a [mm]	b [mm]	F_{max} [kN]	UTS [MPa]	ε_{max} [%]	E_x [GPa]	Failure mode
REF_DY_1	Reference	3.34	25.60	42.19	493.40	1.01	46.03	Cohesive/Adherend
REF_DY_2	Reference	3.35	25.48	40.14	470.22	0.91	46.34	Cohesive/Adherend
REF_DY_3	Reference	3.35	25.53	38.51	450.25	0.88	47.63	Cohesive/Adherend
REF_DY_4	Reference	3.42	25.55	40.01	457.88	0.92	47.41	Cohesive/Adherend
REF_DY_5	Reference	3.45	25.55	39.99	453.66	0.85	49.94	Cohesive/Adherend
MIL_DY_2	Re-milled	3.16	25.54	30.74	380.90	0.61	60.09	Cohesive/Adherend
MIL_DY_3	Re-milled	3.16	25.65	30.28	373.62	0.64	57.77	Cohesive/Adherend
MIL_DY_4	Re-milled	3.17	25.55	35.85	442.58	0.77	51.96	Cohesive/Adherend
MIL_DY_5	Re-milled	3.18	25.55	32.54	400.45	0.69	58.37	Cohesive/Adherend

Table C.2: Comparison between the specimens statically tested after fatigue and the ones statically tested in pristine conditions (the reference values are the medians listed in Table 9.1)

Specimen	Patch configuration	ΔF_{max}	ΔUTS	$\Delta\varepsilon_{max}$	ΔE_x
REF_DY_1	Reference	+3%	+5%	+15%	-12%
REF_DY_2	Reference	-2%	0%	+4%	-12%
REF_DY_3	Reference	-6%	-4%	+1%	-10%
REF_DY_4	Reference	-2%	-2%	+5%	-8%
REF_DY_5	Reference	-2%	-3%	-3%	-1%
MIL_DY_2	Re-milled	-22%	-22%	-26%	+2%

MIL_DY_3	Re-milled	-23%	-23%	-22%	-8%
MIL_DY_4	Re-milled	-9%	-9%	-7%	-9%
MIL_DY_5	Re-milled	-18%	-18%	-16%	-7%

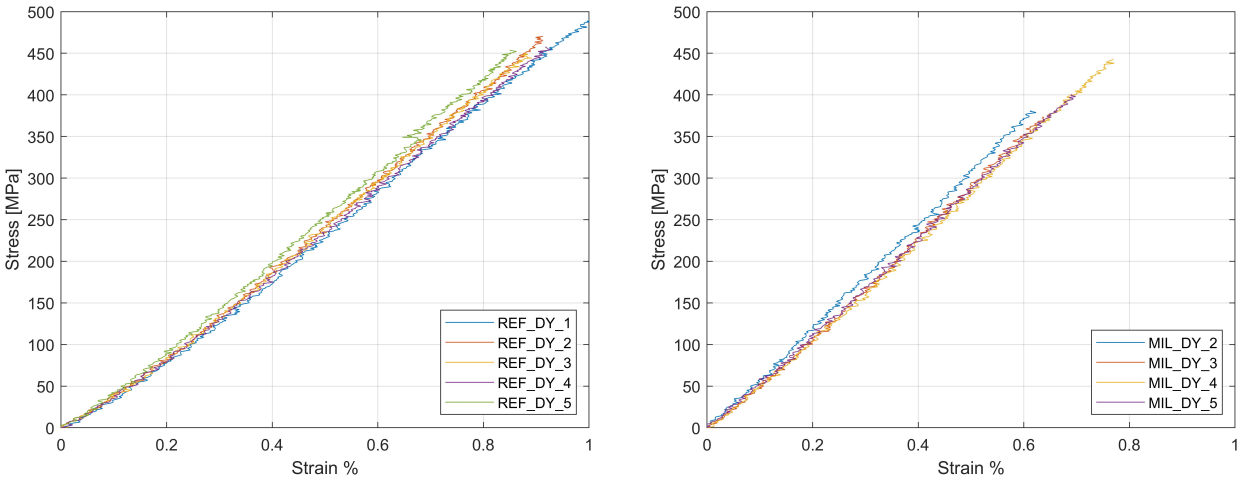

(a) Reference configuration **(b)** Re-milled configuration

Figure C.1: Stress-strain curves for the EN6066 specimens, residual strength static tests

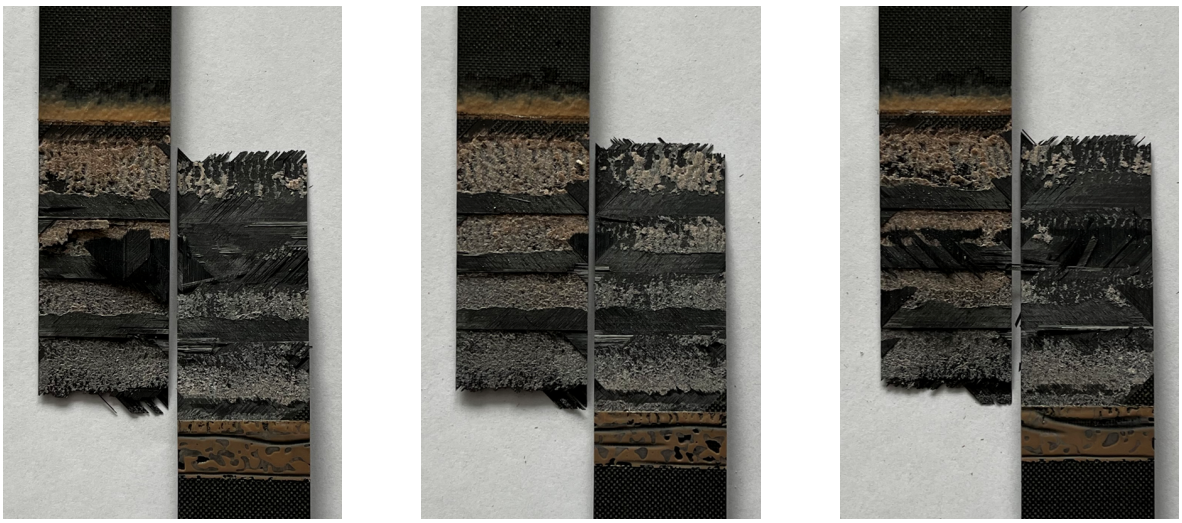

(a) REF_DY_1 **(b)** REF_DY_2 **(c)** REF_DY_3

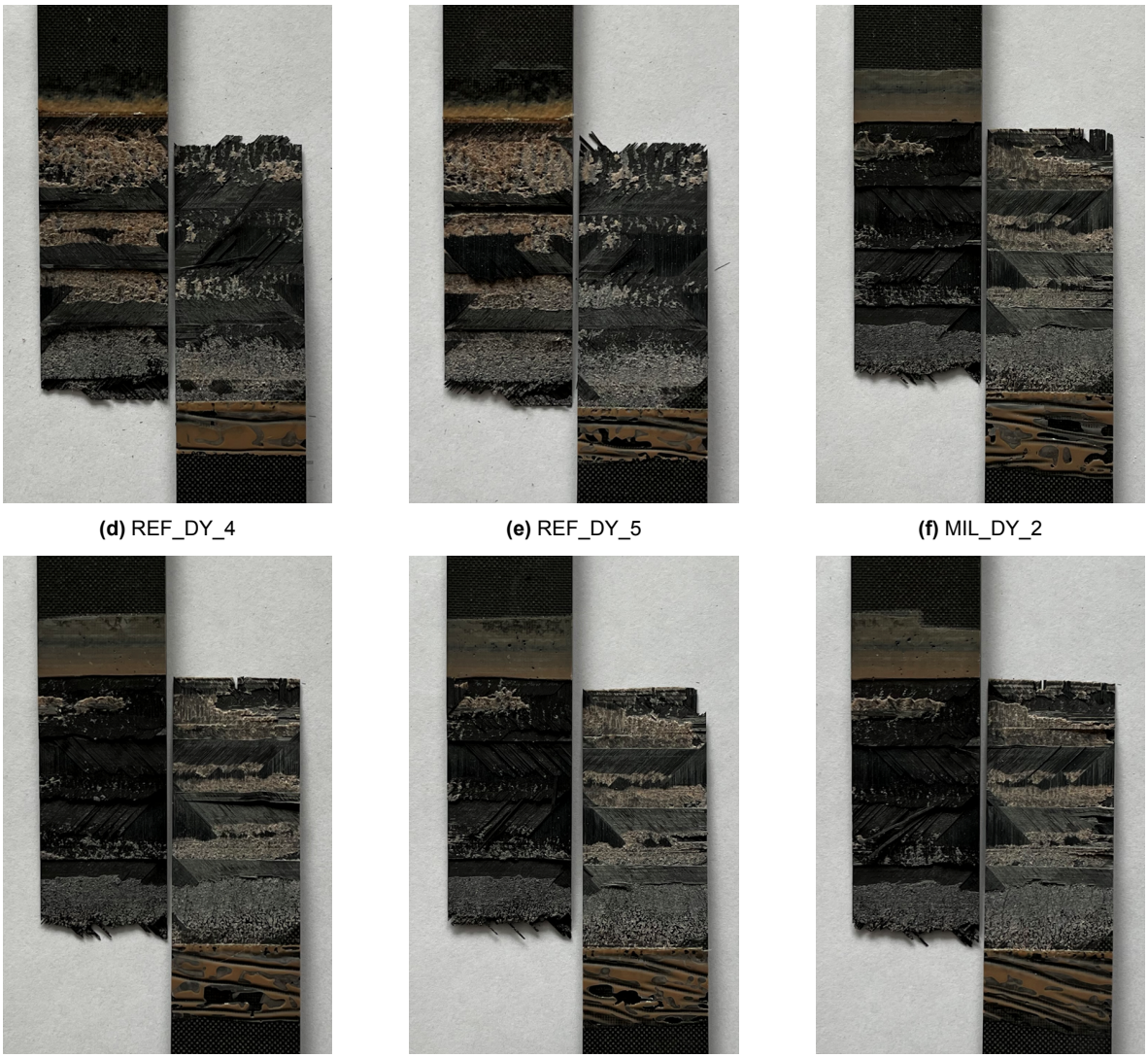

(d) REF_DY_4 **(e)** REF_DY_5 **(f)** MIL_DY_2

(g) MI_DY_3 **(h)** MIL_DY_4 **(i)** MIL_DY_5

Figure C.2: Fracture surfaces of the EN6066 specimens, residual strength tests (in every picture: parent laminate on the LHS, repair patch on the RHS)